THE CORNEAL LAMELLA ANISOTROPIC ELASTIC CONSTITUTIVE RELATION: THEORY AND EXPERIMENT

Thesis for the Degree of Ph. D.
MICHIGAN STATE UNIVERSITY

GERALD WARREN NYQUIST

1970

This is to certify that the

thesis entitled

The Corneal Lamella Anisotropic Elastic

Constitutive Relation: Theory and Experiment

presented by

Gerald W. Nyquist

has been accepted towards fulfillment
of the requirements for

Ph.D. degree in Mechanics

Gary Lee Cloud
Major professor

Gary Lee Cloud

Date July 30, 1970

O-169

ABSTRACT

THE CORNEAL LAMELLA ANISOTROPIC ELASTIC
CONSTITUTIVE RELATION: THEORY AND EXPERIMENT

By

Gerald Warren Nyquist

The structure of the corneal stroma of the higher vertebrates renders it a fascinating example of an anisotropic heterogeneous tissue, and the extreme geometric regularity of the stroma enables realistic analytic modeling of the three-dimensional stress-strain relation.

An analysis of the fluid pressure in the stroma indicates that a simple elastic continuum theory must be abandoned in favor of a mixed-media theory, which enables the tissue to be treated as a fluid-impregnated elastic continuum. The stroma is modeled as a superposition of a large number of randomly-oriented identical linearly-elastic transversely-isotropic layers, and it is shown that anisotropic heterogeneous plate theory may be used to relate the load-deformation properties of the complete stroma to the elastic properties of an individual layer.

The analytical treatment indicates that laboratory experiments are feasible which give results enabling some numerical information to be associated with the elastic constants of the constitutive model. Complete experimental data for fresh pig corneas are included, and details regarding the test equipment and procedures are presented. Pertinent experimental results are that the load-deformation properties are linear for the range of stress representative of intraocular pressure loading, and uniaxial tensile strips of stroma exhibit a Young's modulus of 66.3 gm/mm^2 and a Poisson's ratio of 5.9.

THE CORNEAL LAMELLA ANISOTROPIC ELASTIC CONSTITUTIVE RELATION: THEORY AND EXPERIMENT

By

Gerald Warren Nyquist

A THESIS

Submitted to
Michigan State University
in partial fulfillment of the requirements
for the degree of

DOCTOR OF PHILOSOPHY

Department of Metallurgy,
Mechanics, and Materials Science

College of Engineering

1970

G-65555
1-20-71

ACKNOWLEDGMENTS

The author expresses his gratitude to the many people who gave their assistance and advice. Particular thanks are given to Dr. Gary Cloud for his comments on the manuscript, and to Dr. James Klemm for his helpful discussions during the course of the research.

TABLE OF CONTENTS

LIST OF TABLES

LIST OF FIGURES

INTRODUCTION

The structural complexity of the corneal stroma of the higher vertebrates renders it a fascinating example of an anisotropic heterogeneous viscoelastic tissue, and the extreme geometric regularity of the stroma enables realistic analytic modeling of the three-dimensional stress-strain relation. The combined results of theory and experiment enable some numerical values to be associated with the material constants of the proposed stress-strain constitutive law.

The elastic properties of the cornea have received little attention from researchers to date, even though measurements made by the ophthalmologist in diagnosing a major cause of blindness (glaucoma) are dependent on these properties. Glaucoma is characterized by an abnormal elevation of the intraocular pressure, and the aforementioned measurements give an indication of the pressure by means of the techniques of tonometry and tonography, which are dependent on the elastic response of the cornea.

The above reference to glaucoma and the associated pressure-measuring techniques was made to aid in justifying this study of the elastic properties of the stroma. No further comment on the glaucoma problem will be made other than to point out that tonometric and tonographic procedures in common usage are known to produce inexact indications of intraocular pressure.

Recently the possibility of correlating measurements of the temporary stress-dependent birefringence (double-refraction) of the stroma to the intraocular pressure has been the motivating force of several research efforts. The goal is to develop a purely optical technique for clinical pressure measurement. A feasible technique is yet to be developed, and a knowledge of the stress-strain properties of the tissue is a necessary prerequisite to a complete understanding of the stress-dependence of stromal birefringence.

The research of this Thesis is of a bioengineering nature, heavily weighted toward engineering. Whereas the continuum mechanics theory presented would be difficult for the medically-oriented reader, the brief presentation of the anatomy of the eye in Chapter I will enable the engineering-oriented reader to proceed with little difficulty.

After a short presentation of previous studies on the mechanical properties of the cornea, a detailed analysis of the characteristics of the aqueous fluid pressure in the tissue is presented, and it becomes apparent that a simple elastic continuum theory must be abandoned in favor of a mixed-media theory which enables the cornea to be treated as a fluid-impregnated elastic continuum.

It is shown that the corneal stroma can be modeled as a superposition of a large number of transversely-isotropic elastic layers. The layers are identical, but are randomly oriented, and this leads to the use of an anisotropic heterogeneous plate theory to relate the load-deformation properties of the complete stroma to the elastic properties of an individual layer.

In the context of this Thesis, a "simple test" is defined to be a load-deformation test of the stroma where the stress and/or strain distribution may be evaluated without requiring the solution of a full-scale boundary value problem of the theory of elasticity. Three such simple tests are developed - uniaxial tensile stress, torsion, and uniaxial compressive strain.

Custom-designed test fixtures were fabricated for conducting the above tests, and fresh pig corneas were used for test specimens. Complete details of the laboratory experiments and results are presented, and the analytical and experimental results are combined to yield some numerical information regarding the elastic constants of the constitutive model. The metric system of units is generally adhered to, and force is expressed in grams (a one-gram force is that due to gravity acting on a standard one-gram mass).

The theoretical portion of the Thesis borrows heavily from the research of others, and the formulation of the problem would not have been possible without the mixed-media theory of Biot and the anisotropic heterogeneous elastic plate theory of Reissner and Stavsky (see Refs. 15 and 23). The combining of the two theories to analyze the cornea is of course original, as are all aspects of the experimental portion of the work.

It appears that this research constitutes the first attempt to rigorously analyze the anisotropic elastic properties of the tissue, and it is hoped that the work will not die at this point, but that the theory will enjoy improvements by those who follow.

CHAPTER I

ANATOMY OF THE EYE

The Eyeball

The anatomy of the eye of man and the domestic animals is nearly the same with the exception of dimensional variations among the species. The eye is most simply described as a layer of light-sensitive tissue (the retina) held in shape by surrounding coats of tissue which protect it (the sclera and cornea) and nourish it (the choroid). Further, the retina is served by an optical system consisting of a lens of variable aperture (the latter feature being the function of the iris) positioned behind a transparent anterior extension of the sclera known as the cornea. The cornea, in addition to its role as a structural member and protective shield for the intraocular structures, is a vital part of the optical system. The bending of light rays due to passing through the cornea is several times greater than the same effect experienced while passing through the lens. The configuration of the eye is shown in Figure I-1.

Although the eye is commonly referred to as a ball or globe, it is not a true sphere, but consists of the segments of two nonconcentric somewhat modified spheres.[2] The structural tissue of the posterior spherical segment is the white, opaque sclera. Viewing a horizontal section through the eye, the sclera

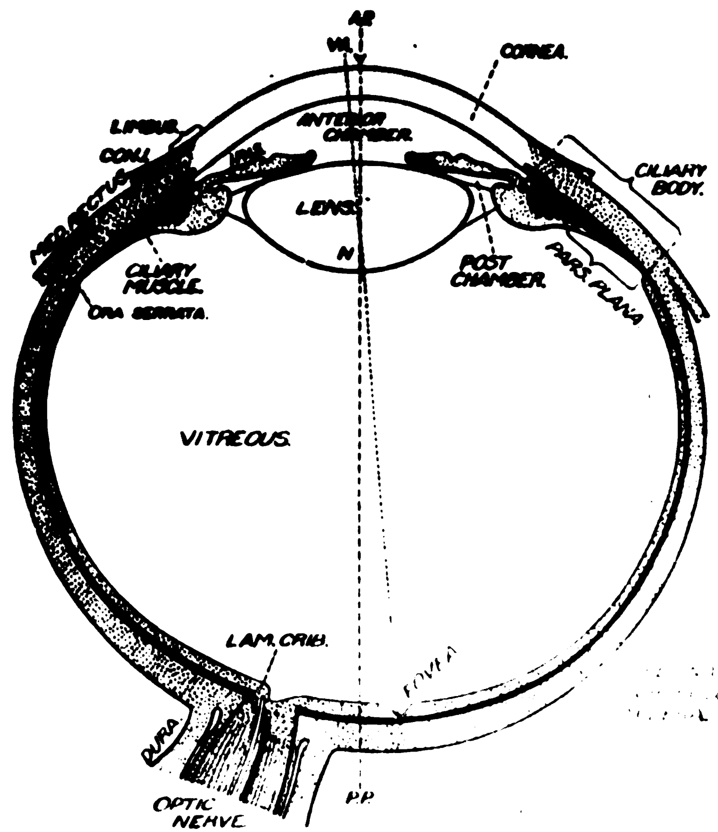

P.P. = posterior pole.
A.P. = anterior pole.
V.A. = visual axis.
PARS PLANA = orbiculus ciliaris.

(Modified from Salzmann.)

Figure I-1. Horizontal Section of the Eye

(Reproduced with permission from Ref. 2)

accounts for approximately five-sixths of the circumference of the eyeball. The remaining anterior one-sixth of the circumference (the cornea) is the segment of a sphere of smaller diameter. The sclera and cornea together are referred to as the fibrous tunic. Although the sclera and cornea appear to be composed of basically different types of tissue (since one is white and opaque whereas the other is clear and transparent), the transition from sclera to cornea (known as the limbus) is of a continuous nature.

The fibrous tunic is the outer coat or structure of the eye that houses and protects the delicate inner structures. In conjunction with the intraocular pressure the fibrous tunic gives the eyeball its resilience and definite shape.

Two fluids within the fibrous tunic are the mediums through which the intraocular pressure is realized. The vitreous humor, which fills the region posterior to the lens, is a clear gelatinous liquid having no provision for reproduction in the event of loss. The aqueous humor is a water-like liquid produced by the ciliary process. It flows through the posterior chamber (the region between the iris and anterior surface of the lens) and pupil into the anterior chamber (the region between the iris and posterior surface of the cornea). The fluid exits through the "angle" of the anterior chamber into the canal of Schlemm which carries it away via the venous pathways.

The Cornea

Since the cornea and sclera are of a continuous nature and together make up the fibrous tunic, a few remarks regarding the structure of the sclera will be made prior to a detailed description of the corneal structure. Strength is imparted to the fibrous tunic by tightly packed collagenous connective tissue fibers along with "elastic" fibers in much smaller numbers and a relatively few stroma cells.

In the sclera the collagen tissues are arranged into lamellae, or broad ribbons, which interweave in intricate strength-increasing patterns.[3] The sclera is thinnest at the equator and becomes progressively thicker anteriorly and posteriorly. The outer layers of the sclera are loosely woven, especially anteriorly, this soft material being known as the episcleral tissue.

The corneoscleral junction, or limbus, is approximately 0.75 to 1.0 mm in width, and is easily recognized as the thin transitional region along the periphery of the cornea where the change from opaqueness to transparency occurs. The scleral lamellae pass through the limbus, the dramatic change from opaqueness to transparency being caused by changes in their hydration and in the orientation of the microscopic structural elements.

The cornea is virtually a continuation of the sclera, but has greater curvature and a more methodical arrangement of its fibrous structure. The limbus is not always completely circular, but varies slightly among the species. Typical variations from a circle are the ellipse and pear-shape. The cornea is classically divided into five distinct anatomical layers lying parallel to the surface (see Figure I-2). Starting anteriorly, the layers are:

1) epithelium
2) Bowman's membrane
3) stroma (or substantia propria)
4) Descemet's membrane
5) endothelium.

A brief description of each of the above layers follows. Dimensions for both man (Ref. 3, pp. 290-302) and the pig (Ref. 1, pp. 217-218) are cited. This Thesis deals specifically with the pig cornea; however, for convenience of comparison the dimensions in man are also given.

The epithelium, built up of many layers of cells, accounts for about 10 per cent of the corneal thickness. There are 5 or 6 layers in man and 6 to 8 layers in the pig. The posterior layer is formed by basal cells which are columnar and closely packed. The middle layers are made up of "wing cells" which become increasingly flatter, thinner, and wider until the anterior layer is reached. The first few anterior layers consist of flat, overlapping squamous (scaly) cells.

Bowman's membrane[4] is 10 to 13 microns thick in man and not more than 2 microns thick in the pig. The anterior surface is smooth, but the posterior is rough due to projections from the membrane, called arcuate fibers, into the stroma. Pores in the membrane allow passage of nerve fibers from the

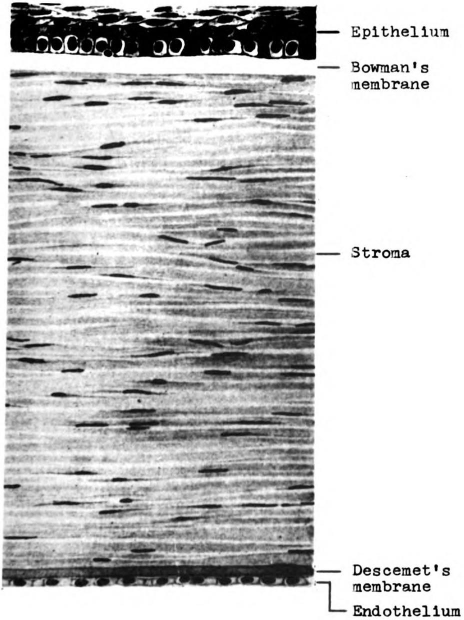

Figure I-2. Transverse Section of the Cornea

(Reproduced with permission from Ref. 2)

epithelium. Bowman's membrane is often referred to as a modified layer of the stroma due to its structural similarity.

Since the stroma makes up the majority of the corneal thickness, is structurally of primary interest, and has a complex structure, the description of this layer is presented in considerable detail. The stroma or "substantia propria" makes up about 90 per cent of the thickness of the cornea. The literature is rather inconsistent in the terminology used in describing its structure. Upon studying a number of the morphological descriptions based on conventional, polarized light, and electron microscopy, the following description seems to be representative.

The stroma of the cornea is composed of thin sheets of tissue called lamellae which are stacked one upon another to form a laminated structure composed of approximately two-hundred layers. Each lamella has a fibrous structure, and the elemental structural unit is the fibril, predominantly composed of collagen. The fibrils of a given lamella are parallel to one-another and to the surfaces of the sheet; however, the fibril directions of adjacent lamellae through the thickness of the stack are randomly oriented.[5,6] The fibrils may be assumed to run uninterruptedly from limbus-to-limbus.

The fibrils are known to have a circular cross-section of constant diameter along their length, varying between approximately 190 Å* and 340 Å,[3] and reportedly

---

* Å denotes the Angstrom unit of length. $(10)^{10}$ Å = 1 meter.

independent of age. The distance between adjacent fibrils is near the same order of magnitude as this diameter, and the thickness of a lamella may be taken as approximately two microns.

Isolated fibrils separated with a minimum of preparation are coated with a sheath of amorphous material that requires vigorous chemical or physical treatment for removal. Analysis of lamellar fragments indicates that the fibrils are embedded within this "ground substance" to the extent that their individual outlines are nearly indiscernible.[3]

The above description of the stroma, using two structural levels (fibril and lamella) and assuming the lamellae are continuous flat sheets stacked one-upon-another, simplifies the exact picture to some degree; but to the writer seems representative of the structure, and is concise and unambiguous.

Additional terms used in the literature are zone, fiber, and band. In accordance with the convention of Naylor,[5] a zone is simply the region of the stroma occupied by a given lamella. Following the recommendations of Naylor[5] and Maurice,[3] the term "fiber" is to be conveniently used to denote bundles of parallel fibrils of arbitrary size, one fiber always comprising the full thickness of a lamella. The term "band" is not as concisely defined. The lamellae, particularly near the anterior surface of the stroma, are not of a perfectly continuous nature in the direction perpendicular to the fibers, but are composed of several individual bands[3] (a band is at least three mm wide). The nature of the transition between bands is not well understood, and photomicrographs indicate that there is a localized

variation in fibril density, giving the impression that the lamella is composed of individual bands.

The above description of the structure of the stroma holds for all of the higher vertebrates, however there is some variation among the species, and the structure in mammals is said to lack this extreme regularity somewhat. An electron micrograph showing the lamellae and fibrils of a well-organized area of the stroma in man is shown in Figure I-3.

The next anatomical layer is Descemet's membrane. This membrane is a sheet which bounds the inner surface of the stroma, from which it is easily separated. The membrane is 5 to 10 microns thick in man, and 8 to 15 microns thick in the pig. Structurally, Descemet's membrane consists of a superposition of a large number of sheets of a meshwork which lie parallel to the surface.

The final (posterior) layer of the cornea is the endothelium. This is a single layer of flattened cells, having a thickness of approximately 4 or 5 microns in man and the pig.

Regarding overall dimensions of the cornea, for man[3] a mean value of the thickness at the central position is 0.55 mm. The radius of curvature of the anterior surface is 8.0 mm, and the corneal diameter (i.e. greatest chord) is 11 mm. For the pig[1], the central corneal thickness is given as slightly less than 1.0 mm. The radius of curvature of the anterior

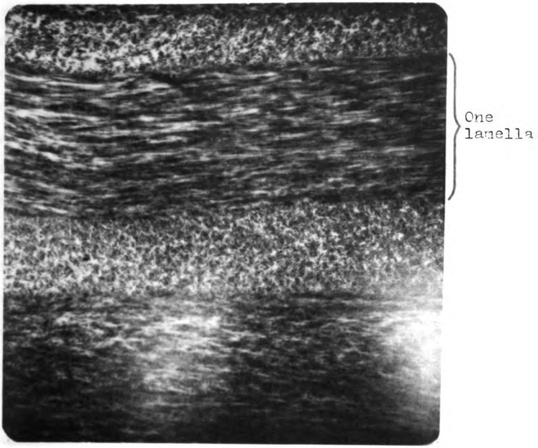

Figure I-3. Well-Organized Section of the Stroma in Man
(Reproduced with permission from Ref. 3)

surface is 10 to 11 mm, and the corneal diameter is 17 to 19 mm horizontally and 14 to 16.5 mm vertically (the pig limbus is somewhat pear-shaped).

Coulombre[7] indicates that since collagen has a high tensile strength, the stroma will determine the structural properties of the cornea, such as its response to mechanical distortion. The stroma is an unusual material from the standpoint of its shear rigidity. If a surface-parallel disc is cut from the laminated stroma and held between the thumb and index-finger, one can easily observe that over limited but quite large shear displacements the rigidity is quite small. According to Maurice (see Ref. 3) this is due to the properties of the matrix of ground substance in which the fibrils of the lamellae are embedded. He reports that it is impossible for the tensile force in a fibril to be dissipated into adjacent fibrils by means of shear stresses.

Since swelling of the excised cornea is a persistent problem, some comments on the hydration properties are in order. One may refer to pages 307 and 322 of Ref. 3 to obtain an introduction to this topic and a number of references to research papers. If the cornea were freely permeable to fluids, then one could expect considerable loss of aqueous humor due to diffusion through the stroma and evaporation at the anterior surface (tear evaporation is known to be of considerable magnitude); however this does not occur. The processes involved are currently not fully understood. Experiments have shown that the barriers to salt passage are the epithelium and endothelium, and that

substances which do not pass through the stroma have very large molecules (proteins and congo red are examples) or are insoluble in water.

The stroma of the in vitro or excised cornea has an affinity for water. When immersed in aqueous solutions it will absorb and hold water in large quantities. The hydration properties of excised pieces of cornea have been studied experimentally with the conclusion that the amount of swelling is not simply dependent on the osmotic pressure of the solution in which the specimen is immersed. The degree of swelling was found to be the same throughout a wide range of concentrations of glucose, urea, glycerine, and even distilled water. The cornea swells to the same extent in solutions of nonelectrolytes as in distilled water. In salt solutions, however, the amount and rate of swelling is dependent on the concentration.

It has been concluded that since the in vivo cornea is in a deturgesced state, that it contains less water than it is capable of imbibing, the hydration is controlled by some mechanism which draws water out. The hydration is maintained by a steady-state existing between water imbibed by the stroma and water removed by some other process (this is though to be associated with the endothelium). One can expect that any disruption of the normal in vivo state of the cornea will affect the steady-state situation; therefore it becomes important in removing a test specimen of corneal tissue from the eye to immerse it immediately in an appropriate liquid in order to mitigate swelling. Viability considerations[8] are of course important in the case of transplants; however since the collagen fibrils and ground-substance are not composed of living cells this is of secondary importance in tests regarding mechanical properties.

The normal corneal stroma consists of about 78 per cent water by weight[3], and the matrix of ground substance around the fibrils is known to be heavily hydrated; however evidence to date indicates that the fibrils themselves are essentially free of hydration since no change of diameter is observed upon desiccation.

CHAPTER II

PREVIOUS STUDIES OF CORNEAL ELASTICITY

A literature survey indicated that little quantitative information is available regarding the elastic properties of the cornea. There has apparently been no methodical theoretical and/or experimental treatment of the anisotropic elastic properties of the lamella.

Stanworth[9] made a brief study of the load-elongation properties of the cat cornea as part of his classical work dealing with corneal birefringence, and a treatise on the mechanical behavior of the cornea intact with the in vitro eyeball has been presented by Schwartz[10] which includes both theoretical and experimental aspects of the problem. Nyquist[6] has studied the viscoelastic properties of uniaxial tensile strips of cornea and concluded that the response of the cornea to an applied stress includes instantaneous and retarded (time dependent) elastic components.

Stanworth's work consisted of load-elongation measurements on the cat cornea with a constant loading rate of 125 grams per minute. The test specimens consisted of cleanly cut strips of cornea 1.5 mm wide with a small length of sclera remaining at each end. The specimens were obtained from fresh cat eyes by means of a double-blade knife. Artery forcepts were used to clamp to the sclera at each end of the test strip, and were fixed to two pillars, the distance between which could be altered by means of a screw arrangement. The distance between the tips of the forceps was used as a measure of the elongation, and was measured to 0.1 mm by means of a fine pointer moving over a scale observed through a magnifying glass. Loads were monitored by means of a recording device.[9]

A load-elongation curve is presented, and Stanworth points out that it approaches a straight line only for relatively large loads and elongations, and that for this range Young's modulus of elasticity is approximately 1800 gm/mm^2, or 2560 psi.

The research of Schwartz was confined to a study of the intact cornea with the intraocular pressure in force. Loads were applied to the anterior corneal surface through a small disc or indenter in a manner similar to that used in tonometry. A theoretical analysis is presented which includes the solution for the constraint of a thin, shallow, spherical shell (the cornea) by a flat plate. The experimental study investigated the rheology of the intact cornea with particular emphasis on its compliance with the requirements of the Boltzmann superposition principle. It is concluded that the corneas of the human and pig behave as linear viscoelastic solids.

Nyquist studied the stress-strain-time properties of the pig cornea, and tested long strips of stroma in tension. Stresses were applied using dead-weight loads, and the resulting strains at midlength of the strip (the central cornea) were recorded by means of photomicrography. Constant loads were suddenly applied, and the strains were measured as a function of time (creep test). Testing strips cut at various orientation angles (i.e. various rotations with respect to an axis normal to the plane of the surface of the cornea) indicated that the uniaxial tensile properties were independent of orientation, which supports theories of random orientation of the stromal fibrils.[5,6]

The response of the cornea to an applied stress includes instantaneous and retarded (time-dependent) elastic components. Figure II-1 shows typical results for a uniaxial tensile creep test (constant nominal stress suddenly applied), and Figure II-2 shows the instantaneous and steady-state stress-strain curves generated by conducting a series of creep tests. It can be seen from Figure II-2 that for the physiological range of stress (say less than 10.0 psi) the stress-strain relation may be approximated quite well by a straight line, whereas nonlinearity cannot be neglected over an extended range.

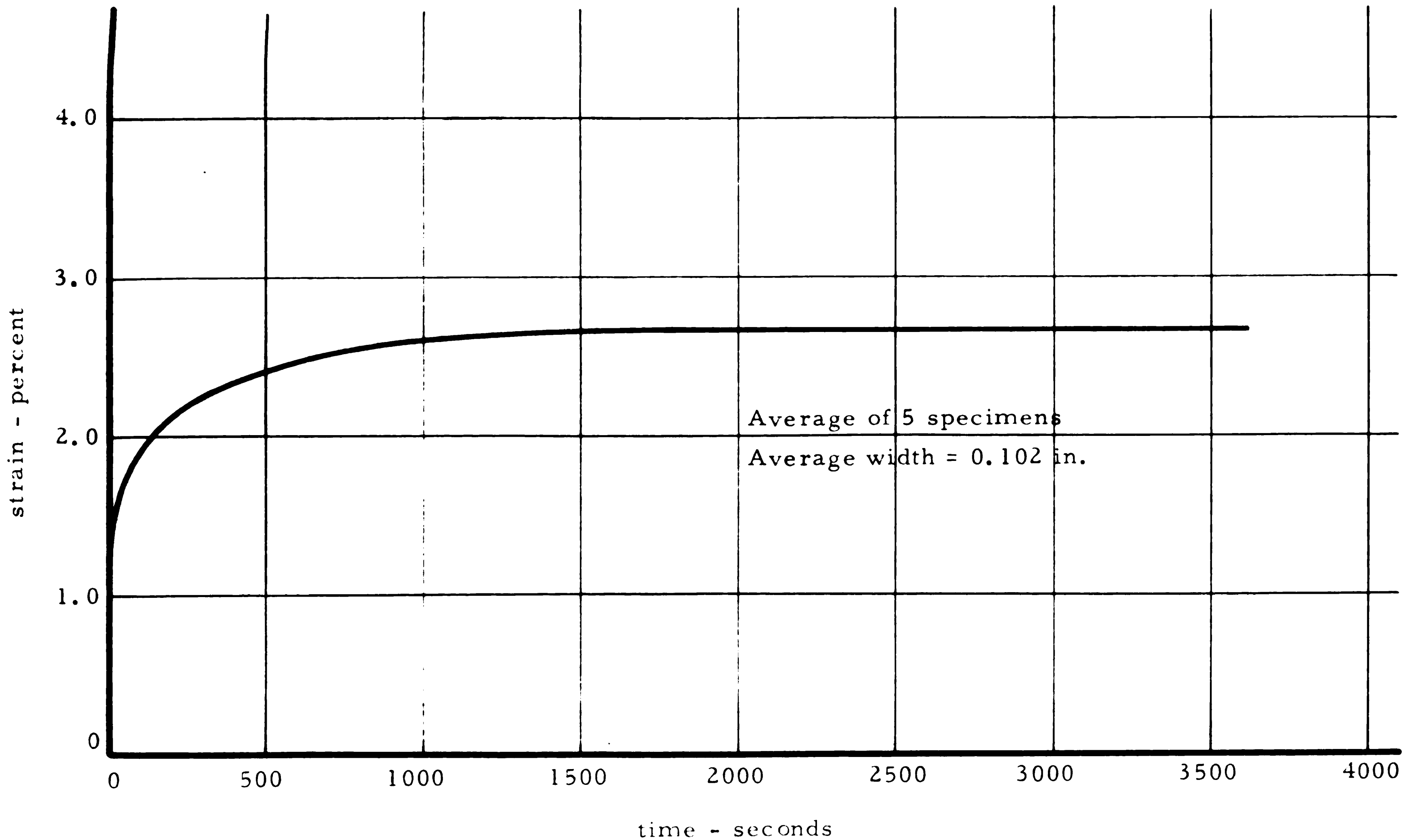

Figure II-1. Longitudinal Strain Versus Time For 0.08 lb. Tensile Load

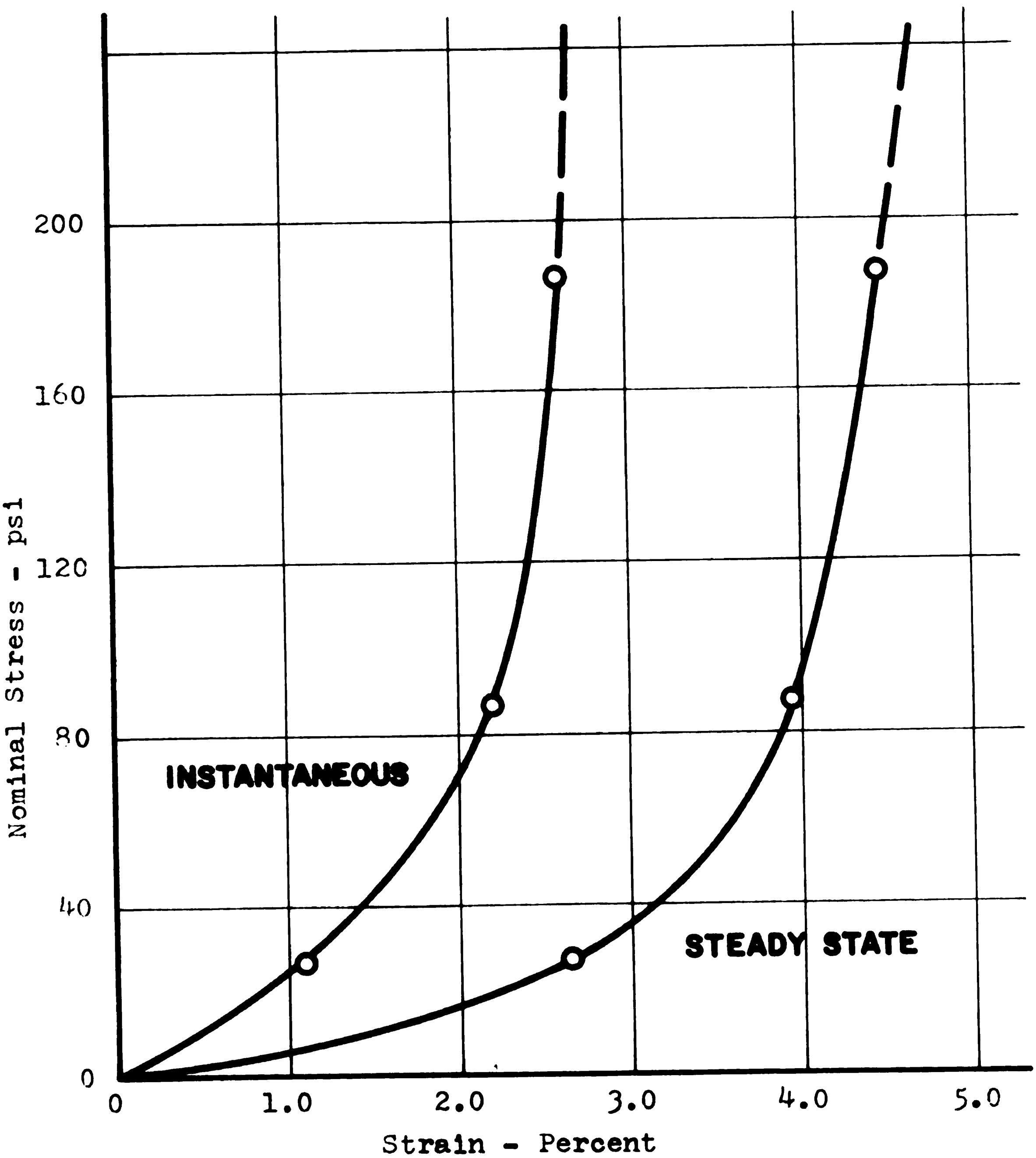

Figure II-2. Uniaxial Tensile Stress-Strain Curves

CHAPTER III

PRESSURE DISTRIBUTION OF THE INTRACORNEAL FLUID

Theoretical Considerations

The fluid pressure equilibrium within the cornea evaded understanding until quite recently, and some of the details are still unclear. Several research programs[11,12,13] since approximately 1940, culminating with the work of Hedbys, Mishima, and Maurice[14] in 1963 led to the currently accepted description of the fluid pressure phenomenon. A complete summary of the research would be lengthy, therefore only the results necessary for an understanding of the mechanism regulating pressure and swelling within the cornea will be considered. Some details must be added in order to present the Ophthalmologist's conceptually-correct descriptions in engineering terms (i.e. using a mathematical framework).

A number of variables must be defined, and fortunately, a fairly standard terminology has evolved. Pressures are reckoned from atmospheric (i.e. gage pressures), and a positive pressure implies a negative stress as usual. The variables are as follows:

Variable	Symbol
Fluid pressure	P_f
Imbibition pressure	P_i
Osmotic pressure	P_o
External pressure	P_e
Mechanical pressure	P_m
Swelling pressure	P_s
Tissue pressure	P_t

A "button" cut from the stroma (full thickness of the cornea, but with epithelium, endothelium, and Descemet's membrane removed) is shown schematically in Figures III-1(a) and III-1(b). The button may be assumed circular with a diameter d, and to have a thickness h normal to the plane of the cornea. In Figure III-1(a) only an external pressure P_e is acting, whereas in Figure III-1(b), in addition to the external pressure, there is a mechanical pressure P_m exerted by porous rigid plates. Details of the state of equilibrium across the (circumferential) side surface is not clearly understood, but this need not be considered if $d/h >> 1$, and only pressure equilibrium in the direction normal to the plate of the stroma is considered. Rigorous justification for this approach is lacking, but the success of the resulting analysis in explaining all experimentally observed phenomena is considered justification enough. Publications to date seem to have overlooked this matter entirely.

The fluid pressure P_f is the hydrostatic pressure of the aqueous solution within the stroma. It is the sum of two separate components; the osmotic pressure P_o caused by solute

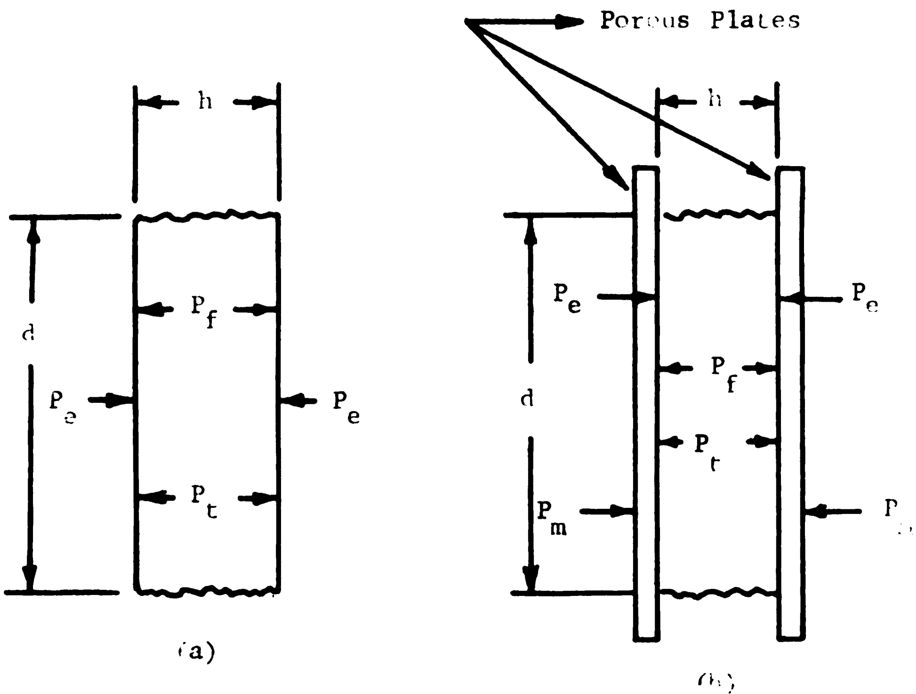

Figure III-1. Schematic Loading Diagrams of a Stromal Button molecules and ions (P_o includes the Donnan effect) in the tissue, and the imbibition pressure P_i which results from capillary action in the fibrous structure. P_i is a negative pressure (An analogous case which is easier to comprehend is the capillary rise of water in a glass tube, where the pressure just below the meniscus is negative). The fluid, osmotic, and imbibition pressures are related as follows:

$$P_f = P_o + P_i. \tag{3-1}$$

The lamellae of the stroma are normally compressed in the direction perpendicular to the plane of the surface, and the tissue pressure P_t is a measure of this compression. The release of this compression is the mechanism by which the stroma swells, and may be thought of as being analogous to the elongation of a compression-type spring as its load is decreased.

To properly analyze the system of pressures acting in the lamellae it is necessary to introduce the notion of porosity as used in the theory of elasticity of a porous solid.[15] At any given state of hydration of a lamella let the total (bulk) volume be denoted by V_b, and let the fluid volume (i.e. the pore volume) be denoted by V_p. Then the porosity f is defined by the ratio

$$f = V_p/V_b. \tag{3-2}$$

For a homogeneous anisotropic material (a lamella is considered macroscopically homogeneous) the porosity is also the ratio of the pore cross-sectional area to the bulk cross-sectional area of any plane section, regardless of its orientation.

The tissue pressure P_t is defined as the force per unit bulk cross-sectional area exerted by the tissue owing to its compressed state. In contrast, the fluid pressure P_f, osmotic pressure P_o, and imbibition pressure P_i are defined as forces exerted per unit cross-section of pore area. These values (P_f, P_o and P_i) must be multiplied by the porosity f if they are to be reckoned per unit bulk cross-sectional area. Hypothetical experimental pressure measurements (say with a small cannula and manometer) would yield values of P_f, P_o, and P_i, whereas in a procedure of adding or equating pressures from various sources one must use fP_f, fP_o, and fP_i. The factor f is only necessary when dealing with "intratissue" fluid pressures.

Suppose the stromal button of Figure III-1(a) is hydrated so as to have some thickness h, and is immersed in a non-imbibable medium at a positive hydrostatic (external) pressure P_e. Then normal-stress continuity at the boundary requires

$$P_e = fP_f + P_t, \tag{3-3}$$

and using eq. (3-1) this becomes

$$P_e = f(P_o + P_i) + P_t. \tag{3-4}$$

With reference to eq. (3-4), it is experimentally feasible to hold P_t and P_o constant while varying P_e and measuring P_i. It has been shown[16] that the thickness h of the excised cornea varies linearly with hydration (weight per unit dry weight), therefore if the state of hydration is fixed, the thickness remains constant. This in turn implies that the tissue pressure P_t remains constant. Since the osmotic pressure P_o is primarily a function of the tissue chemistry and microscopic geometry, it also can be assumed independent of P_e when h is fixed.

The above discussion indicates that when a non-imbibable immersion medium is used, P_i is linearly related to P_e through the constant f, and for incremental changes one can write

$$\Delta P_e = f \Delta P_i .$$

Letting the increments tend to zero, it becomes apparent that an alternate definition for the porosity f is

$$f = \left(\frac{\partial P_e}{\partial P_i}\right)_h \tag{3-5}$$

where the subscript h indicates that the derivative is evaluated for some constant hydration (thickness).

A similar analysis may be made in the case of Figure III-1(b), however the mechanical pressure P_m exerted by the porous plates must be taken into account. Continuity of the normal stress at the boundary between the plate and the tissue requires

$$f_1 P_e + P_m = f P_f + P_t \tag{3-6}$$

where f_1 is the porosity of the plate and P_m is reckoned per unit bulk area of the plate. Applying eq. (3-1), eq. (3-6) becomes

$$f_1 P_e + P_m = f(P_o + P_i) + P_t . \tag{3-7}$$

By definition the swelling pressure P_s is the equilibrium value of the mechanical pressure P_m. Thus from eq. (3-7),

$$P_s = f(P_o + P_i) + P_t - f_1 P_e. \tag{3-8}$$

A common test condition has been the case where P_e is zero and the immersion medium is imbibable. The pressure P_s required to maintain the plates at various distances h apart is measured, and the data are plotted in the form of a swelling pressure versus hydration curve. Such a curve is a measure of the relation

$$P_s = [f(P_o + P_i) + P_t] = g(h) \tag{3-9}$$

where g(h) is some function of the stromal thickness h and is dependent on the type of immersion medium used.

Now, analogous to the analyses of Figures III-1(a) and (b), consider the pressures acting on the cornea in situ, where the intraocular pressure is in force on the posterior surface and the anterior surface is at atmospheric (zero) pressure. The situation is shown schematically in Figure III-2 (curvature has been neglected for the moment). Let the intraocular pressure be denoted by P_a, the subscript "a" being associated with "anterior chamber."

In this case two different equations result when continuity of the normal stress is required at the two surfaces. Let subscripts A and P denote the anterior and posterior surfaces respectively. Then at the posterior surface

$$P_a = (fP_f + P_t)_P,$$

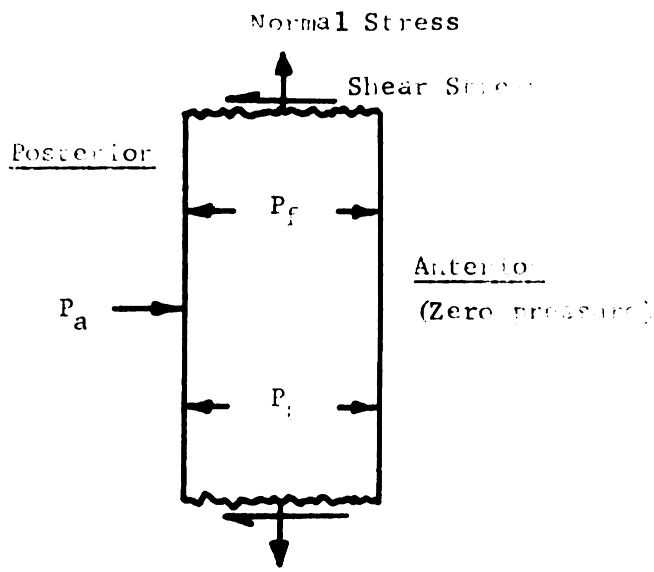

Figure III-2. Schematic Loading Diagram of the In Situ Cornea whereas at the anterior surface

$$0 = (fP_f + P_t)_A.$$

Eq. (3-1) is still applicable, therefore

$$\left.\begin{aligned} P_a &= f(P_o + P_i)_P + (P_t)_P \quad \text{(Posteriorally)} \\ 0 &= f(P_o + P_i)_A + (P_t)_A \quad \text{(Anteriorally)} \end{aligned}\right\} \qquad (3\text{-}10)$$

Maurice[17] has proposed a model which enables both of eqs. (3-10) to hold. This is reproduced in Figure III-3. Curvature of the cornea is taken into account, and the function of the limiting layers (epithelium and endothelium) becomes important. Maurice's variable S is the imbibition pressure P_i. He explains the model as follows:

> "The ground substance is shown enmeshing the collagen fibrils at the bottom right, but its expansile component is represented functionally, upper right, by compressed springs. The tension (T) of the individual fibrils creates a centrally directed pressure, rising cumulatively from the outside to the inside of the stroma, where it is balanced by the intraocular pressure. This would compress the ground substance unevenly across the thickness and cause a displacement of the majority of the fibrils towards the endothelial surface. The endothelial pump meachanism (P), however, maintains a suction (S) in the stromal tissue fluid. The suction acting on the epithelial and endothelial surfaces tend to establish a uniform compression of the ground substance across the thickness. This braces the fibrils apart, giving them a more equal distribution and leading to the formation of a regular lattice on which the transparency of the tissue depends. The compression of the ground substance is manifested as the swelling pressure, 60 mm. Hg, when fluid is allowed free access to the stroma."

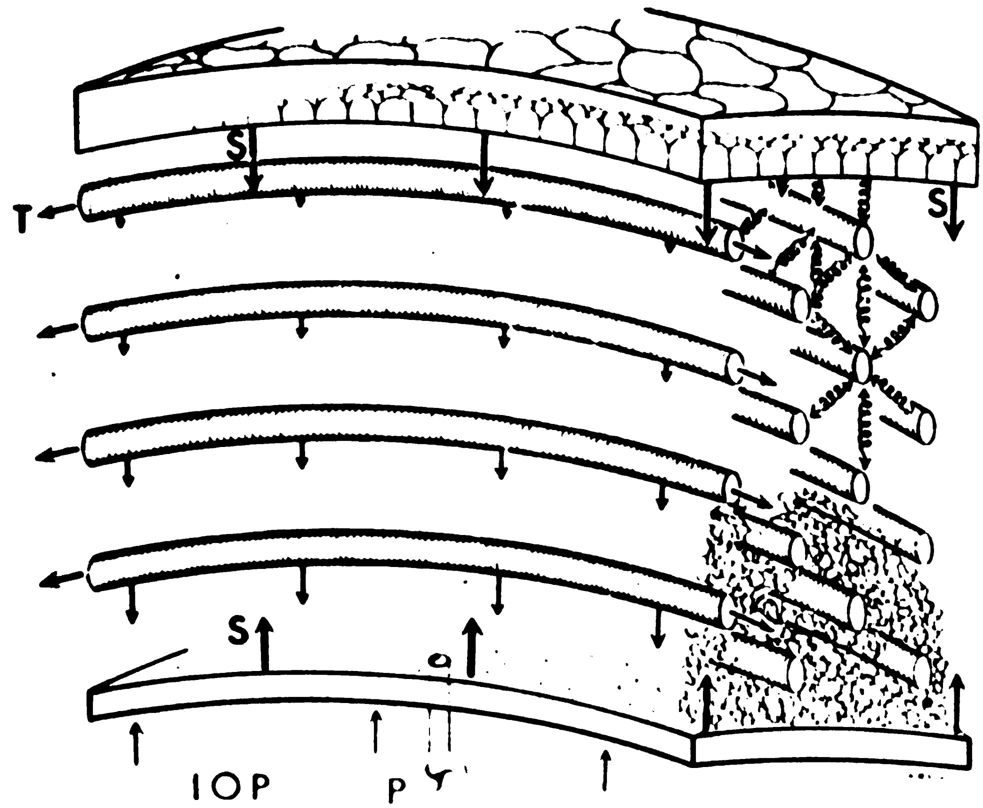

Figure III-3. Maurice's Proposed Scheme of Pressures Within the Cornea

(Reproduced with permission from Ref. 17)

Pressure Distribution Experiments

The most common type of experiment has been the measurement of swelling pressure as a function of hydration,[11,12,13] the general scheme of Figure III-1(b) being used and eq. (3-9) being applicable. Swelling pressure versus hydration curves are, however, not of great use in validating the theory presented in the previous pages. More pertinent information in this respect is given by the work of Hedbys et al[14] where intra-tissue measurements of the imbibition pressure P_i were made, both in vitro (steer cornea) and in vivo (rabbit cornea) using a cannula and pressure transducer with pen-recorder output. In vitro tests were performed under conditions for which eq. (3-4) is applicable, and P_e was zero. P_i was recorded as a function of thickness h and the thickness measurements were converted to hydrations using a steer eye thickness versus hydration curve previously established.[13] It was found that this data gave the same curve as obtained when plotting the negative of the swelling pressure P_s as a function of hydration, conditions being those under which eq. (3-9) is applicable. This correlation is shown in Figure III-4. In short, this can be summarized by saying that for equal hydrations

$$P_i\Big|_{\substack{\text{nonimbibile}\\ \text{fluid}}} \approx -P_s\Big|_{\substack{\text{imbibible}\\ \text{fluid}}} . \qquad (3\text{-}11)$$

In vitro tests were also performed which may be analyzed using Figure III-1(b) and eq. (3-8). In place of the porous plates shown in the figure, a glass plate was used

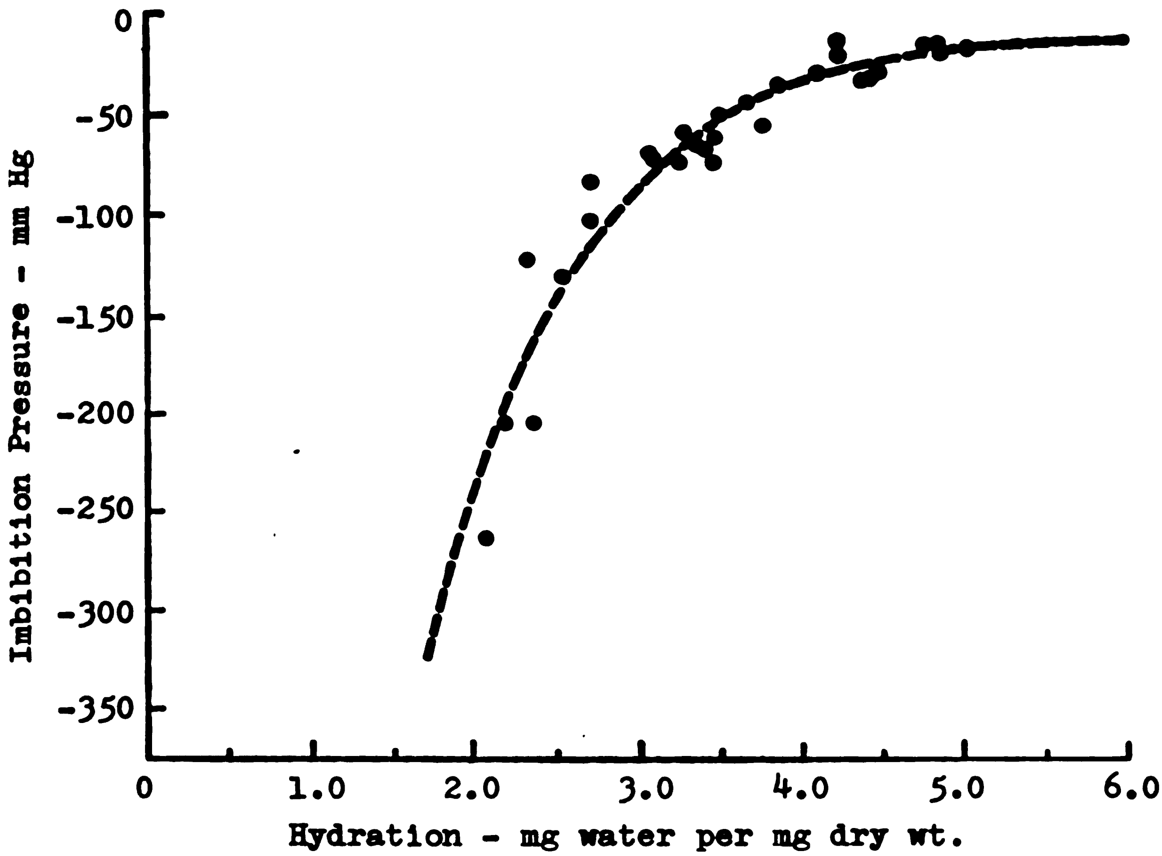

"Variation of imbibition pressure with hydration of excised stroma. Each point represents one equilibrium value. The curve shows the relationship of swelling pressure to hydration (Hedbys and Dohlman, 1963)."

Figure III-4. Correlation Between Imbibition Pressure and Swelling Pressure as a Function of Hydration

(Reproduced with permission from Ref. 14)

on one side, and a pressurized rubber balloon on the other side. The stroma was compressed by increasing the pressure in the balloon. The glass and rubber may be assumed nonporous, therefore f_1 is zero in eq. (3-8), and the swelling pressure P_s may be taken equal to the balloon pressure (P_b). Eq. (3-8) becomes

$$P_b \equiv P_s = f(P_o + P_i) + P_t. \tag{3-12}$$

P_i was measured using a cannula and pressure transducer, and it was found that increments in P_b and $-P_i$ were nearly equal (for a positive increment of P_b the magnitude of the negative imbibition pressure P_i decreased). The correlation diminished as P_b increased, the magnitude of ΔP_i being smaller than those of ΔP_b.

Complete information for analyzing this test is lacking. No data has been presented regarding the thickness (hydration) variation with P_b; therefore, with reference to eq. (3-12), it is not known to what extent P_t varied during the test. It is reasonable to assume that f and P_o are constant with respect to small fluctuations in P_b, therefore from eq. (3-12) one can write

$$\Delta P_b = f\Delta P_i + \Delta P_t. \tag{3-13}$$

The thickness must have decreased somewhat as P_b increased, and therefore some positive value of ΔP_t was present in eq. (3-13), which may be written as

$$\Delta P_i = \frac{1}{f}(\Delta P_b - \Delta P_t). \tag{3-14}$$

It was pointed out at the end of Chapter I that about 78 per cent, by weight, of the corneal stroma is water. In addition, it is easily observed that stromal specimens are heavier than water, therefore the per cent of water by volume is greater than 78 per cent. This implies that the factor $(1/f)$ in eq. (3-14) is of the order of unity and therefore indicates that values of ΔP_i smaller than ΔP_b, as observed, are in fact fully justified, since it is likely that ΔP_t was not negligibly small.

Measurements of the imbibition pressure in vivo in the rabbit cornea[14] showed the same general trends as the tests in vitro. The magnitude of the imbibition pressure in vivo was found to be less than that in vitro, at the same hydration, by an amount comparable to the magnitude of the intraocular pressure. Assuming that f and P_o remain constant for small changes in the intraocular pressure P_a, eqs. (3-10) give

$$\Delta P_a = f(\Delta P_i)_P + (\Delta P_t)_P \quad \text{(Posteriorally)}$$

$$(\Delta P_t)_A = -f(\Delta P_i)_A \qquad \text{(Anteriorally).}$$

Recalling that f is nearly unity, it becomes apparent that the observed correlation between ΔP_a and ΔP_i implies that as P_a is increased, P_t near the posterior surface remains nearly constant whereas near the anterior surface P_t decreases.

In all cases, both in vivo and in vitro, it was found that the imbibition pressure did not vary with position in the stroma, either in the anterior-posterior direction or with distance from the limbus. The research showed that the stroma exerts its full tendency to swell under normal (in vivo) physiological conditions and that the reason swelling does not take place as a result of slow absorption of the aqueous humor is due to an active transport mechanism continuously "pumping down" the stroma. This mechanism is thought to be located in the endothelium (see Ref. 3, p. 334).

CHAPTER IV

THE STRESS-STRAIN CONSTITUTIVE RELATION FOR A SINGLE LAMELLA

Introduction

In order to obtain relations between the components of stress and strain in a lamella it is necessary to formulate a mathematical model which describes the material. The previous chapters make it clear that the lamella is not a simple elastic continuum. It may be treated as a mixed-media problem; more specifically, as a binary mixture composed of a porous elastic solid (or "elastic framework") containing an incompressible viscous fluid. This is a special case of the same problem with a compressible fluid, and Biot[15] has generalized the classical theory of elasticity to cover such a material.

Formulation of General Anisotropic Equations

Consider an elastic framework with a random distribution of interconnected pores. Let the porosity f be defined as in the previous chapter; that is

$$f = \frac{V_p}{V_b} = \frac{A_p}{A_b} \tag{4-1}$$

where V_p and A_p are the volume and cross-sectional area of pores contained in a sample of bulk volume V_b and bulk cross-sectional area A_b (For a macroscopically homogeneous anisotropic material f is independent of location and cross-section orientation).

Consider a unit cube (i.e. having edge lengths of unity and consequently face areas of unity) of the bulk material having edges parallel to orthogonal rectangular cartesian reference axes x_1, x_2, and x_3. Let σ represent the normal tensile force on each face of the cube due to the stress in the fluid. Then if p is the hydrostatic pressure of the fluid one can write

$$\sigma = -fp. \tag{4-2}$$

In a similar manner let σ_{ij} denote the forces applied to the solid part of the cube faces where, in the usual manner, subscripts i and j corresponding to x_i and x_j denote the directions of the normal to the cube face, and the line-of-action of the force respectively $(i,j = 1,2,3)$. No couple stresses are considered, therefore $\sigma_{ij} = \sigma_{ji}$, and the total stresses τ_{ij} are components of a symmetric second-order tensor as follows:

$$\tau_{ij} = \begin{bmatrix} (\sigma_{11}+\sigma) & \sigma_{12} & \sigma_{13} \\ \sigma_{12} & (\sigma_{22}+\sigma) & \sigma_{23} \\ \sigma_{13} & \sigma_{23} & (\sigma_{33}+\sigma) \end{bmatrix}.$$

Let displacements of the solid and the fluid in the directions (x_1,x_2,x_3) be denoted by (u_1,u_2,u_3) and (v_1,v_2,v_3) respectively. Assuming small displacement gradients, the solid strains e_{ij} and fluid strains ϵ_{ij} are defined by the relations

$$\left.\begin{aligned} e_{ij} &= \frac{1}{2}\left(\frac{\partial u_i}{\partial x_j} + \frac{\partial u_j}{\partial x_i}\right) \\ \epsilon_{ij} &= \frac{1}{2}\left(\frac{\partial v_i}{\partial x_j} + \frac{\partial v_j}{\partial x_i}\right) . \end{aligned}\right\} \qquad (4\text{-}3)$$

In each case the strains are components of a symmetric second-order tensor.

The constitutive equations relating the above stresses and strains may be established by generalizing the procedure used in classical elasticity. Let it be assumed that the deformations are completely reversible and that an elastic potential, or strain-energy function V exists such that

$$\left.\begin{aligned} \sigma_{ij} &= \frac{\partial V}{\partial e_{ij}} \\ \sigma &= \frac{\partial V}{\partial \epsilon} \end{aligned}\right\} \qquad (4\text{-}4)$$

where

$$\epsilon = \epsilon_{11} + \epsilon_{22} + \epsilon_{33}.$$

Such a material is said to be "hyperelastic". It is further assumed that the seven stress components (σ_{ij} and σ) are linear functions of the seven strain components (e_{ij} and ϵ); therefore the elastic potential V is a quadratic function of the strains.

Let the following stress and strain notation be used for convenience:

$$\sigma_1 = \sigma_{11} \qquad e_1 = e_{11}$$
$$\sigma_2 = \sigma_{22} \qquad e_2 = e_{22}$$
$$\sigma_3 = \sigma_{33} \qquad e_3 = e_{33}$$
$$\sigma_4 = \sigma_{23} \qquad e_4 = e_{23}$$
$$\sigma_5 = \sigma_{13} \qquad e_5 = e_{13}$$
$$\sigma_6 = \sigma_{12} \qquad e_6 = e_{12}$$
$$\sigma_7 = \sigma \qquad e_7 = \epsilon .$$

Then the quadratic elastic potential V has the general form

$$V = C_o + C_j e_j + C'_{k\ell} e_k e_\ell \quad (j,k,\ell = 1,2,\ldots,7)$$

where the C's are material constants. Expanding the right hand side of this equation and defining

$$C_{k\ell} = C'_{k\ell} + C'_{\ell k}$$

yields

$$\begin{aligned} V = C_o &+ C_1 e_1 + \cdots + C_7 e_7 + \frac{1}{2} C_{11} e_1^2 + \cdots + \frac{1}{2} C_{77} e_7^2 \\ &+ C_{12} e_1 e_2 + \cdots + C_{17} e_1 e_7 \\ &+ C_{23} e_2 e_3 + \cdots + C_{27} e_2 e_7 \\ &+ C_{34} e_3 e_4 + \cdots + C_{37} e_3 e_7 \\ &+ C_{45} e_4 e_5 + \cdots + C_{47} e_4 e_7 \\ &+ C_{56} e_5 e_6 + C_{57} e_5 e_7 \\ &+ C_{67} e_6 e_7 . \end{aligned} \tag{4-5}$$

Insertion of eq. (4-5) into (4-4) gives

$$\begin{bmatrix}\sigma_1\\ \sigma_2\\ \sigma_3\\ \sigma_4\\ \sigma_5\\ \sigma_6\\ \sigma_7\end{bmatrix} = \begin{bmatrix}C_1\\ C_2\\ C_3\\ C_4\\ C_5\\ C_6\\ C_7\end{bmatrix} + \begin{bmatrix}C_{11} & C_{12} & C_{13} & C_{14} & C_{15} & C_{16} & C_{17}\\ C_{12} & & & & & & \vdots\\ C_{13} & & & & & & \\ C_{14} & & & \text{(symmetric)} & & & \\ C_{15} & & & & & & \\ C_{16} & & & & & & \vdots\\ C_{17} & \cdots & & & & \cdots & C_{77}\end{bmatrix} \begin{bmatrix}e_1\\ e_2\\ e_3\\ e_4\\ e_5\\ e_6\\ e_7\end{bmatrix} . \quad (4\text{-}6)$$

This is the most general form of the stress-strain constitutive relation. It differs from that given by Biot in that the constants C_1 through C_7 have been retained. This retention allows a reference configuration $(e_i = 0)$ where the stresses are not identically zero (Additional comments will be made in the following section).

The total stresses τ_{ij} $\left(\tau_{ij} = \sigma_{ij} + \sigma\delta_{ij};\ \delta_{ij} = \begin{cases}1 \text{ for } i = j\\ 0 \text{ for } i \neq j\end{cases}\right)$ of the bulk material satisfy the equilibrium equations

$$\frac{\partial}{\partial x_j}(\sigma_{ij} + \sigma\delta_{ij}) + \rho X_i = 0 \qquad (4\text{-}7)$$

where ρ is the mass density of the bulk material and X_i is the body force per unit mass in the positive x_i-direction. Biot goes on to show that substituting the displacement gradients of eqs. (4-3) for the strains in the constitutive relation (4-6), and using the result to eliminate the stresses from the equilibrium equations (7), gives three equations in the six displacements u_i and v_i. He introduces a generalized form of Darcy's law to describe the flow of fluid in a porous material and obtains an additional three equations in the displacements

u_i and v_i (time derivatives are involved). There is, however, no need to work with the resulting set of six simultaneous partial differential equations in this Thesis.

Specialization of the General Equations to the Lamella

The general applicability of the formulation presented in the previous section was discussed in the Introduction of this Chapter. Some correlation of the variables with those of Chapter III, and additional specialization of the stress-strain relation of eq. (4-6) must be considered. The use of a linear constitutive equation also must be justified.

Figure II-2 indicates that the uniaxial tensile stress-strain relation of the corneal tissue is inherently nonlinear. For the restricted range of stress resulting from the intraocular pressure (say up to 10 psi) the Figure tends to indicate that linearity is a good approximation. It is reasonable to generalize this indication and state that linearity may be assumed regardless of the state of stress as long as the stresses are restricted to be within the physiological range (i.e. stresses caused by intraocular pressure). The correctness of this linearity assumption will be established later in the analysis and discussion of experimental data from fresh tissue experiments.

By restricting the applicability of the proposed constitutive equation to steady-state conditions and dealing with only the quasi-elastostatic properties of the tissue, the viscoelastic effects (see Figure II-1) can be eliminated from the analysis. The viscoelastic properties of the cornea resemble those of a Voigt-element (spring and dashpot in parallel combination). For a given applied load the final elongation of a Voigt-element (after a large interval of time) is not dependent on the presence of the dashpot; that is, the spring-dashpot combination and thé spring alone have identical quasi-elastostatic properties.

With regard to correlation of variables between Chapters III and IV, the porosity f was defined in the same manner in both chapters, and the hydrostatic pressure p of this Chapter may be associated with the fluid pressure P_f, in the stroma, defined in Chapter III. Thus from eqs. (3-1) and (4-2) one can write

$$\sigma = -fp = -fP_f = -f(P_o + P_i) \tag{4-8}$$

where P_o and P_i are the osmotic and imbibition pressures respectively. The elastic solid stresses σ_{ij} may be associated with the tissue stresses of the lamella; that is, the forces on the faces of a unit cube of lamella caused by the stresses in the elastic solid part of the binary mixture. The component of the tissue stress normal to the face of a lamella is the negative of the tissue pressure P_t defined in Chapter III.

The discussion in the previous chapter leads one to assume that the fluid pressure P_f, as a first-order approximation, is independent of the state of <u>tissue</u> strain $(e_1,\dots,e_6)$.

This assumption is based on the notions that the osmotic pressure P_o depends on the solute molecules and ions in the tissue, and the imbibition pressure P_i, induced through capillary action, depends on the gross geometrical structure and material constitution. One can expect that none of these will change significantly with (small) strain.

Recalling that $\sigma_7 = \sigma$ and using eq. (4-8), the independence of P_f with respect to tissue strain implies that in eq. (4-6)

$$C_{17} = C_{27} = \cdots = C_{67} = 0$$

and thus

$$-fP_f = C_7 + C_{77}e_7$$

from which

$$P_f = -\frac{1}{f}(C_7 + C_{77}\varepsilon). \tag{4-9}$$

The variables P_f and ε, however, are directly related through the elastic bulk modulus K of the fluid by the relation

$$P_f = -K\varepsilon.$$

Comparing this equation to eq. (4-9) shows that $C_7 = 0$ and $C_{77} = fK$. Thus the constitutive equation (4-6) may be written as

$$\sigma = fK\varepsilon \tag{4-10}$$

and

$$\begin{bmatrix}\sigma_1\\ \sigma_2\\ \sigma_3\\ \sigma_4\\ \sigma_5\\ \sigma_6\end{bmatrix} = \begin{bmatrix}C_1\\ C_2\\ C_3\\ C_4\\ C_5\\ C_6\end{bmatrix} + \begin{bmatrix}C_{11} & C_{12} & C_{13} & C_{14} & C_{15} & C_{16}\\ C_{12} & & & & & \vdots\\ C_{13} & & & & & \\ C_{14} & & & & & \\ C_{15} & & & & & \vdots\\ C_{16} & \cdots & & & \cdots & C_{66}\end{bmatrix} \begin{bmatrix}e_1\\ e_2\\ e_3\\ e_4\\ e_5\\ e_6\end{bmatrix} .$$

Let the double-subscript indicial notation for the total stresses τ_{ij} given by the matrix on page 39 be changed, for convenience, to a single subscript using the same convention as in the σ_{ij}-to-σ_i conversion on page 41; then

$$\begin{bmatrix}\tau_1\\ \tau_2\\ \tau_3\\ \tau_4\\ \tau_5\\ \tau_6\end{bmatrix} = \begin{bmatrix}C_1-fP_f\\ C_2-fP_f\\ C_3-fP_f\\ C_4\\ C_5\\ C_6\end{bmatrix} + \begin{bmatrix}C_{11} & C_{12} & C_{13} & C_{14} & C_{15} & C_{16}\\ C_{12} & & & & & \vdots\\ C_{13} & & & & & \\ C_{14} & & & & & \\ C_{15} & & & & & \vdots\\ C_{16} & \cdots & & & \cdots & C_{66}\end{bmatrix} \begin{bmatrix}e_1\\ e_2\\ e_3\\ e_4\\ e_5\\ e_6\end{bmatrix} . \qquad (4\text{-}11)$$

In the Introduction to this Thesis it was pointed out that this research is linked to the glaucoma problem, where the increased intraocular pressure causes above-normal stresses in the cornea. Let it be required that the constitutive equation be applicable only for the range of stresses and strains associated with the physiologically normal, and elevated intraocular pressures; then the material behavior outside this range need not be considered. Since eq. (4-11) is linear, the superposition principle is applicable, and one can deal with the problem by reckoning the stresses and strains from the normal condition (i.e., $\tau_i = 0 = e_i$ at the normal intraocular pressure).

Let the normal fluid pressure P_f be denoted by P_{fo}; then in order for the τ_i and e_i to be zero simultaneously eq. (4-11) requires that

$$C_1 = C_2 = C_3 = fP_{fo}$$

and

$$C_4 = C_5 = C_6 = 0,$$

and the constitutive equation reduces to

$$\begin{bmatrix} \tau_1 \\ \tau_2 \\ \tau_3 \\ \tau_4 \\ \tau_5 \\ \tau_6 \end{bmatrix} = \begin{bmatrix} C_{11} & C_{12} & C_{13} & C_{14} & C_{15} & C_{16} \\ C_{12} & & & & & \vdots \\ C_{13} & & & & & \\ C_{14} & & & & & \\ C_{15} & & & & & \vdots \\ C_{16} & \cdots & & & \cdots & C_{66} \end{bmatrix} \begin{bmatrix} e_1 \\ e_2 \\ e_3 \\ e_4 \\ e_5 \\ e_6 \end{bmatrix} . \qquad (4\text{-}12)$$

Equation (4-12) may be simplified further using symmetry arguments. Consider the geometric symmetry of the lamella. The anatomy discussion of Chapter I showed that a lamella is a sheet made up of parallel fibrils in an amorphous matrix. The fibrils are parallel to the surfaces of the sheet, and the sheet thickness is large compared to the diameter of an individual fibril; also, the fibril spacing is near the same order of magnitude as the diameter. Although some tests have given vague indications of regularity of the fibril array (see Ref. 3, pp. 320-322) there seems to be no strong evidence that the parallel fibrils are not randomly disposed, therefore random disposition will be assumed in the following analysis.

The literature on the theory of fiber-reinforced composites (see, for example, Refs. 18 thru 21) shows that in a macroscopic sense the material may be treated as homogeneous and anisotropic, and further that geometric symmetry implies elastic symmetry.

Let rectangular orthogonal cartesian reference axes (x_1,x_2,x_3) be defined for a given lamella such that the x_1-axis is parallel to the fibril axis and the x_3-axis is normal to the plane of the lamella, having positive sense in the anterior direction. Then the x_2-axis is also in the plane of the lamella, and is normal to the fibrils. An element of a lamella is shown in Figure VI-1. It is apparent that the coordinate planes are planes of symmetry, and the x_1-axis is an axis of rotational symmetry.

The reduction of the number of independent constants in the elastic constant matrix of eq. (4-12), using symmetry arguments, proceeds as follows. First consider the $x_2 - x_3$ plane of symmetry. Define a new set of axes $(\bar{x}_1,\bar{x}_2,\bar{x}_3)$ by simply taking the $\bar{x}_1$-axis in the negative x_1-direction, the other axes remaining unchanged. Therefore

$$\bar{\tau}_{13} = -\tau_{13} \quad \text{and} \quad \bar{\tau}_{12} = -\tau_{12}.$$

That is,

$$\bar{\tau}_5 = -\tau_5 \quad \text{and} \quad \bar{\tau}_6 = -\tau_6$$

and similarly

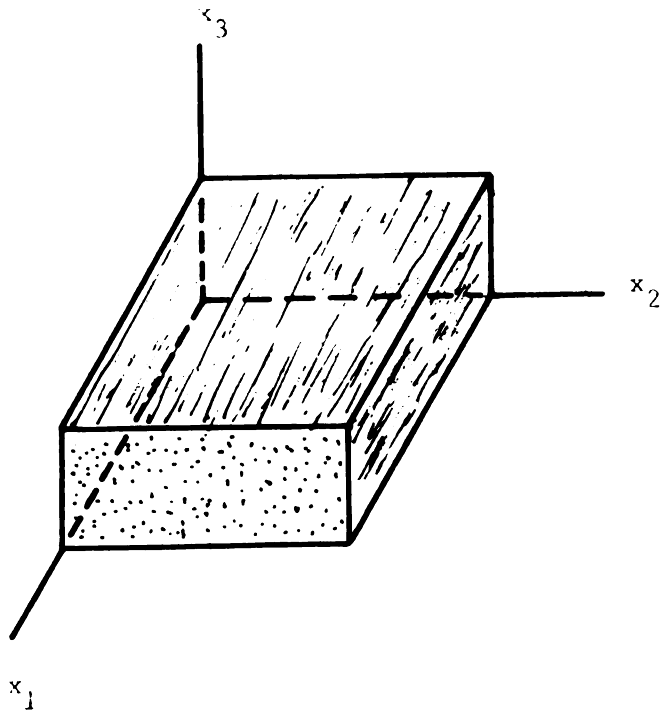

Figure IV-1. An Element of a Lamella

$$\bar{e}_5 = -e_5 \quad \text{and} \quad \bar{e}_6 = -e_6.$$

All other stresses and strains remained unchanged. Since the stress-strain constitutive law must hold for both coordinate systems, from eq. (4-12) one can write

$$\tau_5 = C_{15}e_1 + C_{25}e_2 + C_{35}e_3 + C_{45}e_4 + C_{55}e_5 + C_{56}e_6$$

and

$$-\tau_5 = C_{15}e_1 + C_{25}e_2 + C_{35}e_3 + C_{45}e_4 - C_{55}e_5 - C_{56}e_6.$$

Subtract the latter equation from the former to get

$$2\tau_5 = 2C_{55}e_5 + 2C_{56}e_6$$

for arbitrary values of e_1 through e_4. This requires that

$$C_{15} = C_{25} = C_{35} = C_{45} = 0.$$

Using exactly the same procedure with the two expressions for τ_6 shows that

$$C_{16} = C_{26} = C_{36} = C_{46} = 0.$$

Therefore the symmetric matrix of elastic constants reduces to

$$\begin{bmatrix} C_{11} & C_{12} & C_{13} & C_{14} & 0 & 0 \\ C_{12} & C_{22} & C_{23} & C_{24} & 0 & 0 \\ C_{13} & C_{23} & C_{33} & C_{34} & 0 & 0 \\ C_{14} & C_{24} & C_{34} & C_{44} & 0 & 0 \\ 0 & 0 & 0 & 0 & C_{55} & C_{56} \\ 0 & 0 & 0 & 0 & C_{56} & C_{66} \end{bmatrix}$$

which has 13 independent elements.

Now consider the $x_1 - x_3$ plane of symmetry. Define new axes $(\bar{x}_1, \bar{x}_2, \bar{x}_3)$ by taking the $\bar{x}_2$-axis in the negative

x_2-direction, the other axes remaining unchanged. Then

$$\bar{\tau}_{23} = -\tau_{23} \quad \text{and} \quad \bar{\tau}_{12} = -\tau_{12}.$$

That is,

$$\bar{\tau}_4 = -\tau_4 \quad \text{and} \quad \bar{\tau}_6 = -\tau_6$$

and similarly

$$\bar{e}_4 = -e_4 \quad \text{and} \quad \bar{e}_6 = -e_6.$$

All other stresses and strains remain unchanged. The symmetry conditions have already been imposed on $\bar{\tau}_6$ and $\bar{e}_6$, but using the previously established procedure on $\bar{\tau}_4$ and $\bar{e}_4$ shows that

$$C_{14} = C_{24} = C_{34} = C_{45} = 0$$

and the symmetric matrix of elastic constants is further reduced to

$$\begin{bmatrix} C_{11} & C_{12} & C_{13} & 0 & 0 & 0 \\ C_{12} & C_{22} & C_{23} & 0 & 0 & 0 \\ C_{13} & C_{23} & C_{33} & 0 & 0 & 0 \\ 0 & 0 & 0 & C_{44} & 0 & 0 \\ 0 & 0 & 0 & 0 & C_{55} & 0 \\ 0 & 0 & 0 & 0 & 0 & C_{66} \end{bmatrix}$$

which has 9 independent elements.

Following the above procedure using the $x_1 - x_2$ plane of symmetry gives no further reduction of constants; however a rotation of 90 degrees about the x_1-axis gives an additional simplification. The 90 degree rotation places the

$\bar{x}_2$-axis along the positive x_3-axis and the $\bar{x}_3$-axis along the negative x_2-axis. Then

$$\bar{\tau}_{22} = \tau_{33} \qquad \bar{\tau}_{12} = \tau_{13}$$
$$\bar{\tau}_{33} = \tau_{22} \qquad \bar{\tau}_{13} = -\tau_{12}$$
$$\bar{\tau}_{23} = -\tau_{23} \ .$$

That is,

$$\bar{\tau}_{2} = \tau_{3} \qquad \bar{\tau}_{6} = \tau_{5}$$
$$\bar{\tau}_{3} = \tau_{2} \qquad \bar{\tau}_{5} = -\tau_{6}$$
$$\bar{\tau}_{4} = -\tau_{4}$$

and similarly

$$\bar{e}_{2} = e_{3} \qquad \bar{e}_{6} = e_{5}$$
$$\bar{e}_{3} = e_{2} \qquad \bar{e}_{5} = -e_{6}$$
$$\bar{e}_{4} = -e_{4} \ .$$

All other stresses and strains remain unchanged. Comparing corresponding expressions for each stress component expressed in the two coordinate systems and simplifying using the above expressions, shows that

$$C_{22} = C_{33}$$
$$C_{12} = C_{13}$$
$$C_{55} = C_{66}$$

and the elastic constant matrix has only six independent elements as follows:

$$\begin{bmatrix} C_{11} & C_{12} & C_{12} & 0 & 0 & 0 \\ C_{12} & C_{22} & C_{23} & 0 & 0 & 0 \\ C_{12} & C_{23} & C_{22} & 0 & 0 & 0 \\ 0 & 0 & 0 & C_{44} & 0 & 0 \\ 0 & 0 & 0 & 0 & C_{55} & 0 \\ 0 & 0 & 0 & 0 & 0 & C_{55} \end{bmatrix} .$$

The final reduction of constants comes from considering an arbitrary rotation about the x_1-axis. Let the angle of rotation be α and define the direction cosine a_{ij} as the cosine of the angle between the positive $\bar{x}_i$ and x_j axes. Then

$$\left.\begin{array}{lll} a_{11} = 1 & a_{21} = 0 & a_{31} = 0 \\ a_{12} = 0 & a_{22} = \cos\alpha & a_{32} = -\sin\alpha \\ a_{13} = 0 & a_{23} = \sin\alpha & a_{33} = \cos\alpha\,. \end{array}\right\} \tag{4-13}$$

The stresses and strains in the rotated coordinate system may be found by using the transformation equation for a second-order tensor; that is

$$\left.\begin{array}{l} \bar{\tau}_{ij} = a_{ik}a_{j\ell}\tau_{k\ell} \\ \bar{e}_{ij} = a_{ik}a_{j\ell}e_{k\ell}\,. \end{array}\right\} \tag{4-14}$$

Expanding eqs. (4-14) and applying eqs. (4-13) yields the following expressions:

$$\left.\begin{array}{l} \bar{\tau}_{11} = \tau_{11} \\ \bar{\tau}_{12} = \tau_{12}\cos\alpha + \tau_{13}\sin\alpha \\ \bar{\tau}_{13} = \tau_{13}\cos\alpha - \tau_{12}\sin\alpha \\ \bar{\tau}_{22} = \tau_{22}\cos^2\alpha + \tau_{33}\sin^2\alpha + 2\tau_{23}\sin\alpha\cos\alpha \\ \bar{\tau}_{23} = \tau_{23}(\cos^2\alpha - \sin^2\alpha) + (\tau_{33} - \tau_{22})\sin\alpha\cos\alpha \\ \bar{\tau}_{33} = \tau_{22}\sin^2\alpha + \tau_{33}\cos^2\alpha - 2\tau_{23}\sin\alpha\cos\alpha\,. \end{array}\right\} \tag{4-15}$$

The strains in the rotated coordinate system are found simply by replacing the stresses in the above equations by their corresponding strains. Converting the stresses and strains to single-subscripted variables using the relations on page 41, and writing the expressions for the stresses in terms of strains in both the original and the rotated coordinates, it can be shown after applying eqs. (4-15) that in order for the constitutive equation to hold in both coordinate systems it is necessary that

$$C_{44} = (C_{22} - C_{23}).$$

Therefore the final elastic constant matrix contains five independent elements, and the constitutive equation takes the following form:

$$\begin{bmatrix} \tau_1 \\ \tau_2 \\ \tau_3 \\ \tau_4 \\ \tau_5 \\ \tau_6 \end{bmatrix} = \begin{bmatrix} C_{11} & C_{12} & C_{12} & 0 & 0 & 0 \\ C_{12} & C_{22} & C_{23} & 0 & 0 & 0 \\ C_{12} & C_{23} & C_{22} & 0 & 0 & 0 \\ 0 & 0 & 0 & (C_{22}-C_{23}) & 0 & 0 \\ 0 & 0 & 0 & 0 & C_{55} & 0 \\ 0 & 0 & 0 & 0 & 0 & C_{55} \end{bmatrix} \begin{bmatrix} e_1 \\ e_2 \\ e_3 \\ e_4 \\ e_5 \\ e_6 \end{bmatrix} . \qquad (4\text{-}16)$$

A material described by eq. (4-16) is said to have a "plane of isotropy" normal to the x_1-axis, and is referred to as "transversely isotropic". The corneal lamella, then, is transversely isotropic with respect to the fibril axis.

CHAPTER V

LAMINATED PLATE ANALYSIS OF THE STROMA

Introduction

The formulation of a generalized plane-stress or plane-strain elasticity problem using the transversely isotropic stress-strain relation, eq. (4-16), developed for a corneal lamella, is conceptually straight-forward. Unfortunately, this is not the case for the complete stroma of the cornea, which is a laminate composed of a large number of randomly-oriented lamellae. It is reasonable to assume that the individual lamellae are identical, therefore the same stress-strain relation holds for each lamella in its own coordinate system.

It is apparent that the stroma is heterogeneous, and this is the stumbling-block in formulating the elasticity problem. Procedures for analyzing laminated anisotropic heterogeneous plates and shells have been developed[22,23,24,25] in recent years largely as a result of the interest in using laminated fibrous composite materials in aircraft structures (because of their characteristically high strength-to-weight ratios). One of these procedures is suitable for analyzing the stroma, and is presented in the following section.

Analysis of Laminated Anisotropic Elastic Plates

The problem formulation which might be referred to as "classical," for the analysis of a laminated anisotropic elastic plate subjected to bending and stretching, may be attributed to Reissner and Stavsky (1961)[23].

The formulation closely parallels that of classical homogeneous plate theory, and the Kirchhoff assumption, that normals of the middle-plane of the plate before bending and stretching are deformed into the normals of the middle-plane after bending and stretching, is used. An element of the plate is shown in Figure V-1.

Let stresses τ_i and strains e_i $(i = 1,\dots,6)$ be defined in a manner analogous to that on page 41. Stress-resultants and couples are defined as follows:

$$\left.\begin{aligned} N_1 &= \int_{-h/2}^{h/2} \tau_1 dx_3 \\ N_2 &= \int_{-h/2}^{h/2} \tau_2 dx_3 \\ N_{12} &= \int_{-h/2}^{h/2} \tau_6 dx_3 = N_{21} \equiv N_6 \end{aligned}\right\} \qquad (5\text{-}1)$$

$$\left.\begin{aligned} M_1 &= \int_{-h/2}^{h/2} \tau_1 x_3 dx_3 \\ M_2 &= \int_{-h/2}^{h/2} \tau_2 x_3 dx_3 \\ M_{12} &= \int_{-h/2}^{h/2} \tau_6 x_3 dx_3 = -M_{21} \equiv M_6 . \end{aligned}\right\} \qquad (5\text{-}2)$$

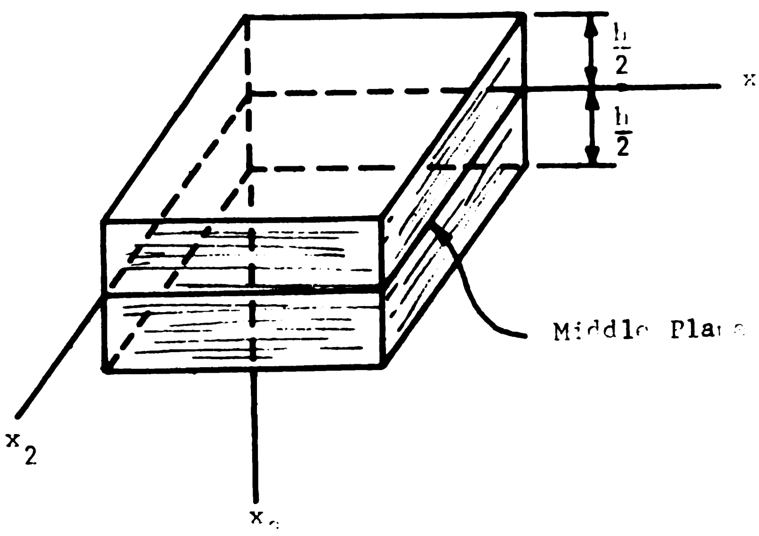

Figure V-1. An Element of the Plate

Transverse shearing forces are defined as

$$\left.\begin{aligned} Q_1 &= \int_{-h/2}^{h/2} \tau_5 dx_3 \\ Q_2 &= \int_{-h/2}^{h/2} \tau_4 dx_3. \end{aligned}\right\} \tag{5-3}$$

Classical plate theory gives the equilibrium relations

$$\left.\begin{aligned} N_{1,1} + N_{6,2} + P_1 &= 0 \\ N_{2,2} + N_{6,1} + P_2 &= 0 \\ M_{1,1} + M_{6,2} - Q_1 &= 0 \\ M_{2,2} + M_{6,1} - Q_2 &= 0 \\ Q_{1,1} + Q_{2,2} + q &= 0 \end{aligned}\right\} \tag{5-4}$$

where the comma indicates partial differentiation with respect to the direction indicated by the numbers is preceeds. P_1, P_2, and q are the body forces per unit volume in the x_1 and x_2 directions, and the distributed surface force per unit area acting in the x_3- direction.

Displacements of the middle-plane $(x_3 = 0)$ in the x_1, x_2, and x_3 directions are denoted by u_1, u_2, and u_3 respectively and the in-plane strains are

$$\left.\begin{aligned} e_1 &= e_1^o + x_3 K_1 \\ e_2 &= e_2^o + x_3 K_2 \\ e_6 &= e_6^o + x_3 K_6 \end{aligned}\right\} \tag{5-5}$$

where

$$\left.\begin{aligned} e_1^o &= u_{1,1} \\ e_2^o &= u_{2,2} \\ e_6^o &= \tfrac{1}{2}(u_{1,2} + u_{2,1}) \end{aligned}\right\} \tag{5-6}$$

and K_1, K_2, and K_6 are curvatures defined as follows:

$$
\begin{aligned}
K_1 &= -u_{3,11} \\
K_2 &= -u_{3,22} \\
K_6 &= -u_{3,12}.
\end{aligned}
\tag{5-7}
$$

It should be noted that the shear strain e_6 is a component of a second-order tensor, and represents half the angle-change (γ_{12}).

The plane-stress generalized Hooke's law is used; therefore the assumption of classical plate theory, that the shearing forces Q_1 and Q_2, and the stress τ_3 produced by q, have negligible effect on the bending, is in force (see Ref. 26, p. 81). Let the stress-strain relation be written in the form

$$
\begin{bmatrix} \tau_1 \\ \tau_2 \\ \tau_6 \end{bmatrix} = \begin{bmatrix} E_{11} & E_{12} & E_{16} \\ E_{12} & E_{22} & E_{26} \\ E_{16} & E_{26} & E_{66} \end{bmatrix} \begin{bmatrix} e_1 \\ e_2 \\ e_6 \end{bmatrix}
\tag{5-8}
$$

where it is understood that the E_{ij} vary with x_3 because the plate is heterogeneous (the elements E_{ij} of eq. (5-8) will later be defined in terms of the elements C_{ij} of eq. (4-16) for the corneal lamella).

Substituting eq. (5-5) into (5-8) and the result into eqs. (5-1) and (5-2) yields a constitutive relation between the stress-resultants and couples and the middle-plane strains and curvatures as follows:

$$\begin{bmatrix} N_1 \\ N_2 \\ N_6 \\ M_1 \\ M_2 \\ M_6 \end{bmatrix} = \left[\begin{array}{ccc|ccc} A_{11} & A_{12} & A_{16} & B_{11} & B_{12} & B_{16} \\ A_{21} & A_{22} & A_{26} & B_{21} & B_{22} & B_{26} \\ A_{61} & A_{62} & A_{66} & B_{61} & B_{62} & B_{66} \\ \hline B_{11} & B_{12} & B_{16} & D_{11} & D_{12} & D_{16} \\ B_{21} & B_{22} & B_{26} & D_{21} & D_{22} & D_{26} \\ B_{61} & B_{62} & B_{66} & D_{61} & D_{62} & D_{66} \end{array}\right] \begin{bmatrix} e_1^o \\ e_2^o \\ e_6^o \\ K_1 \\ K_2 \\ K_6 \end{bmatrix} . \tag{5-9}$$

The constants in the above 6×6 matrix are given by the following relations $(i,j = 1,2,6)$:

$$\left.\begin{aligned} A_{ij} &= \int_{-h/2}^{h/2} E_{ij} dx_3 \\ B_{ij} &= \int_{-h/2}^{h/2} E_{ij} x_3 dx_3 \\ D_{ij} &= \int_{-h/2}^{h/2} E_{ij} x_3^2 dx_3 \ . \end{aligned}\right\} \tag{5-10}$$

Equations (5-4) and (5-9) may be considered to be a system of eleven equations in eleven unknowns $(Q_1, Q_2, N_i, M_i, u_i;$ $i = 1,2,6)$, and with appropriate boundary conditions may, in theory, be solved. Reissner and Stavsky[23] show that the system may be reduced to three equations in displacements u_i, or two equations in terms of u_3 and an Airy stress function F.

There are two controversial points of the formulation. The use of the plane-stress constitutive relation (eq. (5-8)) is obviously an approximation. This same approximation is made in classical plate theory, and has been shown to give negligible error for thin plates. Timoshenko and Woinowsky-Krieger[26] make several comments regarding this matter. Secondly, the applicability of the assumption that straight lines normal to the middle-surface before deformation are straight line normal to the deformed middle surface is questionable in the case of a heterogeneous plate. The good correlation of theory and experiment in the research of Azzi and Tsai[25], however, indicates that one can be optimistic in this regard.

Application of the Laminated Plate Analysis to the Corneal Stroma

The laminated plate formulation presented in the previous section is a practical means for analyzing the stroma as a laminated structure of a large number of randomly oriented anisotropic lamellae. The quasi-elastostatic stress-strain constitutive equation of the transversely isotropic lamella given by eq. (4-16) will be used along with some arguments based on qualitative observations of corneal mechanical properties to yield expressions enabling partial evaluation of elastic constants from simple tests.

The first task at hand is the evaluation of A_{ij}, B_{ij}, and D_{ij} using eqs. (5-10) and the plane-stress specialization of eq. (4-16). The plane-stress specialization of the elastic constant matrix is obtained by setting τ_3 to zero and solving for e_3 in terms of e_1 and e_2. The result is that the E_{ij} of eq. (5-8) are related to the C_{ij} of eq. (4-16) as follows:

$$\left.\begin{aligned}
E_{11} &= C_{11} - \frac{C_{12}^2}{C_{22}} \\
E_{12} &= E_{21} = C_{12}\left(1 - \frac{C_{23}}{C_{22}}\right) \\
E_{16} &= E_{61} = 0 \\
E_{22} &= C_{22} - \frac{C_{23}^2}{C_{22}} \\
E_{26} &= E_{62} = 0 \\
E_{66} &= C_{55} \ .
\end{aligned}\right\} \qquad (5\text{-}11)$$

The E_{ij} of eq. (5-11) are defined with respect to the specific coordinate system (x_1, x_2, x_3) shown in Figure V-1. Suppose new axes $(\bar{x}_1, \bar{x}_2, \bar{x}_3)$ are defined by a rotation through an angle ξ about the x_3-axis as shown in Figure V-2. The elastic constants $\bar{E}_{ij}$ of the new coordinate system can be expressed in terms of the original E_{ij} and the angle ξ by employing the transformation relation for a fourth-order tensor; that is,

$$\bar{E}_{ijk\ell} = a_{im} a_{jn} a_{ko} a_{\ell p} E_{mnop} \qquad (5\text{-}12)$$

where a_{ij} is the cosine of the angle between the positive $\bar{x}_i$ and x_j axes, and the indices take on the values of 1 and 2. The correlation between the E_{ij} of eqs. (5-11) and the E_{mnop} of eq. (5-12) is as follows:

$$\left.\begin{aligned}
E_{11} &= E_{1111} \\
E_{12} &= E_{21} = E_{1122} = E_{2211} \\
E_{16} &= E_{61} = E_{1112} = E_{1121} = E_{1211} = E_{2111} \\
E_{22} &= E_{2222} \\
E_{26} &= E_{62} = E_{2212} = E_{2221} = E_{1222} = E_{2122} \\
E_{66} &= E_{1212} = E_{2121} \ .
\end{aligned}\right\} \qquad (5\text{-}13)$$

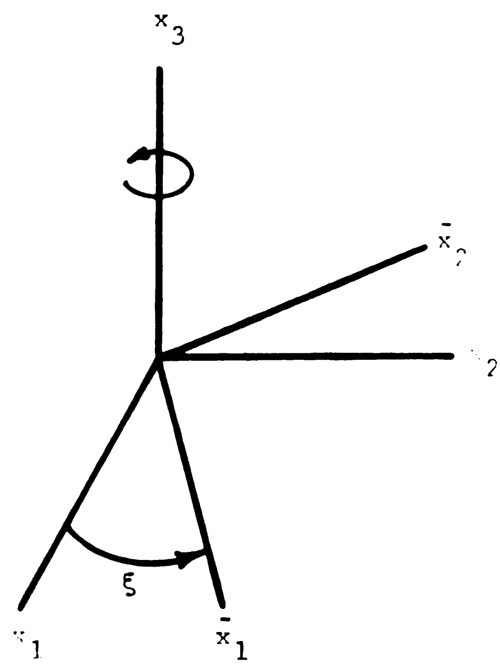

Figure V-2. Rotation of Axes

Taking direction cosines from Figure V-2 and using eqs. (5-13), eq. (5-12) may be expanded to yield the following results:

$$\begin{aligned}
\bar{E}_{11} &= E_{11}\cos^2\xi + E_{22}\sin^2\xi + (2E_{12} + 4E_{66} - E_{11} - E_{22})\sin^2\xi\cos^2\xi \\
\bar{E}_{12} &= E_{12} + (E_{11} + E_{22} - 2E_{12} - 4E_{66})\sin^2\xi\cos^2\xi \\
\bar{E}_{16} &= (2E_{66} + E_{12} - E_{11})\cos^3\xi\sin\xi - (2E_{66} + E_{12} - E_{22})\sin^3\xi\cos\xi \\
\bar{E}_{22} &= E_{11}\sin^2\xi + E_{22}\cos^2\xi + (2E_{12}+4E_{66}-E_{11}-E_{22})\sin^2\xi\cos^2\xi \\
\bar{E}_{26} &= (2E_{66} + E_{12} - E_{11})\sin^3\xi\cos\xi - (2E_{66}+E_{12}-E_{22})\cos^3\xi\sin\xi \\
\bar{E}_{66} &= E_{66} + (E_{11} + E_{22} - 2E_{12} - 4E_{66})\sin^2\xi\cos^2\xi
\end{aligned} \tag{5-14}$$

and

$$\bar{E}_{ij} = \bar{E}_{ji}.$$

Equations (5-10) may be evaluated in an approximate sense by introducing the notion of macroscopic transverse isotropy of the plate with respect to the x_3-axis. The lamellae are large in number (approximately 200 in the 0.5 mm thick human stroma), and their orientation angles (ξ) are randomly distributed in the x_3-direction (ξ is constant for a given lamella, and has random jump-discontinuities between adjacent lamellae). Let average values (E^*_{ij}) of the $\bar{E}_{ij}$ be introduced. Since all lamellae are identical, and are large in number, the above described random disposition with respect to x_3 implies that all the E^*_{ij} associated with increments of plate thickness Δx_3 (arbitrarily located in the plate) are equal. The values of E^*_{ij} may be defined by the relation

$$E^*_{ij} = \frac{1}{h}\int_{-h/2}^{h/2} \bar{E}_{ij}(x_3)dx_3$$

or equivalently

$$E^*_{ij} = \frac{1}{2\pi}\int_{o}^{2\pi} \bar{E}_{ij}(\xi)d\xi, \tag{5-15}$$

and eqs. (5-10) may be approximated as follows:

$$A_{ij} = E^*_{ij}\int_{-h/2}^{h/2} dx_3 = h\, E^*_{ij} \tag{5-16}$$

$$B_{ij} = E^*_{ij}\int_{-h/2}^{h/2} x_3 dx_3 = 0 \tag{5-17}$$

$$D_{ij} = E^*_{ij}\int_{-h/2}^{h/2} x_3^2 dx_3 = \frac{h^3}{12} E^*_{ij}. \tag{5-18}$$

Equations (5-15) may be evaluated by substituting $\bar{E}_{ij}(\xi)$ from eqs. (5-14), and it is easily shown that

$$\left.\begin{aligned}
E^*_{11} &= \frac{1}{8}(3E_{11} + 3E_{22} + 4E_{66} + 2E_{12}) \\
E^*_{12} &= \frac{1}{8}(6E_{12} + E_{11} + E_{22} - 4E_{66}) \\
E^*_{16} &= 0 \\
E^*_{22} &= E^*_{11} \\
E^*_{26} &= 0 \\
E^*_{66} &= \frac{1}{8}(4E_{66} + E_{11} + E_{22} - 2E_{12}).
\end{aligned}\right\} \tag{5-19}$$

Since $B_{ij} = 0$ there is no coupling between in-plane stretching and transverse bending, and using eqs. (5-16) through (5-18) the matrix equation (5-9) may be separated into the following two simpler expressions:

$$\begin{bmatrix} N_1 \\ N_2 \\ N_6 \end{bmatrix} = h \begin{bmatrix} E^*_{11} & E^*_{12} & 0 \\ E^*_{12} & E^*_{11} & 0 \\ 0 & 0 & E^*_{66} \end{bmatrix} \begin{bmatrix} e^o_1 \\ e^o_2 \\ e^o_6 \end{bmatrix} \tag{5-20}$$

$$\begin{bmatrix} M_1 \\ M_2 \\ M_6 \end{bmatrix} = \frac{h^3}{12} \begin{bmatrix} E^*_{11} & E^*_{12} & 0 \\ E^*_{12} & E^*_{11} & 0 \\ 0 & 0 & E^*_{66} \end{bmatrix} \begin{bmatrix} K_1 \\ K_2 \\ K_6 \end{bmatrix} . \tag{5-21}$$

Equations (5-20) and (5-21) hold for any orientation of axes x_1 and x_2 in the plane of the stroma because the E^*_{ij} are average values, independent of direction in the plane. It is important to note that this theoretical analysis predicts the earlier experimentally observed[6] in-plane isotropy of the stroma.

Equations (5-20) and (5-21) may be used to analyze laboratory experiments that lead toward evaluation of the elastic constants in the matrix of eq. (4-16). A discussion of the theory behind the experiments follows. In all cases the body forces P_1 and P_2 and the distributed force q are zero (see page 58).

Uniaxial Tensile Stress Test

For the case of uniaxial tension of a long strip of stroma, eq. (5-20) is applicable, and it may be assumed, except near the end restraints (St. Venant boundary region), that $N_2 = 0 = N_6$ and N_1 is uniformly distributed. The equilibrium equations (5-4) are identically satisfied, and from eq. (5-20) one can write

$$N_1 = h(E^*_{11}e^o_1 + E^*_{12}e^o_2)$$

$$0 = h(E^*_{12}e^o_1 + E^*_{11}e^o_2).$$

Eliminating e^o_2 gives

$$\frac{N_1}{h} = \frac{1}{E^*_{11}}[(E^*_{11})^2 - (E^*_{12})^2]e^o_1.$$

The quantity N_1/h is the nominal tensile stress in the strip, thus the "apparent** Young's modulus" E_a is

$$E_a = E^*_{11} - \frac{(E^*_{12})^2}{E^*_{11}}$$

and the "apparent** Poisson's Ratio" μ_a, in the $x_1 - x_2$ plane, is

$$\mu_a = \frac{E^*_{12}}{E^*_{11}}.$$

From the above two equations one can write

$$E^*_{11} = \frac{E_a}{1 - \mu_a^2}$$

$$E^*_{12} = \frac{\mu_a E_a}{1 - \mu_a^2},$$

and applying eqs. (5-19) these relations become

$$\left.\begin{aligned} 3(E_{11} + E_{22}) + 2E_{12} + 4E_{66} &= \frac{8E_a}{1 - \mu_a^2} \\ E_{11} + E_{22} + 6E_{12} - 4E_{66} &= \frac{8\mu_a E_a}{1 - \mu_a^2}. \end{aligned}\right\} \tag{5-22}$$

** The term "apparent" is included because of the fact that the concept of Young's modulus and Poisson's ratio are not simply defined as for an isotropic material. Subscript a is added to E and μ in order that this be kept in mind.

Torsion Test

The quantity E^*_{66} may be evaluated by using eq. (5-21) to analyze a torsion test. Consider a long strip of stroma of width W having a length ℓ in the x_1-direction. Let the strip be clamped rigidly at $x_1 = 0$ and let a torque T be applied (about the axis of the strip) at $x_1 = \ell$, and let ϕ be the resulting angle-of-twist (Use the left-hand rule for the directions of T and ϕ).

If the strip is centered with respect to the x_1-axis one may approximate the middle-plane displacement (it is assumed $u_1 \equiv 0 \equiv u_2$) by taking

$$u_3 = -\phi x_2 (\frac{x_1}{\ell}).$$

Applying eqs. (5-2) and (5-7), it is apparent that

$$M_6 = \frac{T}{W}$$

and

$$K_6 = \frac{\phi}{\ell}.$$

It may be assumed, except near the end restraints, that only the stresses τ_5 and τ_6 are nonzero, and that both are uniformly distributed in the x_1-direction. Then from eqs. (5-1) through (5-3) it is clear that all the equilibrium equations (5-4) are satisfied.

Using the above expressions for M_6 and K_6, from eq. (5-21) one can write

$$E^*_{66} = \frac{12\ M_6}{h^3\ K_6} = \frac{12\ \ell}{W\ h^3}\ (\frac{T}{\phi}).$$

Applying eqs. (5-18) this becomes

$$E_{11} + E_{22} - 2E_{12} + 4E_{66} = \left(\frac{96\,\ell}{W\,h^3}\right)K_T \tag{5-23}$$

where K_T is the "torsional rigidity of the strip"; that is

$$K_T = \frac{T}{\phi}\,.$$

Tension and Torsion Data Analysis

For convenience let the right hand side of eqs. (5-22) and (5-23) be denoted as follows:

$$\left.\begin{aligned} \frac{8\,E_a}{1-\mu_a^2} &= E_A \\ \frac{8\mu_a\,E_a}{1-\mu_a^2} &= E_B \\ \left(\frac{96\,\ell}{W\,h^3}\right)K_T &= E_C. \end{aligned}\right\} \tag{5-24}$$

Then

$$3(E_{11} + E_{22}) + 2E_{12} + 4E_{66} = E_A$$

$$(E_{11} + E_{22}) + 6E_{12} - 4E_{66} = E_B$$

$$(E_{11} + E_{22}) - 2E_{12} + 4E_{66} = E_C.$$

These three equations give only two independent relations in the three quantities $(E_{11} + E_{22})$, E_{12}, and E_{66}. It is easily shown from the first two of the equations that

$$\left.\begin{aligned} E_{12} &= \frac{1}{16}(3E_B - E_A) + E_{66} \\ (E_{11} + E_{22}) &= \frac{1}{8}(3E_A - E_B) - 2E_{66}. \end{aligned}\right\} \tag{5-25}$$

If one solves the third equation for E_{66} and substitutes the expression into eqs. (5-25), the resulting two equations may be combined to show that

$$E_A - E_B = 2E_C. \tag{5-26}$$

Numerical values of E_A, E_B, and E_C may be determined from laboratory experiments, and the degree to which they satisfy eq. (5-26) gives an indication of the validity of the theoretical formulation of the problem.

The plane stress elastic constants E_{ij} in eqs. (5-25) may be expressed in terms of the constants C_{ij} of eq. (4-16) by using the relationships presented in eqs. (5-11). The result is two independent equations in the five elastic constants C_{ij}. Before carrying out these calculations it is convenient to discuss a uniaxial strain test that leads to the evaluation of the constant C_{22}. Arguments also will be presented to show that C_{55} is small.

Uniaxial Strain Test

With reference to eq. (4-16), consider a uniaxial strain test in the x_3-direction. This implies that e_1 and e_2 are zero, and therefore

$$\tau_3 = C_{22}e_3. \tag{5-27}$$

Since the x_3-axis of each lamella is normal to the surfaces of the stroma, all the x_3-axes are parallel, and no transformation-of-axes relations need be used.

A uniaxial compressive strain test of the stroma in the x_3-direction may be conducted as illustrated in Figure V-3. The test specimen is a disc of corneal stroma having a circular cross-section in the $x_1 - x_2$ plane. The specimen lies on a flat surface, and the circumfrential edges are in contact with a rigid surface to prevent displacements in the $x_1 - x_2$ plane. The plunger and guide are coupled in such a manner that, at the end in contact with the specimen, the plunger face always remains flush with the face of the guide (i.e. the plunger never moves relative to the guide).

The diameter of the test specimen is large compared to its thickness h, and the ratio of guide-to-plunger outside diameters is sufficiently large so that "edge effects" at the periphery of the specimen may be assumed to have a negligible influence on the state of stress in the vicinity of the plunger.

Let the plunger/guide assembly be displaced in the negative x_3-direction by an amount Δh so as to compress the specimen, and let the change in the axial force in the plunger be ΔP. If the cross-sectional area of the plunger face is denoted by A, then eq. (5-27) may be written in the form

$$\frac{\Delta P}{A} = C_{22}\left(\frac{\Delta h}{h}\right)$$

and therefore

$$C_{22} = \frac{h}{A}\left(\frac{\Delta P}{\Delta h}\right). \qquad (5\text{-}28)$$

Note: All parts appear circular when viewing in the x_3-direction.

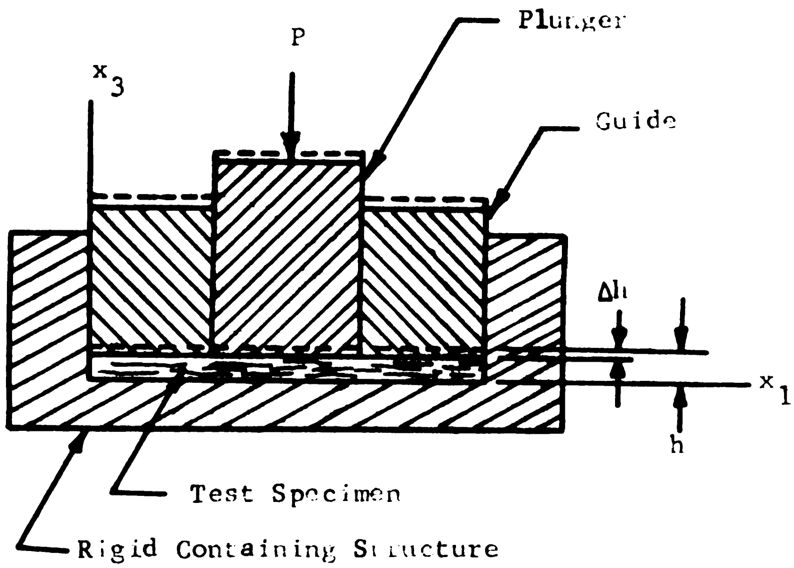

Figure V-3. Uniaxial Compressive Strain Test Configuration

Analysis of the Stroma Small Shear Rigidity

As pointed out in Chapter I (see also Ref. 3, p. 306 and 311), the stroma has a small shear rigidity for shear displacements of planes relative to one-another parallel to the anterior and posterior surfaces of the cornea. Recall that the stroma is composed of a stack of a large number of randomly-oriented lamellae as indicated in Figure V-4.

The matrix of elastic constants of eq. (4-16) defines the stress-strain relations for any one of the lamellae with respect to its axes (x_{1n}, x_{2n}, x_3). Since the lamellae are large in number, and are randomly oriented (with respect to rotations about the x_3-axis), it may be assumed that there always exists a value for n (see Figure V-4) such that the x_{1n} axis is parallel to any arbitrarily selected direction in the plane of the stroma. This leads one to conclude that the observed small shear rigidity across the stack of lamellae could be due to any one, or all, of the following possible properties:

1) The shear rigidity between adjacent lamellae is small.
2) The shear rigidity related to distortion in the $x_1 - x_3$ plane is small.
3) The shear rigidity related to distortion in the $x_2 - x_3$ plane is small.

Possibility (1) does not directly influence the form of the elastic constant matrix of the lamella; however possibilities

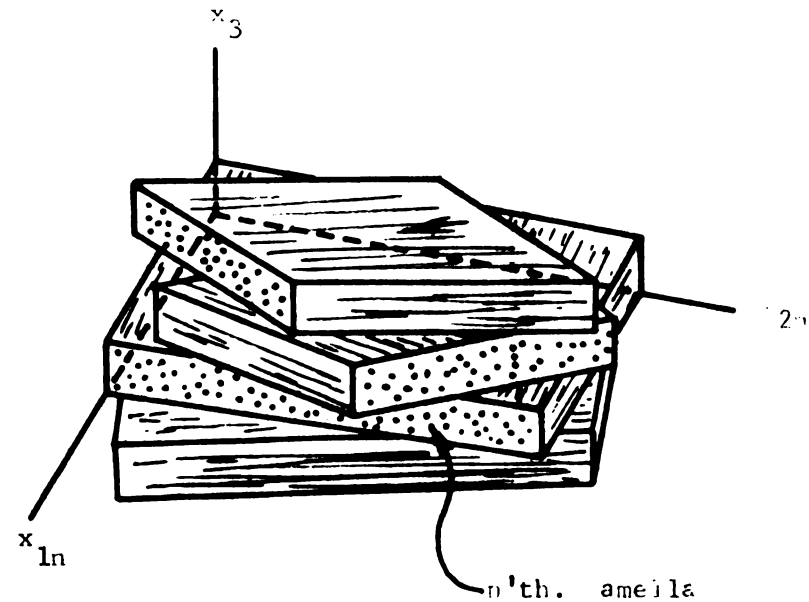

Figure V-4. The Stack of Lamellae

(2) and (3) imply that C_{55} and $(C_{22} - C_{23})$ are approximately zero respectively (see eq. (4-16)).

Possibility (3) may be eliminated by considering the physical consequences it implies. If $(C_{22} - C_{23}) = 0$, then the constitutive equation (4-16) requires that the stresses τ_2 and τ_3 be identically equal, regardless of the state of strain. Since sections of stroma stretched in the x_3-direction show normal elastic action (see Ref. 3, p. 307) it appears that τ_2 and τ_3 are in fact independent. This evidence is assumed to be sufficient justification for throwing-out possibility (3) above.

If possibility (1) alone is the mechanism responsible for the small shear rigidity, then microscopic examination of the side surfaces (i.e. surfaces parallel to the x_3-axis) of a section of stroma after shear deformation should reveal a staircase-type profile, since there would be discontinuities in the displacements from one lamella to the next as one proceeded in the x_3-direction. There is no evidence in the literature that this easily-recognizable phenomenon has been observed, and on this basis it will be assumed that possibility (1) does not exist <u>alone</u>. It is concluded, then, that possibility (2), perhaps supplemented by (1), exists and is responsible for the observed small shear rigidity. As discussed previously, this implies that

$$C_{55} \approx 0. \tag{5-29}$$

It should be pointed out, in support of the argument leading to eq. (5-29), that there are no contradictions with the stroma model proposed by Maurice (see Fig. III-3).

Analysis of the Simple-Test Relationships

With regard to the use of simple tests to evaluate the elastic constants, the three tests presented in the previous sections of this Chapter - uniaxial tensile stress, torsion, and uniaxial compressive strain - exhaust the list of possibilities.

Recapitulating, the three-dimensional set of elastic constants is shown in eq. (4-16), and contains five nonzero entries (C_{11}, C_{12}, C_{22}, C_{23}, and C_{55}). The constant C_{22} may be evaluated directly from the uniaxial strain test data by using eq. (5-28), and applying eqs. (5-11) to the uniaxial tensile stress relations of eqs. (5-25) and rearranging gives

$$
\begin{aligned}
C_{11} &= \frac{1}{8}(3E_A - E_B - 16C_{55}) + \frac{C_{12}^2}{C_{22}} + \frac{1}{C_{12}}\left[\frac{C_{22}}{8}(16C_{55} - 3E_B + E_A)\right] \\
&\quad + \frac{C_{22}}{C_{12}^2}\left[\frac{1}{16}(16C_{55} - 3E_B + E_A)\right]^2 \qquad (5\text{-}30) \\
C_{23} &= C_{22} + \frac{1}{C_{12}}\left[\frac{C_{22}}{16}(16C_{55} - 3E_B + E_A)\right].
\end{aligned}
$$

The consequences of setting $C_{55} = 0$, as suggested by the analysis leading to eq. (5-29) will be discussed in Chapter VIII where the experimental results are applied to eqs. (5-30). The quantity C_{55} has been retained in eqs. (5-30) so that the effects of nonzero values may be observed. Details of the laboratory experiments follow next.

CHAPTER VI

EXPERIMENTAL EQUIPMENT

Introduction

Experimental equipment was designed specifically for carrying out the three types of tests discussed in the previous Chapter (uniaxial tension, torsion, and uniaxial strain). The same specimen preparation and mensuration equipment, and constant temperature immersion bath system, were used for all three types of experiments. The equipment was fabricated using the facilities of the Departmental experimental mechanics laboratories and the Division of Engineering Research machine shop.

The topic of specimen preparation is an appropriate starting point in discussing the equipment, and will be followed by descriptions of the specimen mensuration equipment, immersion bath system, and the test fixtures used in conducting the three basic experiments.

Specimen Preparation

A double-blade knife was used to cut a uniform strip of cornea from a "hemispherical shell" of the eyeball (specifically, the quasi-hemisphere anterior from the equator, which contains the cornea). A photograph of the knife is shown in Figure VI-1. The plastic spherical seat of the knife enabled the eyeball hemisphere to be positioned with the cornea directed toward the knife blades. The tissue was held in place by means of a vacuum applied through small holes in the plastic seat. This held the sclera, adjacent to the periphery of the cornea, tightly against the seat.

Two parallel slots machined in the spherical seat enabled the knife blades to cut through the entire width and thickness of the cornea and adjacent sclera, and resulted in a long-strip specimen of uniform rectangular cross-section. This preparation eliminated excessive handling which might have lead to inadvertent straining of the tissue. The knife blades consisted of two razor-blades, and were held a specific distance apart by a spacer. The blades could be moved in the vertical direction by sliding their mounting frame along four rigid guide-rods extending from the heavy steel base of the fixture.

The circular disc-shaped specimens used in the uniaxial strain tests were cut from the cornea using a standard type 7 mm diameter corneal trephine. The trephine is shown in Figure VI-12.

Specimen Mensuration

The initial thickness (h) of the strip specimens in the anterior-posterior direction (the x_3-direction) was always measured immediately after preparation. The measurement was made using an Ames dial-indicator (0.0001 inch scale divisions) mounted on a ring-stand, and a simple electrical circuit. The

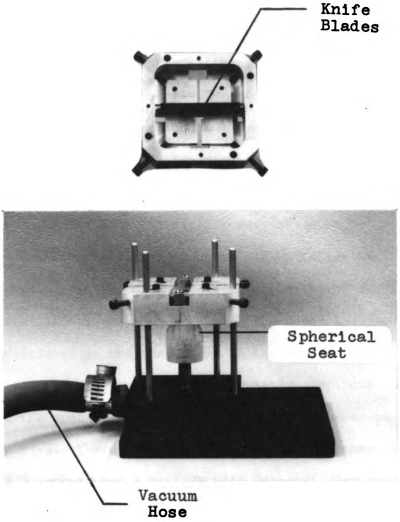

Figure VI-1. Double-Blade Knife

device is shown in Figure VI-2.

A small electrical probe protruding from the tip of the dial-indicator was coupled through an ohm-meter to a stainless-steel plate cemented to the base of the ring-stand. The probe was moveable in the vertical direction, and could be adjusted, so as to contact a surface beneath the dial-indicator, by means of a screw-mechanism above the indicator. The probe position at the point of incipient contact could be precisely determined by noting the dial reading at the point where continuity of the electrical circuit was indicated by the meter. The specimen thickness was obtained by taking the difference between successive dial readings for incipient contact with the stainless-steel plate and with the upper specimen surface when positioned on the plate beneath the probe.

Length and width measurements of the strip specimens were made using the specially-constructed measuring microscope shown in Figure VI-3. The microscope had a working distance of approximately 1.5 inches, and a reticle with perpendicular cross-hairs. The vertical position was given by an Ames dial-indicator (0.001 inch scale divisions; one-inch travel), and the horizontal position was read directly from a micrometer-head (Starrett model 465M; 0.002 mm divisions). Length and width measurements were made by taking the difference between successive readings of the dial-indicator and micrometer respectively. The standard deviations associated with the precision of the microscope may be taken as 0.0015 mm and 0.010 mm for the width and length measurements respectively (Specimen dimensions are given in

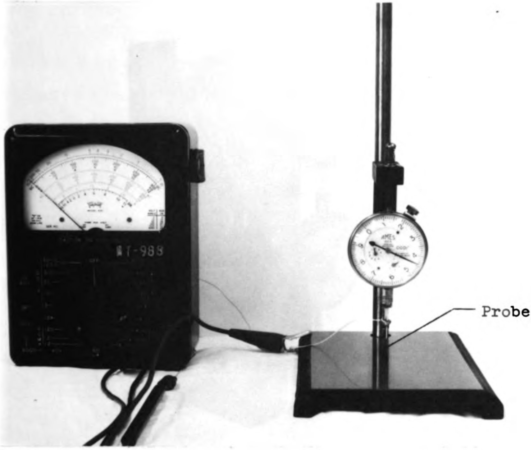

Figure VI-2. Thickness Measuring Fixture

Figure VI-3. Measuring Microscope

Tabl

The

a

de

ab

th

of

thi

a t

a t

An

bott

of th

Tables VII-1 and VII-2).

Immersion Bath System

All tests were conducted with the corneal specimens immersed in a constant-temperature bath so that the in vivo temperature and hydration of the tissue could be approximated. The constant-temperature system consisted basically of two coupled heat-exchangers, one immersed in a tank containing the test-specimen and immersion medium, and the other immersed in a drum of water maintained at a constant temperature of 91.5 deg. F. A schematic diagram is shown in Figure VI-4.

The two heat-exchangers were coupled by plastic tubing, and this closed system was filled with water. At one point the tubing ran through a variable-speed pump (Varistaltic pump no. 72-590-60; Manostat Corp.). This enabled the water to be pumped through the closed circuit and thereby transmit heat from one exchanger to the other. The specimen-tank heat-exchanger consisted of a three-foot length of 1/8-inch copper tubing soldered to a five-inch by nine-inch thin copper plate. The water-drum heat-exchanger consisted of a twenty-foot length of 1/4-inch copper tubing coiled around a ten-inch diameter cylinder. The cylinder was mounted in a twenty-gallon insulated steel drum nearly filled with water. An immersion heater (Aqua-Lite immersion water heater; Vogelzang Bros., Inc., Holland, Mich.) was mounted at the bottom of the drum, and a motor-driven mixer near the center of the drum circulated the water continuously (a mixer was

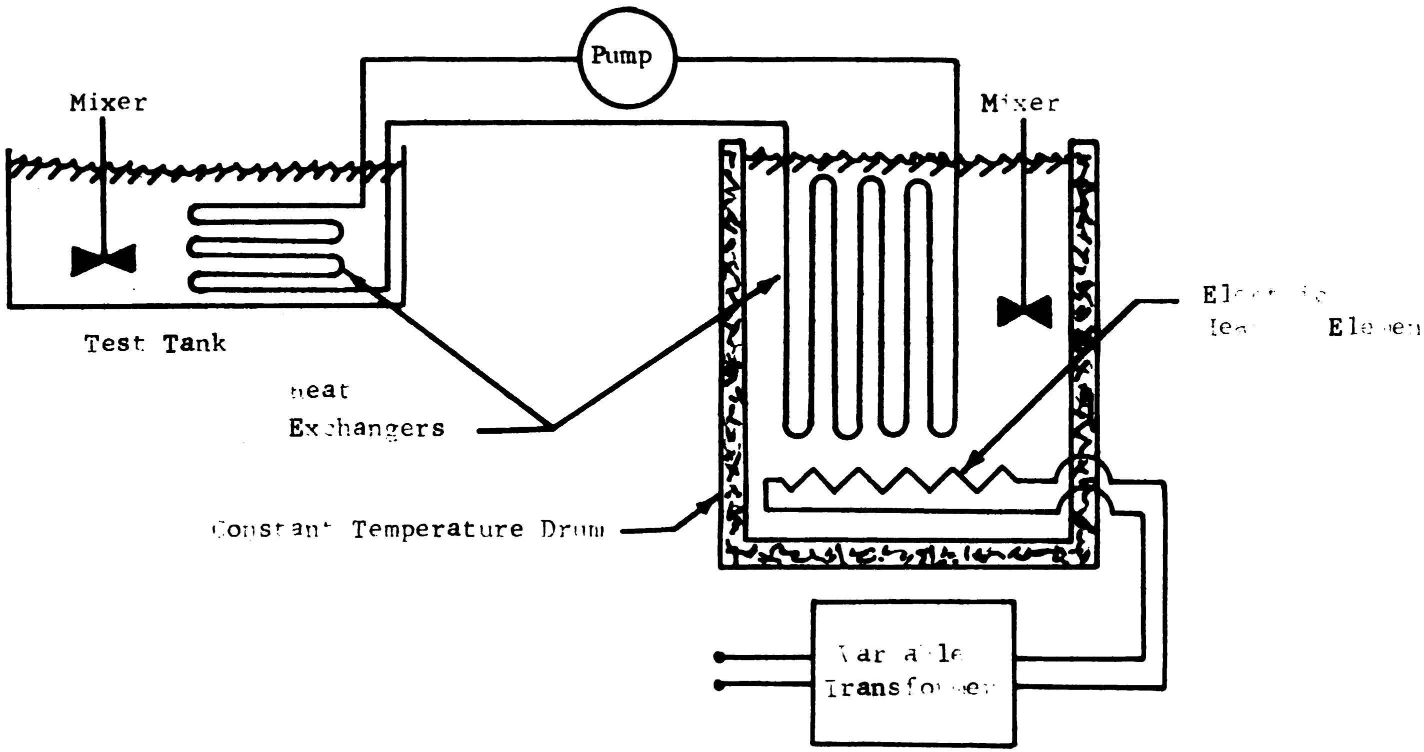

Figure VI-4. Schematic Diagram of Constant Temperature Immersion Bath System

employed in the test tank also).

The immersion heater was powered through a Variac variable transformer, which enabled the rate of heat input to be controlled. A given constant temperature in the test tank was achieved by operating the immersion heater, pump, and mixers continuously and simply varying the pump speed and/or heater voltage to change the equilibrium temperature in the test tank.

Uniaxial Tensile Stress Test

For the uniaxial tensile test the immersion tank was a six-inch by eight-inch glass container eight inches in depth, and the heat exchanger was positioned parallel to, and approximately 1/4 inch above the bottom. A rigid vertical post behind the container was used as an attachment point for the immersion-fluid mixer and the tensile test fixture. These were held in place in the tank by cantilever-type structures extending forward from the post (see Figure VI-5).

The tensile test fixture was positioned in the tank so that the long axis of the test specimen (strip of cornea) was aligned with the vertical direction, and was clamped in place by means of two thumb-screws. This configuration enabled the tensile test fixture to be easily and quickly installed in the immersion tank after a test specimen had been mounted in the fixture (The fixture was mobile, and could be moved away from the tank, for convenience, while installing the test specimen).

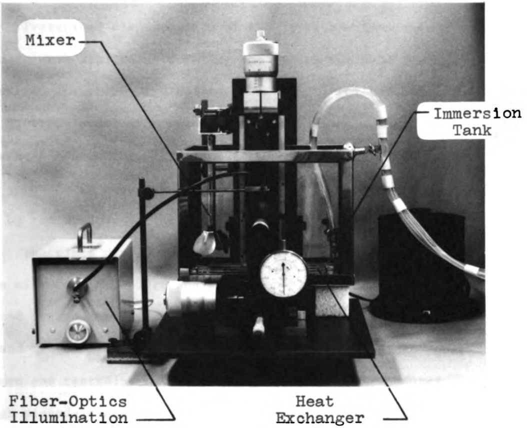

Figure VI-5. Overall View of Tensile Test Equipment

The uniaxial tensile test fixture is shown in Figure VI-6. The fixture enabled the application of a prescribed specimen elongation and measurement of the resulting tensile load.

Prescribed displacements of the upper specimen end restraint were applied by rotating the micrometer head through the desired increment of displacement. The micrometer head was a Starrett model 465M with 0.002 mm divisions. Rotation of the head caused the micrometer coupler to be displaced upward, the force required for this displacement being provided by the preload spring which was always in the compressed state. The rigid displacement bar was attached to the bottom of the micrometer coupler, and slid smoothly in the guide block. The load transducer was affixed to the end of the displacement bar, and the clevis-like transducer coupler connected the upper specimen end restraint to the loading stud of the transducer through pinned-joints that were free to pivot in order to accommodate small misalignments of the system.

The upper and lower specimen end restraints were identical (see Figure VI-7 for a close-up photograph). Each restraint consisted of two machined aluminum components coupled by an aluminum pin, and was attached to the specimen by a simple clamping-action, the clamping force being provided by a brass screw. The lower specimen end restraint was pinned to the attachment bracket, which was simply a rigid L-shaped bracket with provision for adjusting its vertical position in order that test specimens of varying lengths could be accommodated.

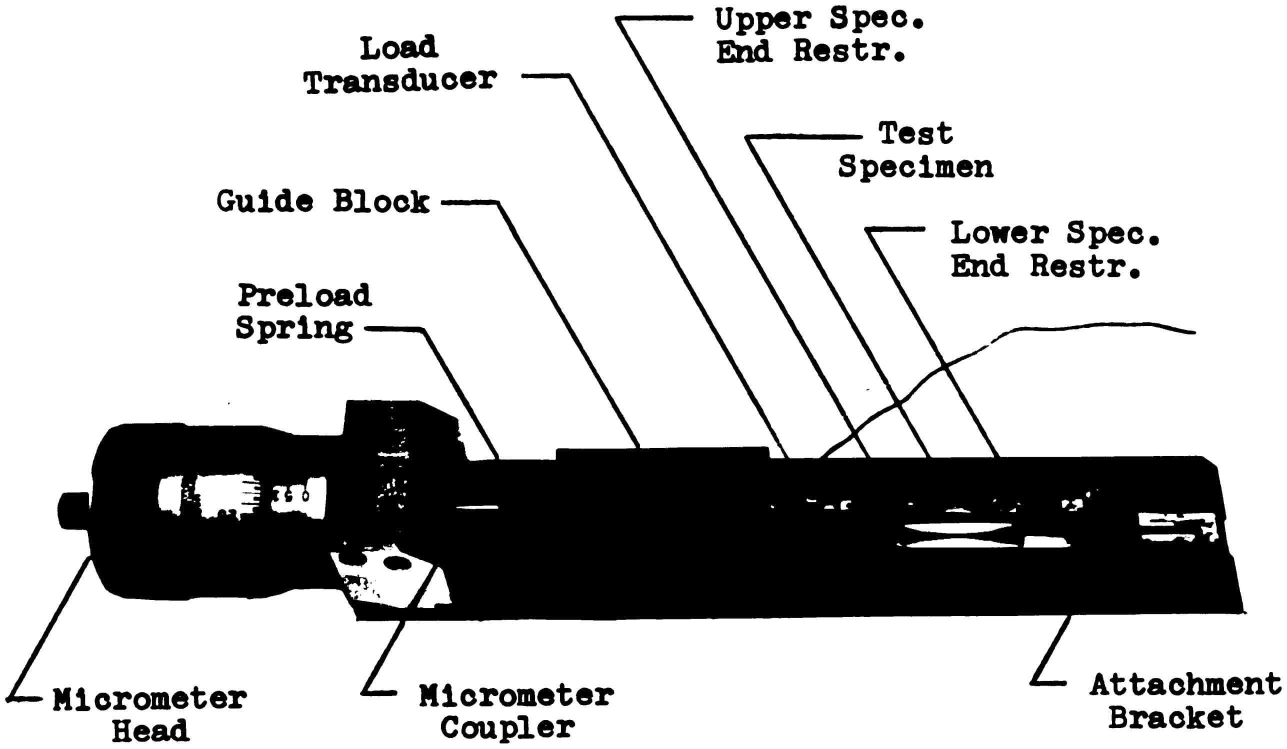

Figure VI-6. Uniaxial Tensile Stress Test Fixture

The load transducer was especially designed and fabricated for this research by Kulite Semiconductor Products, Inc., and consisted basically of a miniature phosphor-bronze cantilever beam with a full four-arm bridge of Kulite semiconductor electrical resistance strain gages. A close-up photograph of the transducer is shown in Figure VI-8. The basic specifications were as follows:

Impedance: 1000 ohms

Sensitivity: Nominally 8.0 mv/gram at 10 volts D.C.

Input: 10 volts DC or AC max.

Rated (max.) load: 50 grams

Temp. sensitivity: Less than 0.2 mv/deg. F. at 100 deg. F.

Rigidity: 0.00083 mm deflection/gram.

The transducer was coupled to a Tektronix type Q transducer preamplifier plug-in unit, and loads were indicated by the vertical trace deflection on an oscilloscope screen.

Torsion Test

The torsion test was conducted in a five-inch by eight-inch sheet steel container ten-inches in depth. The heat-exchanger and immersion-fluid mixer used for the tensile tests were also used in the torsion tests. The basic configuration is shown in Figure VI-9.

The torsion test fixture was clamped to the base of the immersion tank, and was easily removable to facilitate installation of the test-specimens. The fixture is shown in

Figure VI-7. Specimen End Restraint

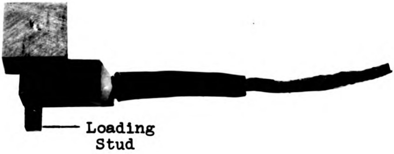

Figure VI-8. Load Transducer

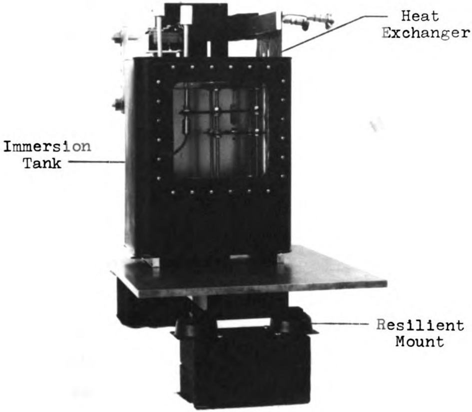

Figure VI-9. Overall View of Torsion Test Equipment

Figure VI-10, and a discussion of the principles of operation follows.

The torsional rigidity of a strip of cornea is small compared to that of specimens normally tested in torsion, therefore no existing torsion test equipment was applicable. The primary difficulty was that commercially available torque transducers do not have the capability of measuring torsional loads in the range of interest for the cornea (of the order of 0.05 gram-millimeter). This difficulty was overcome by using an optical system to measure the torque. The technique consisted of using laser beams and mirrors to measure the twist in a length of wire having a known torsional rigidity.

The torsion test specimens had the same geometry as the tensile specimens, and the same upper and lower specimen end restraints were used in each case. The long-axis of the test strip was vertical, and the torsion test consisted basically of measuring the torque necessary to rotate the lower specimen end restraint, about the vertical axis, through a known angle relative to the upper specimen end restraint.

The upper specimen end restraint was pinned to the attachment bracket, and the bracket was affixed (with provision for rotation about the vertical axis) to the body of the torsion fixture. The bracket could be clamped in place at an arbitrary orientation, which facilitated initial alignment of the system. The lower specimen end restraint was pinned to a small block of brass that served as a mounting point for the specimen-twist mirror and also as a coupling between the end restraint and

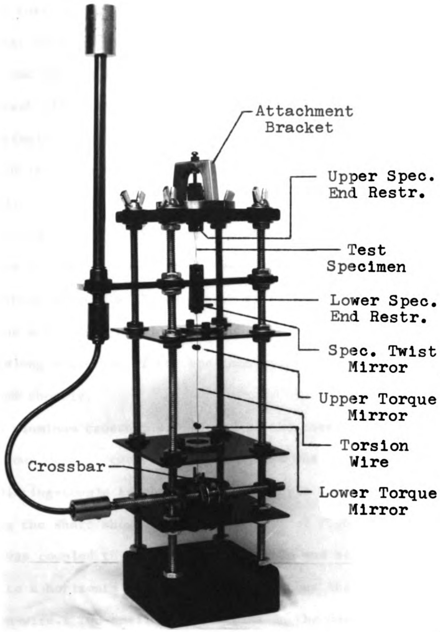

Figure VI-10. Torsion Test Fixture

the torsion-wire.

The torsion-wire was a steel music-wire of 0.008 inch diameter that extended downward from the lower specimen end restraint, and was supported laterally by two horizontal platens. Each platen had a guide for the torsion wire. The guide was simply a small disc of 0.005 inch steel shim stock with a 0.020 inch diameter hole through which the torsion wire passed.

Two small first-surface mirrors were clamped to the torsion-wire a known distance apart (approximately 46 millimeters). These mirrors will henceforth be referred to as the upper torque mirror and the lower torque mirror, and their function, along with that of the specimen-twist mirror will be discussed shortly.

An aluminum crossbar was pinned to the torsion-wire below the lower of the two guide-platens, and was used to apply a twisting-couple to the wire. The couple was applied by rotating the shaft shown in the upper left of Figure VI-10. The shaft was coupled through a flexible cable and screw-mechanism to a horizontal disc that rotated about the axis of the torsion-wire. Two small vertical pins in the disc made contact with the crossbar and caused it to rotate as the upper shaft was turned.

A preload hanger bracket was attached to the lower end of the torsion-wire. This bracket enabled preload weights to be suspended from the torsion-wire in order to vary the axial tensile stress in the test specimen, a capability that was required in order to check for coupling between tensile and torsional modes of loading.

As pointed out earlier, the torque and associated specimen twist angle were measured optically using the specimen-twist mirror and the two torque mirrors. Since the upper specimen end restraint was clamped rigidly in place, the angle-of-twist across the test specimen was equal to the angle-of-rotation of the lower specimen end restraint. The torque responsible for this specimen twist was of the same magnitude as that in the torsion-wire. Assuming the torsional rigidity of the torsion-wire is known, it is apparent that the torque and specimen angle-of-twist can be evaluated if the angles of rotation of the three mirrors, about the vertical torsion-wire axis, can be measured. The torsional rigidity of the wire was evaluated by means of a torsional pendulum, and may be expressed as a torsional spring constant (k) per unit length of wire. The result was

$$k = 1402 \ \frac{\text{gm mm}^2}{\text{radian}}$$

with a standard deviation of 4.0. Details of the calibration procedure are presented in Appendix A.

The angles of rotation of the three mirrors were determined by reflecting laser beams from the mirrors and measuring the beam displacements on a distant screen. In order to keep the tensile preload on the test specimen small, it was necessary to use mirrors weighing only a fraction of a gram. Light-beam oscillograph galvanometer mirrors fulfilled the requirements. These first-surface mirrors were rectangular, having a length and width of 3.14 and 0.64 mm respectively. The weight of one torsion mirror, complete with its torsion-wire mounting attachment, was approximately 0.10 gram.

The small size of the mirrors introduced an unanticipated optical problem. The laser light reflected from the mirrors was no longer well-collimated, but took the form of a rectangular aperture diffraction pattern, and the light impinging on the screen was an interference-fringe pattern rather than a small circular spot of light. Since accurate measurements in the horizontal direction were necessary, the problem was overcome by having the long-axis of the mirrors horizontal. This caused the fringe pattern to be acceptably narrow in the horizontal direction (approx. 3 mm wide), although quite lengthy in the vertical direction (approx. 30 mm long).

The laser beams were provided by means of a one-milliwatt 6328 angstrom Spectra-Physics laser and a three-way beam splitter. The three beams were directed onto auxiliary adjustable first-surface mirrors positioned in the laboratory to give convenient angles of incidence at the torsion test fixture.

Complications in the data-reduction procedure stemmed from two nonnegligible sources. Firstly, the incident light beams propagated from air through a glass plate and into the immersion medium, and the reflected beams propagated from the immersion medium, through the glass plate, and back into the air. Secondly, there was no means to accurately mount the mirrors in a vertical plane (i.e. parallel to the torsion-wire axis), and this misalignment necessitated the introduction of a complicated three-dimensional analysis of the change-in-path of the light beams with rotation of the mirrors about a vertical axis.

The effect of the glass plate may be neglected since it only caused a small offset of the beams, and not a change-in-direction. This leaves one to deal with an air/immersion medium interface and misaligned mirrors. A coordinate system was established so that the rectangular components of the three torsion-fixture mirrors and the three reflected points on the measurement screen could be determined. The coordinates of arbitrary points on each of the incident beams were also measured. This information, recorded both before and after application of torque increments, was sufficient to determine the angles of rotation of the mirrors about the torsion-wire axis. The analysis was rather lengthy, and is presented in Appendix B. A computer program was used to carry out the calculations.

The angle of twist across the test specimen was given directly by the incremental change in the angle θ of equation (B-13) computed for the specimen-twist mirror. The torque was calculated by subtracting the incremental angle-change of the upper-torque mirror from that of the lower-torque mirror and dividing the result by the distance between the mirrors to get the twist per unit length of the torsion-wire. Multiplying this figure by the torsional spring constant (k) gave the applied torque.

Uniaxial Strain Test

The uniaxial strain test fixture configuration was identical to that of the uniaxial stress tests except for the details in the immediate vicinity of the test specimen. The overall view of the tensile test equipment shown in Figure VI-5 is equally applicable for the uniaxial strain test. The details of the uniaxial strain test fixture are shown in Figure VI-11. It is instructive at this point to return to the schematic drawing of Figure V-3 in order to recall the basic geometry required for the uniaxial strain experiment.

The rigid containing structure of Figure V-3 was the corneal trephine of Figure VI-11 (see the detail photograph of Figure VI-12). It was a Castroviejo transplant trephine that cut a seven-millimeter diameter disc from the cornea. The foot of the trephine, which normally has a concave surface with a radius of curvature to match the central cornea, was filled with an epoxy resin and ground to a smooth flat surface. The trephine was clamped to a mounting bracket on the test fixture of Figure VI-11 by means of a clamping action that enabled quick installation with assured accurate alignment.

The plunger and guide assembly of Figure V-3 are shown in the close-up photograph of Figure VI-13. The plunger had a diameter of 2.53 mm, and the guide outside diameter was 6.63 mm. Both parts were made of aluminum, and the mating surfaces

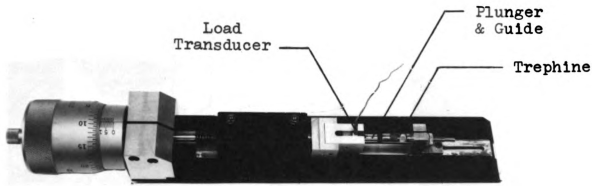

Figure VI-11. Uniaxial Compressive Strain Test Fixture

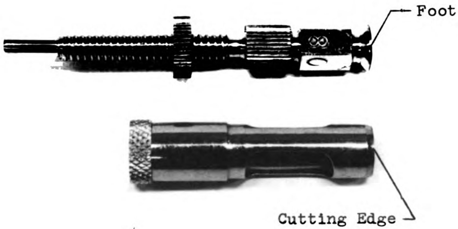

Figure VI-12. Corneal Trephine

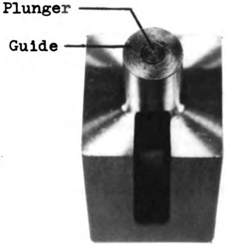

Figure VI-13. Plunger and Guide Assembly

were smoothly finished to minimize frictional effects. The same load transducer used in the uniaxial tensile stress experiments (see Figure VI-8) was used to measure the plunger load in the uniaxial strain tests. The transducer was clamped in a slot machined in the housing above the plunger and guide, and the upper end of the plunger was coupled to the loading stud of the transducer through a small ball-bearing seated in a detent in the end of the plunger. A small spring-clip compressed the ball between the stud and the plunger in order to assure that no backlash was present. The position of the transducer in the mounting slot was adjusted while viewing the bottom end of the plunger and guide assembly through a microscope, and the transducer was clamped in place when the end face of the plunger was aligned coincident with the face of the guide.

The complete transducer-plunger-guide assembly was coupled to the uniaxial strain fixture of Figure VI-11 by means of a clevis-type bracket and set-screw, and the assembly could be moved in the vertical direction in exactly the same manner as the upper specimen end restraint was displaced in the uniaxial tensile stress experiments. The same Tektronix equipment used for the tensile stress experiments was used in conjunction with the transducer to measure the plunger loads.

CHAPTER VII

EXPERIMENTAL PROCEDURES AND DATA

Introduction

All experiments were performed using mature pig corneas because these were readily available, and the pig eye is nearly the same as that of man except for overall size (see Chapter I). The Peet Packing Co. of Chesaning, Michigan cooperated by making eyes available on a daily basis. The eyes were shipped to the University - a distance of approximately 50 miles - by refrigerated truck, and were available within four-hours of the time of death. Unfortunately, it was not possible to remove the eyes until after the animal had passed through a scalding process (140 deg. F. water for five to tén minutes). Although the eyelids remained tightly closed during this time, there would be no justification for ignoring the possibility that mechanical properties of the corneal stroma may have been altered.

A limited number of pig eyes were available within the University. The Meats Laboratory of the Food Science Department slaughtered several pigs in the course of this research, and the eyes of these animals were enucleated immediately after death, prior to the scalding process.

If one attempts to store corneal tissue in the presence of aqueous solutions, it will swell profusely regardless of the salinity. This swelling would have been unacceptable, because in order to get stress-strain information indicative of the in vivo cornea it was necessary that no dimensional changes take place. The problem was solved by using mineral oil as an immersion medium, both during storage at reduced temperature, and during the tests which were performed at the in vivo temperature.

Immediately upon receiving eyes an incision was made through the sclera, along the equator, and only the anterior hemisphere was retained. The contents (i.e. vitreous humor, ciliary process, lens, aqueous humor, etc.) were removed, and the remaining shell, composed of the cornea and adjacent sclera, was immersed in mineral oil. The specimen was refrigerated at 50 deg. F. until tested. The mineral oil was not imbibed by the stroma, and the moisture content (thickness) remained constant during storage because the mineral oil eliminated evaporation of water from the tissue. During the tests the mineral oil was held at approximately 91.5 deg. F. According to the measurements of Lele and Weddell[27] this is one degree warmer than the anterior surface temperature of the human cornea, therefore it seemed a reasonable immersion temperature.

The Kulite load transducer (see Figure VI-8) was dead-weight calibrated using a set of gram-weights. For the uniaxial tensile stress calibration the weights were suspended from the end of the upper specimen end restraint. The compression calibration for the uniaxial strain test was carried out with the transducer mounted in the test configuration except that it was adjusted so that the plunger extended approximately 0.5 mm beyond the end of the guide (see Figure VI-13). This adjustment enabled the gram-weights to be placed on the plunger so as to load the transducer in the same manner as during the actual tests. The transducer response in both tension and compression was linear in the load range of interest.

Uniaxial Tensile Stress Test

Uniaxial tensile stress tests were conducted using strips of cornea having nominal widths of 2.4 and 3.5 mm. The strips were cut using the double-blade knife described in Chapter VI. The pig cornea is somewhat pear-shaped, and all specimens were cut from the direction yielding a strip of maximum length. Approximately two-to-three mm of sclera was retained at the ends of the strip to serve as points for clamping on the end restraints, and the epithelium and endothelium were removed by gently scraping with a sharp scalpel.

Immediately after preparing the strip the excess mineral oil was blotted from the surfaces, and the specimen was placed on the thickness measuring fixture of Figure VI-2. The mid-length thickness was measured with four replications, and the thickness at each end of the strip, approximately two-to-three mm from the limbus, was measured with three replications.

During this process the specimen was handled at the scleral ends with tweezers, and immediately after completion of the measurements additional mineral oil was spread on the strip in order to guard against dehydration.

The two end restraints (see Figure VI-7) were temporarily affixed to a small jig that approximated the juxtaposition necessary for insertion of the corneal strip. The ends of the strip were aligned in the end restraints and clamped in place, after which the two end restraints were removed from the jig and pinned to the test fixture as shown in Figure VI-6 (the test strip was in a "limp" conditions at this point).

Next the test fixture was inserted into the immersion tank of mineral oil, and clamped in place by means of two thumb-screws. After waiting several minutes for temperature stabilization, the transducer strain gage bridge was balanced and the specimen was quickly elongated until a small load of approximately 0.2 gram was applied (This small load immediately began to diminish due to viscoelastic effects). For lack of a more specific criterion, after the specimen had relaxed for approximately 15 minutes, this was referred to as the zero load-zero elongation initial condition for the ensuing test.

The measuring microscope of Figure VI-3 was used next in order to determine the length and exact width of the test specimen. The length was defined as the distance between the adjacent ends of the two end restraints. The width was measured at three positions on the specimen - at midlength of the strip and also 0.10 inch from each of the end restraints. The length measurement was replicated three times and each of the three width measurements was replicated twice.

The above measurement procedure required approximately 15 to 20 minutes, and after this time the load transducer bridge was rebalanced and a series of elongations were applied. It was found that a time increment of 15 minutes was sufficient for the transient viscoelastic effects to decay to a negligible magnitude. The elongation increments were limited to 1.0 and 2.0 percent of the initial length of the specimen, and the tensile load and specimen width at midlength were measured and recorded for each increment (always after the 15 minute relaxation). This data enabled the load versus elongation and width versus elongation curves of Figures C-1 through C-8 to be plotted. It will be shown in Chapter VIII that it is the slope of the linear portion of the curves that is of interest, therefore the slopes are presented in Table VII-1 along with other pertinent information regarding the specimens. It was estimated that a standard deviation of 0.01 mm may be associated with each of the length measurements, and that standard deviations of 0.2 gm/mm and 0.03 mm/mm may be associated with each of the load versus elongation and width versus elongation slopes.

Specimens 70 and 76 were used to examine the reversibility of the deformation process by subjecting the same specimen to two identical tensile tests, the second test being conducted after the specimen had recovered for one

Table VII-1. Uniaxial Tensile Stress Test Data

Specimen Number	Source	Hours Since Death	Length (mm)	Average Width (mm)	Average Thickness (mm)	Std. Deviation Width (mm)	Std. Deviation Thickness (mm)	Slope** Load Vs. Elongation (gm/mm)	Slope** Width Vs. Elongation (mm/mm)
26	Peet	30	17.88	2.52	.96	.28	.06	10.67	-0.97
27	Peet	32	16.43	2.46	.95	.13	.04	8.51	-1.08
28	Peet	36	17.15	2.31	1.03	.06	.03	7.40	-0.87
29	Peet	38	15.82	2.31	.84	.14	.03	15.70	-0.86
30	Peet	51	17.22	2.29	.98	.05	.03	6.78	-0.94
31	Peet	53	17.02	2.45	.94	.16	.03	4.86	-0.63
32	Peet	11	16.18	3.54	.93	.11	.05	14.62	-1.33
33	Peet	14	17.58	3.50	.96	.18	.03	10.17	-1.39
34	Peet	31	17.78	3.45	1.10	.14	.04	8.12	-0.94
35	Peet	33	18.80	3.40	1.09	.14	.03	15.39	-0.97
37	Peet	25	17.65	3.53	1.09	.24	.03	8.68	-1.06
38	Peet	28	17.17	3.62	1.04	.30	.05	11.56	-1.24
65	Meats Lab	5	18.77	3.28	.86	.04	.03	14.75	-1.09
66	Meats Lab	8	17.58	3.37	.88	.16	.06	11.42	-0.68
67	Meats Lab	11	17.63	3.35	.84	.07	.03	11.42	-0.66
68	Meats Lab	24	17.78	3.53	.85	.10	.03	17.50	-1.37
69	Meats Lab	26	17.32	3.53	.86	.13	.14	16.14	-1.18
70 *	Meats Lab	55	16.76	3.15	.91	.09	.04	-	-

Table VII-1 (cont'd.)

Specimen Number	Source	Hours Since Death	Length (mm)	Average Width (mm)	Average Thickness (mm)	Std. Deviation Width (mm)	Std. Deviation Thickness (mm)	Slope** Load Vs. Elongation (gm/mm)	Slope** Width Vs. Elongation (mm/mm)
71	Meats Lab	34	16.64	2.44	.89	.07	.03	8.08	-1.09
72	Meats Lab	38	16.94	2.39	.95	.04	.02	5.37	-0.78
73	Meats Lab	48	19,13	2.40	.84	.07	.03	9.03	-1.20
74	Meats Lab	50	17.15	2.37	.89	.03	.02	6.06	-0.84
75	Meats Lab	52	17.42	2.30	.97	.07	.02	6.06	-0.93
76 *	Meats Lab	54	18.52	2.34	.89	.05	.03	-	-

* Specimens 70 and 76 were used to check the reversibility of the load vs. elongation process.

** Physiologically normal range and above (righ-hand portion of curve).

hour with the elongation set to zero. The load versus elongation data for these specimens are plotted in Figures C-9 and C-10.

Torsion Test

The torsion test specimens had the same nominal dimensions as the uniaxial tensile stress specimens, and were prepared following the same procedures, including thickness measurement and attachment of the end restraints. The end restraints were pinned to the test fixture as shown in Figure VI-10, and after a brief series of fixture alignments the assembly was installed in the immersion tank of Figure VI-9. The tensile preload on the test specimen was in force immediately upon installing the specimen in the test fixture. Length and width measurements were made using the measuring microscope in the same manner as for the uniaxial tensile stress tests.

Upon completing the mensuration process, the laser was turned on and a series of preliminary optical adjustments of the torque and specimen twist measuring system were made. The auxiliary mirrors were adjusted so that the light beams propagated through the immersion tank window and impinged on the test fixture mirrors, and the complete test specimen and torsion-wire assembly was rotated so that the light beams propagated outward from the immersion tank in a direction approximately perpendicular to the glass window (the incident beams also had nearly this same azimuth). The light beams propagating from the fixture impinged on the measuring screen, which was in a plane parallel to the immersion tank window and located approximately 3.4 meters from the torsion-wire axis (the screen was actually the wall on the opposite side of the room).

The light beam positions on the screen were unstable because of air currents in the room and building vibration. Placing the test fixture on a resilient mounting helped to some degree, but it was necessary to apply a small preload torque to the specimen to reduce the vibration to an acceptable level. The preload was equivalent to a test specimen twist angle of approximately 4 to 5 degrees.

The coordinates of points on the incident beams were measured with a scale and tripod-mounted plumb bob, and the reflected-beam coordinates were measured from the screen after a time-interval of 15 to 20 minutes had elapsed from the time of preload application. Three increments of specimen twist, each of approximately 0.07 radian magnitude were applied successively at 15 minute intervals, and screen-coordinates of the three light beams were recorded at the end of each interval.

The data reduction procedure presented in Appendix C was required to convert the light beam coordinate experimental data into twist-angle and torque information. The procedure was lengthy, and required the use of a computer program. The results were somewhat disheartening because for many of the tests the maximum applied torque was below the limit of resolution of the system. Discussion regarding this matter will be presented in Chapter VIII. A precision analysis indicated that the limit of resolution of the system was at best 0.008 gm mm torque, and any torque below this value was discarded from the analysis. In order to treat the remaining data in an unbiased manner, the following procedure was adhered to:

1. All first-increment torque data was discarded because the values were generally near or below the limit-of-resolution of the system.
2. The average twist angle and average torque was computed for each specimen, and the torsional rigidity (gm mm/radian) was expressed as the quotient of this torque divided by this twist.

The individual data points are presented in Figure C-11, and the torsional rigidities are listed in Table VII-2 along with other pertinent information regarding the specimens. All discarded specimen data are included in the Table for completeness. The standard deviation of the length measurement may be taken as 0.01 mm (the same as for the uniaxial tensile stress tests), and it was estimated that a standard deviation of 0.08 gm mm/rad may be associated with each of the torsional rigidities.

Uniaxial Strain Test

Uniaxial compressive strain tests were conducted using circular disc specimens cut from the central cornea with the trephine shown in Figures VI-11 and VI-12. The epithelium and endothelium were removed from the cornea by gently scraping with a sharp knife, and the trephine was used in the normal manner (lightly pressing the blade into the tissue while continuously

Table VII-2. Torsion Test Data

Specimen Number	Source	Hours Since Death	Length (mm)	Average Width (mm)	Average Thickness (mm)	Std. Deviation Width (mm)	Std. Deviation Thickness (mm)	Tensile Preload (gm)	Torsional Rigidity (gm mm/rad)
39	Peet	12	18.03	3.48	.97	.03	.08	3.11	.232
40	Peet	30	19.58	2.02	1.01	.27	.09	3.11	*
41	Peet	27	18.64	3.30	.94	.15	.04	3.11	*
42	Peet	14	18.95	3.23	1.03	.10	.05	3.11	.046
43	Peet	5	19.05	3.45	.95	.07	.05	3.11	*
44	Peet	32	19.00	1.97	.86	.23	.06	3.11	*
45	Peet	28	19.94	2.26	1.01	.12	.04	3.11	*
46	Peet	8	20.57	3.32	.97	.14	.09	3.11	*
47	Peet	10	20.17	3.49	.98	.06	.07	3.11	.177
48	Peet	12	19.71	2.21	.99	.09	.07	3.11	*
49	Peet	33	17.73	2.24	.92	.05	.05	3.11	*
50	Peet	37	19.20	2.20	.98	.23	.07	3.11	.112
51	Meats Lab	17	18.39	3.22	.86	.07	.03	3.11	.065
52	Meats Lab	19	17.27	3.21	.84	.13	.04	3.11	*
53	Meats Lab	20	19.38	3.47	.93	.09	.04	3.11	.120
54	Meats Lab	24	18.29	3.45	.81	.20	.03	3.11	.047
55	Meats Lab	26	17.78	3.20	.85	.06	.03	3.11	*
56	Meats Lab	29	18.31	3.31	.87	.11	.02	3.11	.046
57	Meats Lab	44	17.86	3.29	.87	.19	.05	3.11	.134

Table VII-2 (cont'd.)

Specimen Number	Source	Hours Since Death	Length (mm)	Average Width (mm)	Average Thickness (mm)	Std. Deviation Width (mm)	Std. Deviation Thickness (mm)	Tensile Preload (gm)	Torsional Rigidity (gm mm/rad)
58	Meats Lab	43	19.43	3.13	.87	.10	.03	3.11	*
59	Peet	32	17.58	3.51	1.17	.08	.04	7.20	.383
60	Peet	34	19.48	3.32	1.15	.13	.05	7.20	**
61	Peet	36	17.88	3.43	.96	.09	.03	7.20	.459
62	Peet	38	19.10	3.36	1.21	.06	.03	7.20	**
63	Peet	27	18.92	3.42	1.13	.17	.04	7.20	.426
64	Peet	52	18.14	3.02	1.11	.16	.04	7.20	.366

* Below the limit of resolution of the system.

** Suspected end-restraint slippage.

rotating the trephine).

The trephine and specimen were mounted in the test fixture as shown in Figure VI-11, and the plunger and guide assembly was displaced downward sufficiently so that the lower face had entered into the end of the trephine. The fixture was then installed in the immersion tank and allowed to temperature-stabilize for several minutes, after which the plunger and guide assembly was lowered until a plunger load of approximately 0.2 grams was achieved. This criterion was used to define the zero displacement condition, and after allowing a relaxation period of approximately 15 minutes the load transducer bridge was re-balanced and a series of compressive displacements were applied at 15 minute intervals. The resulting plunger load versus displacement data are presented in the curves of Figures C-12 and C-13. The reversibility of the deformation process was examined by subjecting the same specimen to two identical uniaxial strain tests, the second test having been conducted after the specimen had recovered for one and one-half hours with the compressive displacement set to zero. The plunger load versus displacement data for these specimens are plotted in Figures C-14 and C-15.

An initial attempt was made to measure the thickness of the disc-shaped specimens immediately after installing the trephine in the test fixture. The procedure was to back-off the trephine-handle locknut and rotate the handle until the foot of the trephine had threaded itself upward to expose the edges of the test specimen, after which optical measurements using the measuring microscope were attempted. Unfortunately the edges of the specimen had been sufficiently distorted from the cutting process that representative measurements could not be obtained.

An alternate source of thickness information was considered more reliable. The average value of the central corneal thickness of all of the tensile and torsion test specimens was used. The average value of the thickness was 0.989 mm with a standard deviation of 0.13 mm.

It will be shown in Chapter VIII that the slope of the linear portion of the plunger load versus displacment curves is the information of interest, and this is presented in Table VII-3 along with additional specimen information. It was estimated that the standard deviation of each of the slopes may be taken as 1.0 gm/mm.

Table VII-3. Uniaxial Strain Test Data

Specimen Number	Source	Hours Since Death	Slope (gm/mm)
77	Meats Lab	73	100.0
78	Meats Lab	77	51.2
79 *	Meats Lab	79	47.4
80	Meats Lab	83	74.3
81	Meats Lab	96	102.0
82	Meats Lab	99	98.0
83 *	Meats Lab	101	-
84	Peet	12	42.5
85	Peet	14	50.2
86	Peet	28	48.7
87	Peet	31	51.5
88	Peet	33	43.5
89	Peet	37	86.0

* Specimens 79 and 83 were used to check the reversibility of the load vs. deflection process.

CHAPTER VIII

RESULTS AND CONCLUSIONS

Linearity

The problem formulation of this research was based on the premise that a linear theory was applicable, and it was indicated in the previous Chapter that the slopes of the linear region of the experimental curves (load versus elongation, etc.) were the data of interest. Some simple calculations can be used to show that the linear region of the curves may be associated with the range of corneal stresses caused by intraocular pressure loading.

Dimensional and pressure information for the human eye are given by Davson (see Ref. 3, pp. 158, 161, 290 and 291). The radius of curvature of the outer surface of the central cornea may be taken as 7.86 mm, and the thickness is 0.54 mm. A value of 16 mm Hg is representative of the normal intraocular pressure, and this may rise as high as 80 mm Hg in cases of angle-block glaucoma.

To calculate order-of-magnitude stresses in the cornea it is reasonable to assume the stresses are equal to those of a thin-walled sphere having the same mean radius and thickness as the central cornea, and an internal pressure equal to that of the intraocular pressure. The strength-of-materials solution for the in-plane tensile stress (σ) is simply

$$\sigma = \frac{\pi r^2 p}{2\pi r h} = \frac{rp}{2h}$$

where r, h, and p are the mean radius, thickness, and internal pressure respectively.

The normal intraocular pressure of 16 mm Hg is equivalent to 0.218 gm/mm^2, therefore the tensile stress in the cornea may be taken as

$$\sigma = \frac{(7.86 - 0.67)(0.218)}{2(0.54)} = 1.53 \text{ gm/mm}^2.$$

The average thickness and width of the tensile test specimens were as follows:

Thickness: 0.939 mm

$$\text{Width}\begin{cases}\text{Narrow Specimens:} & 2.38 \text{ mm}\\ \text{Wide Specimens:} & 3.44 \text{ mm}\end{cases}$$

These measurements lead to the following tensile loads necessary to produce a uniaxial tensile stress of 1.53 gm/mm^2:

Narrow Specimens: 3.42 gm

Wide Specimens: 4.94 gm.

The 3.42 and 4.94 gm loads associated with normal intraocular pressure fall on the linear portion of the load versus elongation curves of Figures C-1 through C-4, and furthermore if the elongations at these loads are located on width versus elongation curves of Figures C-5 through C-8, the points fall on the linear portion of these curves.

A similar analysis may be carried out for the uniaxial strain data. The normal intraocular pressure of 1.53 gm/mm^2

may be converted to an equivalent plunger load by multiplying by the cross-sectional area of the plunger. The plunger diameter was 2.53 mm, therefore the plunger load (P) associated with normal intraocular pressure may be taken as

$$P = \frac{\pi(2.53)^2}{4}(1.53) = 7.69 \text{ gm.}$$

It must be remembered that although a pressure of 1.53 gm/mm^2 is acting at the posterior surface of the cornea, the pressure is zero at the anterior surface, therefore in an order-of-magnitude sense it seems more realistic to use one-half of the above 7.69 gram plunger load as a representative value for the cornea in vivo. It may be seen in Figures C-12 and C-13 that the half-value of 3.85 gm falls on the linear portion of the load versus displacement curves.

The torsion test data has already been treated in a linear manner due to lack of resolution of the test equipment, and nothing can be added here to further justify the action taken.

In conclusion, it appears that the linearity assumption was acceptable over the physiologically important range of loads.

Reversibility

In addition to linearity it was assumed that the deformation process is completely reversible. This assumption may be justified by the observation that the in vivo eye undergoes reversible deformation as the intraocular pressure fluctuates (for example in the water-test for glaucoma where the intraocular pressure commonly undergoes a transient fluctuation of 10 mm Hg over an interval of an hour or two). It was of interest to establish the degree of reversibility of the deformations in the uniaxial tensile stress experiments and the uniaxial strain experiments.

One could not expect complete reversibility, as observed in vivo, because the aqueous solution impregnating the tissue could not flow out of the specimens, and then back in, in a reversible manner. This was evidenced by the formation of small water droplets on the surfaces of the tensile specimens during elongation, and the fact that the droplets remained after the elongation had been reduced to zero. Figures C-9 and C-10 for the uniaxial tensile stress experiments, and Figures C-14 and C-15 for the uniaxial compressive strain experiments, show the degree of reversibility that was retained. This does not imply that the load versus deformation curves are not representative of the in vivo tissue, however, because the initial mode of deformation, where moisture was forced out of the tissue, would remain unchanged regardless of the nature of the reversibility of the process.

Statistical Procedures

Before proceeding with the analysis it is timely to discuss the method of error analysis used. The simplifying assumption was made that all statistical distributions were normal, and the propagation of errors resulting from the use of equations in the data reduction procedure were accounted for by using elementary statistical analysis. Suppose one has a function f of several variables $(u,v,w,\ldots)$ of the form

$$y = f(u,v,w,\ldots). \tag{8-1}$$

Let the standard deviations of $u,v,w,\ldots$ be denoted by $S_u, S_v, S_w, \ldots$, and let the resulting standard deviation of y be denoted S_y. Then it can be shown[28] that

$$S_y^2 = \left(\frac{\partial f}{\partial u}\right)^2 S_u^2 + \left(\frac{\partial f}{\partial v}\right)^2 S_v^2 + \left(\frac{\partial f}{\partial w}\right)^2 S_w^2 + \cdots. \tag{8-2}$$

In the following material the standard deviations of all calculated quantities were evaluated using eqs. (8-1) and (8-2), and if S is the standard deviation of X the convention of writing this as $X \pm S$ has been adhered to.

Final Analysis

The uniaxial tensile stress test data of Table VII-1 were used to calculate the apparent Young's modulus E_a and the apparent Poisson's ratio μ_a (see p. 67). Let the load versus elongation slope and the width versus elongation slope be denoted as follows:

Load vs. elong.: $\left(\frac{dP}{d\ell}\right)$

Width vs. elong.: $\left(\frac{dW}{d\ell}\right)$

Then the nominal values of E_a and μ_a are given by the expressions

$$E_a = \frac{\ell}{Wh}\left(\frac{dP}{d\ell}\right)$$

$$\mu_a = -\frac{\ell}{W}\left(\frac{dW}{d\ell}\right)$$

where ℓ, w, and h are the original (unloaded) values of the test specimen length, width, and thickness respectively. The results are shown in Table VIII-1.

Cumulative results are shown in Table VIII-2 where the data from similar types of test specimens have been grouped in several manners in order that the effects of the various test specimen characteristics may be observed. Since the standard deviations are quite large it is unwise to draw any strong conclusions regarding dependence of E_a and μ_a on the variables tabulated, and the results for "all specimens" will be used in forthcoming calculations; that is,

$$E_a = 66.32 \pm 24.14 \text{ gm/mm}^2$$

$$\mu_a = 5.90 \pm 1.38$$

The above values of E_a and μ_a may be substituted into the first two of eqs. (5-24) to evaluate the parameters E_A and E_B. The result is

$$\left.\begin{aligned} E_A &= -15.69 \pm 9.47 \text{ gm/mm}^2 \\ E_B &= -92.59 \pm 25.60 \text{ gm/mm}^2 \end{aligned}\right\} \qquad (8\text{-}3)$$

The shortcomings of the torsion test were already pointed out in Chapter VII, and it seems reasonable to expect the data to indicate only trends and order-of-magnitude quantitative results.

The torsion test data of Table VII-2 may be used to evaluate the parameter E_C by applying the last of eqs. (5-24), and in addition the tensile stress in the specimen may be

Table VIII-1. Young's Modulus and Poisson's Ratio

Specimen Number	Source	Size	Young's Modulus E_a (gm/mm^2)	Poisson's Ratio μ_a (unitless)	Std. Deviation E_a (gm/mm^2)	Std. Deviation μ_a (unitless)
26	Peet	Narrow	79.00	6.89	10.32	.21
27			60.05	6.80	4.30	.19
28			53.07	6.32	2.39	.22
29			127.91	5.56	9.01	.19
30			52.21	6.87	2.59	.22
31			35.79	4.07	3.09	.19
32		Wide	71.52	5.87	4.78	.13
33			52.92	6.66	3.46	.15
34			38.00	4.61	2.40	.18
35			77.88	5.11	4.08	.16
37			39.77	4.87	3.11	.14
38			52.56	5.32	5.11	.13

Table VIII-1. (cont'd.)

Specimen Number	Source	Size	Young's Modulus E_a (gm/mm^2)	Poisson's Ratio μ_a (unitless)	Std. Deviation E_a (gm/mm^2)	Std. Deviation μ_a (unitless)
71	Meats Lab.	Narrow	62.11	7.57	2.90	.21
72			40.03	5.49	1.90	.21
73			85.45	9.21	4.09	.23
74			49.47	6.13	2.07	.22
75			47.28	7.28	2.31	.24
65		Wide	98.21	6.11	4.01	.17
66			67.45	3.36	5.97	.15
67			71.44	3.36	3.10	.15
68			104.35	6.71	4.42	.15
69			92.64	5.55	3.89	.14

Table VIII-2. Young's Modulus and Poisson's Ratio by Groups

Specimen Group	Average E_a (gm/mm^2)	Average μ_a (unitless)	Std. Deviation E_a (gm/mm^2)	Std. Deviation μ_a (unitless)
All narrow Peet	68.00	6.08	32.50	1.11
All wide Peet	55.44	5.41	16.29	0.75
All narrow & wide Peet	61.72	5.74	25.32	0.97
All narrow Meats Lab.	56.87	7.14	17.85	1.44
All wide Meats Lab.	86.82	5.02	16.45	1.57
All narrow & wide Meats Lab.	71.84	6.08	22.61	1.80
All narrow specimens	62.94	6.56	26.26	1.32
All wide specimens	69.70	5.23	22.57	1.14
All specimens	66.32	5.90	24.14	1.38

evaluated by dividing the tensile preload force by the cross-sectional area. The results of these calculations are presented in Table VIII-3. The data of Table VIII-3 is plotted in Figure VIII-1, and the least-squares straight line is shown. It appears that the torsional properties are dependent on the magnitude of the tensile preload stress, a result not predicted by the theoretical analysis.

The theory of Chapter V lead to eq. (5-26) which requires

$$E_C = \frac{1}{2}(E_A - E_B),$$

thus if the values of E_A and E_B given by eqs. (8-3) are applied it is predicted that $E_C = 38.45 \pm 13.7$ gm/mm^2. If a number is to be assigned to E_C from the torsion test results, it is reasonable to select the point on the least-squares line of Figure VIII-1 that is representative of the stress due to normal intraocular pressure. This stress was calculated earlier in the Chapter to be 1.53 gm/mm^2, and yields a value of $E_C = 123 \pm 50$ gm/mm^2 which is too large by a factor of 3.2 $\pm$ 1.7.

The uniaxial strain data of Table VII-3 may be used to evaluate the elastic constant C_{22} by applying eq. (5-28). As discussed in the previous Chapter, the thickness (h) of the specimen is to be taken as 0.989 mm with a standard deviation of 0.13 mm. The diameter (d) of the plunger was 2.53 mm with an estimated standard deviation of 0.005 mm. In eq. (5-28) the area (A) is given by

Table VIII-3. Torsion Test Results

Specimen Number	Tensile Preload Stress (gm/mm^2)	E_C (gm/mm^2)	Std. Deviation E_C (gm/mm^2)
39	.92	127.7	54.2
42	.94	23.8	41.5
47	.91	103.1	51.6
50	1.44	100.1	75.4
51	1.13	56.5	69.8
53	.96	80.1	54.4
54	1.12	45.8	78.2
56	1.08	36.94	64.3
57	1.09	105.3	65.7
59	1.75	115.2	26.9
61	2.19	261.6	52.2
63	1.86	155.1	34.3
64	2.15	153.8	38.4

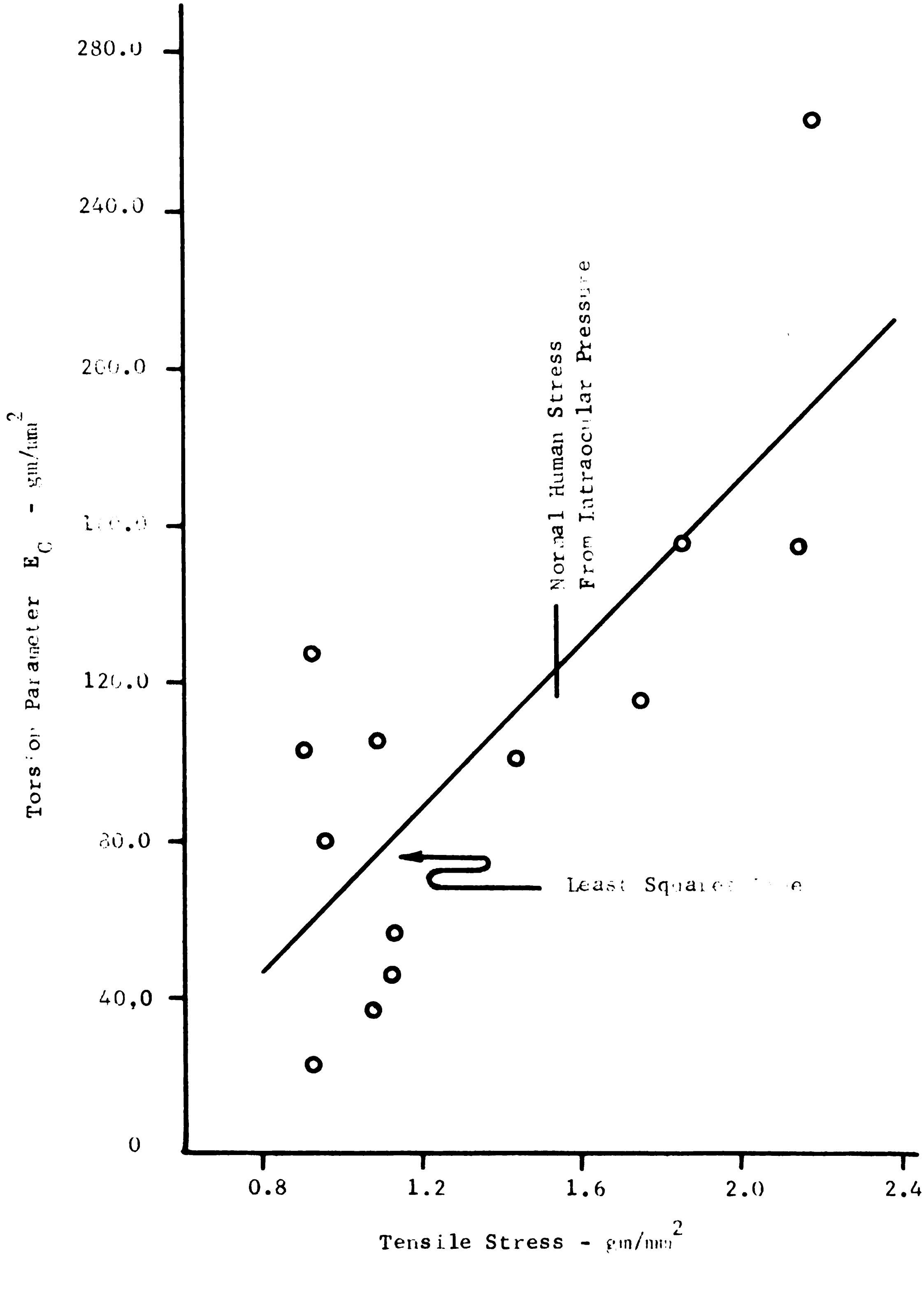

Figure VIII-1. Torsion Parameter E_C Versus Tensile Preload Stress

$$A = \frac{\pi d^2}{4}$$

therefore

$$C_{22} = \frac{4h}{\pi d^2}(\frac{\Delta P}{\Delta h}).$$

The results of the calculations are presented in Table VIII-4. Cumulative results were calculated by grouping the data as previously done for the uniaxial tensile test analysis, and the information is shown in Table VIII-5.

The results of Table VIII-5 tend to indicate quite strongly that the Peet Packing Co. test specimens have a reduced uniaxial compressive strain rigidity as compared to the Meats Laboratory specimens. It must be remembered, however, that the total number of specimens tested was small, and the discrepancy could possibly reduce with increasing specimen quantity. The plausible reason for the reduced rigidity of the Peet specimens is that Meats Laboratory eyes were enucleated prior to the scalding bath operation, whereas Peet eyes were not. Since results indicative of in vivo tissue are desired, the cululative Meats Laboratory value of $C_{22} = 15.55 \pm 4.93$ gm/mm^2 will be used in all forthcoming calculations.

Combined Results of Theory and Experiment

The numerical values of E_A, E_B, and C_{22} may be substituted into eqs. (5-30) to obtain expressions for C_{11} and C_{23} in terms of C_{12} and C_{55}. The following values are appropriate:

Table VIII-4. Uniaxial Strain Test Results

Specimen Number	Source	C_{22} (gm/mm^2)	Std. Deviation (gm/mm^2)
77	Meats Lab.	19.73	2.68
78		10.10	1.38
79		9.35	1.28
80		14.66	1.99
81		20.12	2.73
82		19.33	2.62
84	Peet	8.38	1.15
85		9.90	1.35
86		9.61	1.32
87		10.16	1.39
88		8.58	1.18
89		16.97	2.30

Table VIII-5. Uniaxial Strain Test Cumulative Results

Specimen Group	C_{22} (gm/mm^2)	Std. Deviation (gm/mm^2)
All Meats Lab.	15.55	4.93
All Peet	10.60	3.20
All Specimens	13.07	4.73

$$E_A = -15.69 \pm 9.47 \ \text{gm/mm}^2$$

$$E_B = -92.59 \pm 25.60 \ \text{gm/mm}^2$$

$$C_{22} = 15.55 \pm 4.93 \ \text{gm/mm}^2 \ .$$

Equations (5-30) become

$$\begin{aligned} C_{11} &= 5.69 - 2C_{55} + \frac{C_{12}^2}{15.55} + 15.55(Q^2 + 2Q) \\ C_{23} &= 15.55(1 + Q) \end{aligned} \qquad (8\text{-}4)$$

where

$$Q = \frac{C_{55} + 16.38}{C_{12}}$$

and all the C_{ij} are expressed in units of gm/mm^2.

The data reduction procedure cannot be catried further because two additional independent relationships among the elastic constants are needed. Comments regarding this matter are included in the following section of this Chapter.

It is interesting to select hypothetical values for C_{12} and C_{55} and compute the resulting elastic constants. In Chapter V the analysis of the small shear rigidity of the stroma indicated that the elastic constant C_{55} is likely to be small compared to the other constants, therefore it is logical to compute the C_{ij} and E_{ij} over a reasonable range of assumed C_{12} values while incrementing C_{55} from zero. Figures VIII-2 through VIII-6 show families of curves of C_{ij} and E_{ij} versus C_{12} for several values of C_{55}.

It is easily shown that

$$E_{12} = -(C_{55} + 16.38)$$

and therefore it is predicted that one of the elastic constants is negative. It can also be shown that

$$(C_{22} - C_{23}) = -(\frac{C_{55} + 16.38}{C_{12}})$$

therefore if C_{55} is assumed positive, then both E_{12} and $(C_{22} - C_{23})$ are negative. This matter is covered further in the Discussion.

Discussion

The research has been fully presented at this point; however some discussion of the work is in order. Additional simple tests enabling complete evaluation of the elastic constants are beyond the scope of this Thesis. Information regarding the shear constants C_{55} and $(C_{22} - C_{23})$ could perhaps be obtained by analyzing some type of shear test of a stroma specimen (full thickness), and additional information might be given by the solution of the elastic shell problem of the cornea constrained around the periphery and loaded on the posterior surface by the intraocular pressure. The latter possibility would be a full-scale boundary value problem of the theory of shells, and would be difficult.

In deriving the stress-strain constitutive relation, the existence of an elastic potential V was assumed (see p. 40).

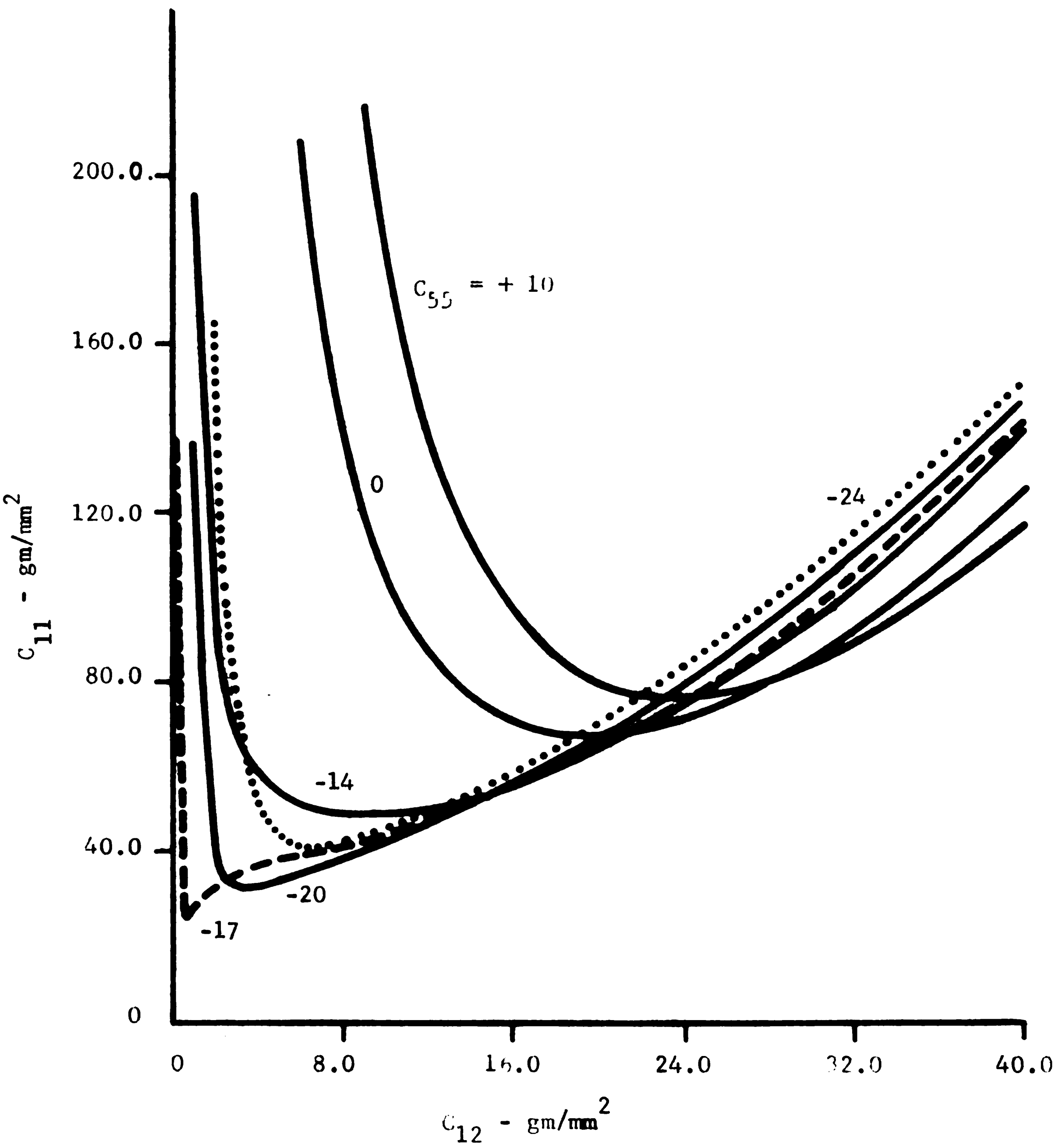

Figure VIII-2. Elastic Constant C_{11} Versus C_{12}

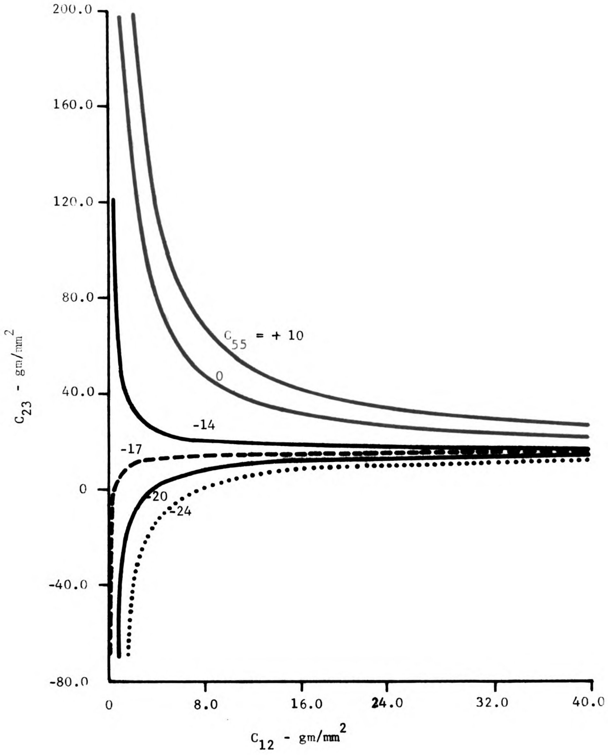

Figure VIII-3. **Elastic Constant** C_{23} Versus C_{12}

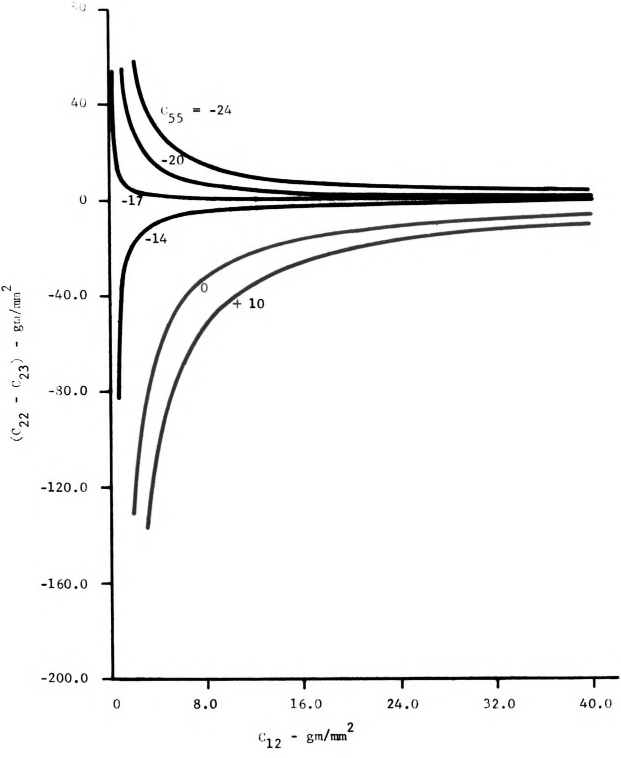

Figure VIII-4. **Elastic Constant** $(C_{22} - C_{23})$ Versus C_{12}

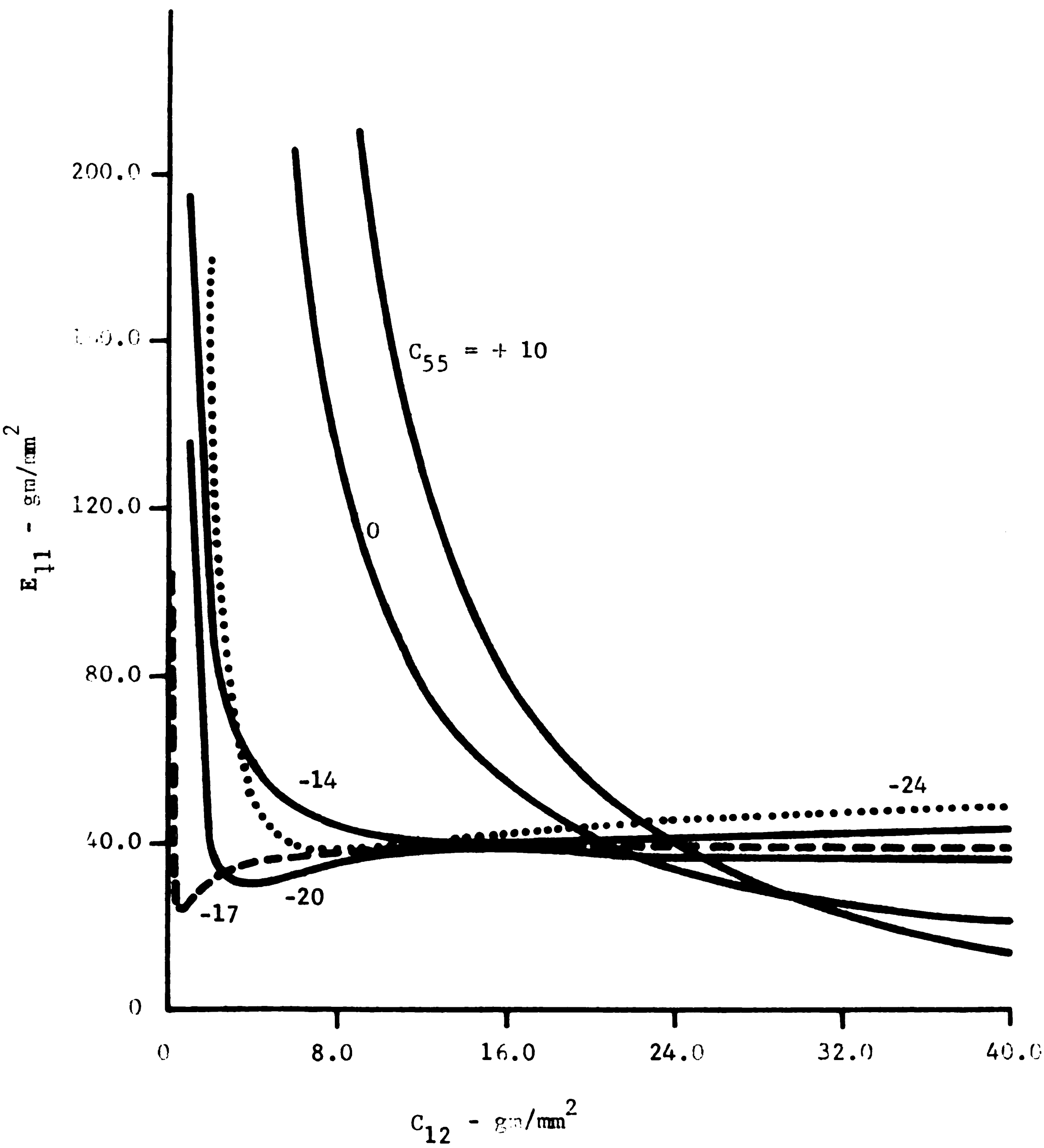

Figure VIII-5. **Elastic Constant E_{11}** Versus C_{12}

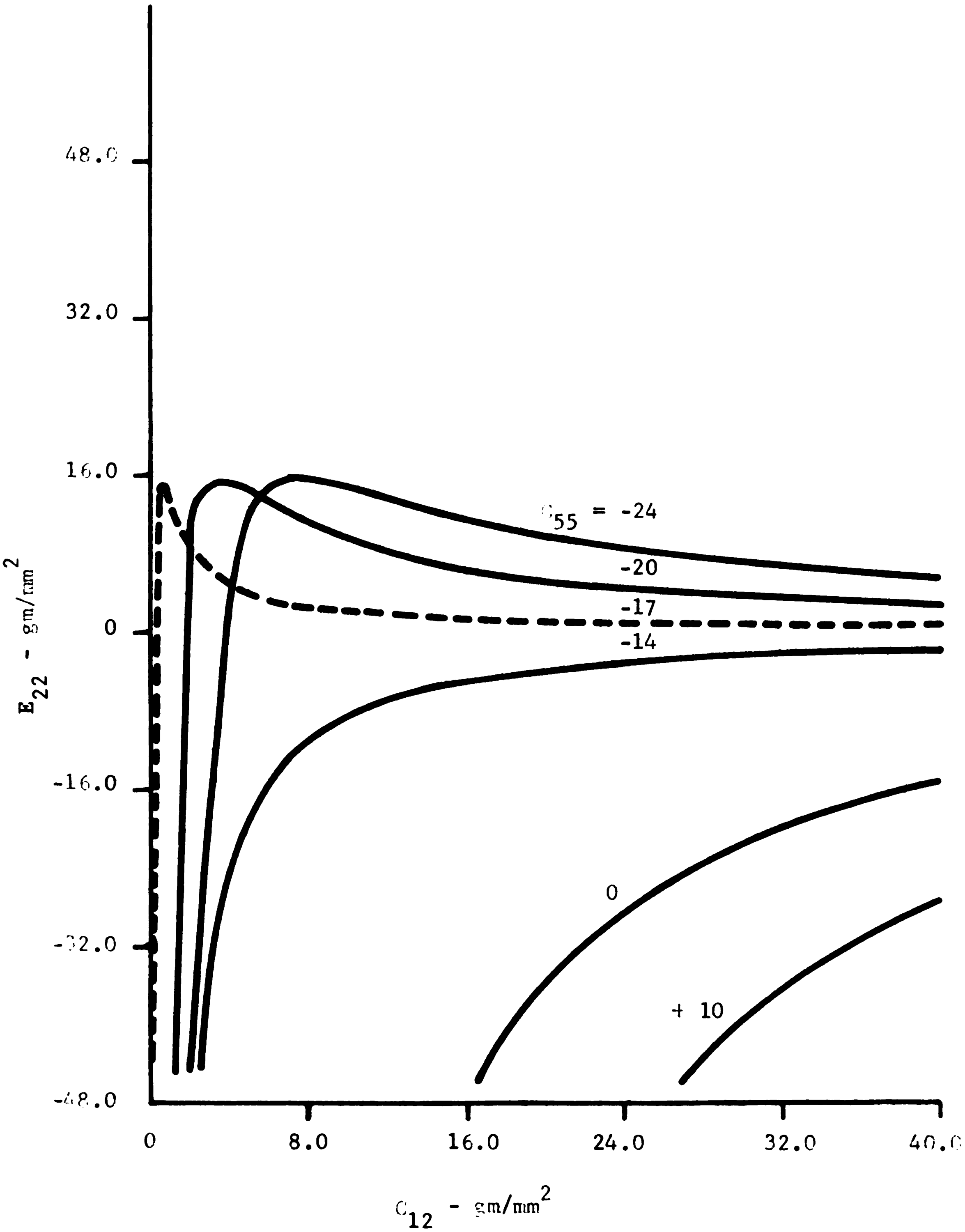

Figure VIII-6. **Elastic Constants** E_{22} Versus C_{12}

Strain-energy arguments of the theory of elasticity show that V must be "positive definite," and this implies that the elastic constants C_{ij} and E_{ij} are non-negative. It was shown at the top of page 133 that negative constants are predicted, and therefore the analytical model for the material is not adequate in its present form. Additional research must be carried out using these results as a basis for postulating a more appropriate theory.

For this reason it seems appropriate to recapitulate and present a comprehensive list of assumptions made in developing the analytical formulation. The assumptions are listed in Appendix D, and are in the same order as they appear in the text. Page numbers are included for convenience.

The discussion of the pressure distribution of the intraocular fluid given in Chapter III is an important development in its own right. It appears to be the first analysis using the notion of porosity, along with pressure equilibrium equations, to correlate the results of previous experiments with analytical relations.

APPENDICES

APPENDIX A

TORSION-WIRE CALIBRATION

The torsional spring constant of the torsion test fixture wire was determined indirectly by measuring the period of vibration of a torsional pendulum constructed with the wire (see Figure A-1). The spring constant (K) of a length (ℓ) of the wire is defined by the equation

$$T = K\phi \tag{A-1}$$

where (T) is the applied torque and ϕ is the relative angle-of-twist, measured in radians, between two points on the wire separated by a distance ℓ.

It is easily shown, using the theory of mechanical vibrations[29], that the vibrational frequency (f) of a torsional pendulum is given by the relation

$$f = \frac{1}{2\pi}\left[\frac{K}{I} - \frac{C^2}{4I^2}\right]^{\frac{1}{2}}$$

where (I) is the polar moment of inertia of the pendulum mass and (C) is a damping coefficient. For a slow pendulum in air the effects of damping are negligible, and the coefficient (C) may be set to zero (The validity of this assumption will be discussed later). The above equation then gives

$$K = 4\pi^2 I f^2. \tag{A-2}$$

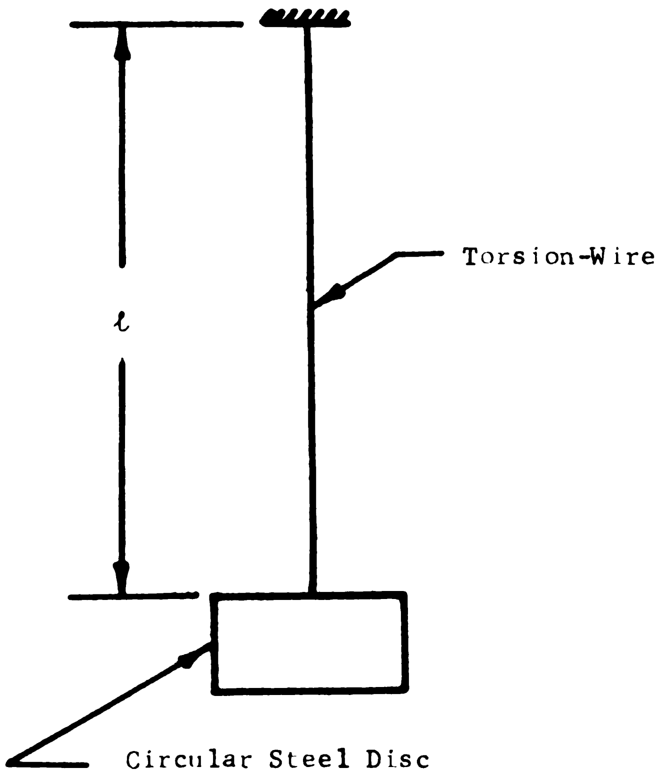

Figure A-1. Torsional Pendulum

The polar moment-of-inertia of a homogeneous circular disc of mass (M) and radius (R) is

$$I = \frac{MR^2}{2} .$$

Substituting this expression for (I) into eq. (A-2) and multiplying by the wire length (ℓ) gives the torsional spring-constant (k) per unit length of wire as follows:

$$k = 2\pi^2 \ell M R^2 f^2. \tag{A-3}$$

If (ℓ) and (R) are measured in centimeters, (M) in grams, and (f) is the reciprocal of the vibrational period in seconds, then the units of k are dyne-centimeters square per radian. If the weight in dynes is divided by the acceleration of gravity in centimeters per second square, the result may be referred to as "grams weight" (simply abbreviated gm). Thus eq. (A-3) gives

$$k = \frac{2\pi^2 \ell M R^2 f^2}{g} \quad \frac{\text{gm cm}^2}{\text{radian}} \tag{A-4}$$

where g is the acceleration of gravity.

The torsion-wire selected was steel music-wire of 0.008 inch diameter. A 46.05 cm effective length of the wire was used, along with a 450.5 gm steel disc of 2.529 cm radius, to construct the pendulum. Replicated measurements of the time required for 20 vibrational cycles all gave 4.60 minutes to within $\pm$ 0.005 minutes. In addition, it was found that the time-interval was independent of the angular amplitude of vibration, which confirms that damping effects were negligible.

Using this data along with eq. (A-4) and taking $g = 980.4$ cm/sec sq. (see Ref. 30) gives

$$k = 14.02 \frac{\text{gm cm}^2}{\text{radian}} .$$

A precision analysis indicated that a reasonable value for the standard deviation of (k) is 0.04 gm cm^2/radian.

APPENDIX B

TORSION TEST LASER BEAM PATH ANALYSIS

The problem at hand is that of computing the angle of rotation of a mirror, about a vertical axis, by analyzing the path of a light beam impinging on the mirror. The spatial rectangular cartesian coordinates of the mirror, and of reference points on the incident and reflected light beams, both before and after rotation, are assumed to be known. The beams pass through a vertical plane air/immersion medium interface located close to the mirror as compared to the distance to the reference points, and the refractive index of the immersion medium is assumed to be different from that of air.

If the air/immersion medium interface is close to the mirror, then from the standpoint of determining the direction cosines of the incident and reflected beams in air, one can neglect the presence of the interface and assume that each beam follows a straight-line between the mirror and the reference point on the beam. The coordinates of two points (mirror and reference point) on the line are known, therefore the direction cosines of the beam in air may be computed.

Take a coordinate system (x_1,x_2,x_3) with origin located at the point the light beam intersects the air/immersion medium interface as shown in Figure B-1, and let the $x_1 - x_3$

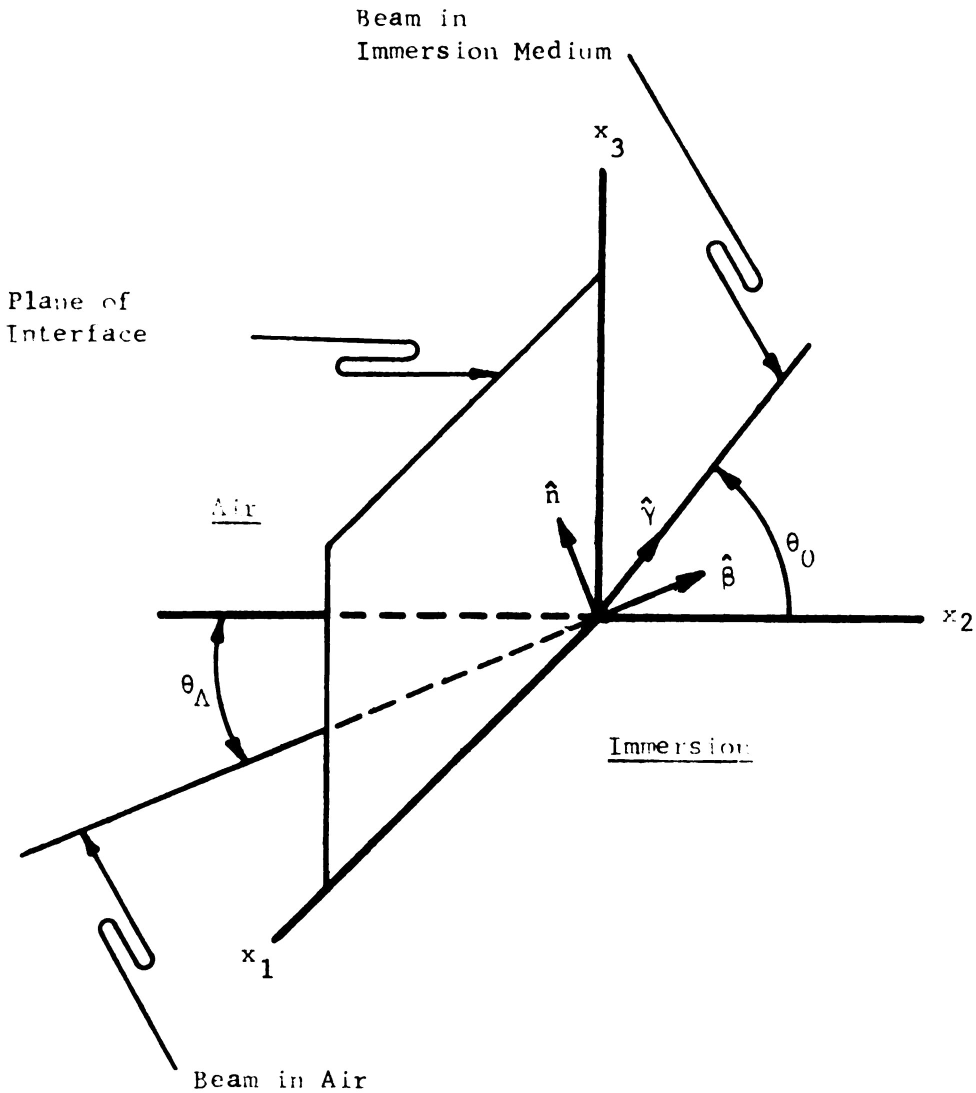

Figure B-1. Light Beam and Air/Immersion Interface plane be the plane of the interface. The light may be assumed to be propagating in either direction across the interface.

Let $\hat{\beta}$ be a unit vector parallel to the beam in air, and pointing into the immersion medium. Then if unit vectors along the positive coordinate directions are denoted by $\hat{i}_1$, $\hat{i}_2$, and $\hat{i}_3$ one can represent $\hat{\beta}$ by the expression

$$\hat{\beta} = \beta_1 \hat{i}_1 + \beta_2 \hat{i}_2 + \beta_3 \hat{i}_3 .$$

Similarly, let $\hat{\gamma}$ be a unit vector parallel to the beam in the immersion medium, and pointing into the immersion medium. Then $\hat{\gamma}$ may be represented by the expression

$$\hat{\gamma} = \gamma_1 \hat{i}_1 + \gamma_2 \hat{i}_2 + \gamma_3 \hat{i}_3 .$$

Since $\hat{\beta}$ and $\hat{\gamma}$ are unit vectors, the quantities $(\beta_1, \beta_2, \beta_3)$ and $(\gamma_1, \gamma_2, \gamma_3)$ are the direction cosines of the air and immersion beams respectively.

According to Snell's law of refraction the refracted beam lies in the plane of incidence; therefore in Figure B-1 the vectors $\hat{\beta}$ and $\hat{\gamma}$ and the x_2- axis are coplanar. Let $\hat{n}$ be a unit vector normal to this plane, and have components (n_1, n_2, n_3) such that

$$\hat{n} = n_1 \hat{i}_1 + n_2 \hat{i}_2 + n_3 \hat{i}_3 .$$

Since $\hat{i}_2$ and $\hat{\beta}$ are in the plane having normal $\hat{n}$ one may write

$$\hat{n} = \frac{\hat{i}_1 \times \hat{\beta}}{|\hat{i}_2 \times \hat{\beta}|}$$

which yields

$$\left.\begin{aligned} n_1 &= \frac{\beta_3}{\sqrt{\beta_1^2 + \beta_3^2}} \\ n_2 &= 0 \\ n_3 &= \frac{-\beta_1}{\sqrt{\beta_1^2 + \beta_2^2}} \end{aligned}\right\} \tag{B-1}$$

The x_2-axis is normal to the interface, therefore the angles θ_A and θ_0 are related by Snell's law of refraction, and one can write

$$n_A \sin \theta_A = n_0 \sin \theta_0$$

where n_A and n_0 are the absolute refractive indices of the air and the immersion medium respectively. It is easily shown from the above expression that

$$\cos \theta_0 = \frac{1}{n_0}\sqrt{n_0^2 - n_A^2(1 - \cos^2\theta_A)} \quad ,$$

but

$$\cos \theta_0 = \gamma_2$$

$$\cos \theta_A = \beta_2$$

therefore

$$\gamma_2 = \frac{1}{n_0}\sqrt{n_0^2 - n_A^2(1 - \beta_2^2)} \, . \tag{B-2}$$

The vector $\hat{\gamma}$ is normal to $\hat{n}$, therefore

$$\hat{\gamma} \cdot \hat{n} = 0$$

which may be written in the form

$$\gamma_1 n_1 + \gamma_2 n_2 + \gamma_3 n_3 = 0 \; . \tag{B-3}$$

Substituting the values of n_1, n_2, and n_3 from (B-1) into (B-3) gives

$$\gamma_3 = \left(\frac{\beta_3}{\beta_1}\right)\gamma_1 \tag{B-4}$$

and since $\hat{\gamma}$ is a unit vector one can write

$$\gamma_1^2 + \gamma_2^2 + \gamma_3^2 = 1 \,.$$

Substituting γ_1 and γ_2 from (B-2) and (B-4) into this equation and simplifying yields

$$\gamma_1^2 = \frac{n_A^2}{n_0^2} \frac{\beta_1^2(1 - \beta_2^2)}{(\beta_1^2 + \beta_3^2)}$$

but since $\hat{\beta}$ is a unit vector it follows that

$$\beta_1^2 + \beta_3^2 = 1 - \beta_2^2$$

and therefore

$$\gamma_1 = \left(\frac{n_A}{n_0}\right)\beta_1 \,. \tag{B-5}$$

Substituting γ_1 from (B-5) into (B-4) gives

$$\gamma_3 = \left(\frac{n_A}{n_0}\right)\beta_3 \,. \tag{B-6}$$

Recapitulating, equations (B-2), (B-5), and (B-6) give the direction cosines of the beam in the immersion medium in terms of the direction cosines of the beam in air and the two refractive indices, therefore the direction cosines of the incident and reflected beams in the immersion medium may be calculated. The next step in the analysis is to calculate the direction cosines of the normal to the mirror surface in terms of the direction cosines of the incident and reflected beams.

It is convenient now to redefine $\hat{\gamma}$ to be a unit vector along the beam impinging on the mirror, and pointing into the mirror. Similarly let $\hat{\gamma}'$ be a unit vector along the beam reflected from the mirror, and pointing into the mirror. Then as indicated previously, if the direction cosines of $\hat{\gamma}$ and $\hat{\gamma}'$ are $(\gamma_1,\gamma_2,\gamma_3)$ and $(\gamma_1',\gamma_2',\gamma_3')$ one can write

$$\hat{\gamma} = \gamma_1\hat{i}_1 + \gamma_2\hat{i}_2 + \gamma_3\hat{i}_3$$

$$\hat{\gamma}' = \gamma_1'\hat{i}_1 + \gamma_2'\hat{i}_2 + \gamma_3'\hat{i}_3 \; .$$

These two vectors are shown in Figure B-2.

Let $\hat{\mu}$ be a unit vector normal to the mirror as shown in Figure B-2, and let the direction cosines of $\hat{\mu}$ be (μ_1,μ_2,μ_3) so that

$$\hat{\mu} = \mu_1\hat{i}_1 + \mu_2\hat{i}_2 + \mu_3\hat{i}_3 \; .$$

Snell's law of reflection requires that the angle of incidence must be equal to the angle of reflection. These angles are denoted by ϕ in Figure B-2, and it is obvious that

$$\left.\begin{aligned} \hat{\gamma} \cdot \hat{\mu} &= \cos\phi \\ \hat{\gamma}' \cdot \hat{\mu} &= \cos\phi \\ \hat{\gamma}' \cdot \hat{\gamma} &= \cos 2\phi \; . \end{aligned}\right\} \qquad \text{(B-7)}$$

Also, since $\hat{\mu}$ is a unit vector one can write

$$\hat{\mu} \cdot \hat{\mu} = 1 \; . \qquad \text{(B-8)}$$

Equations (B-7) and (B-8) constitute a system of four simultaneous equations in the four unknowns μ_1,μ_2,μ_3, and ϕ.

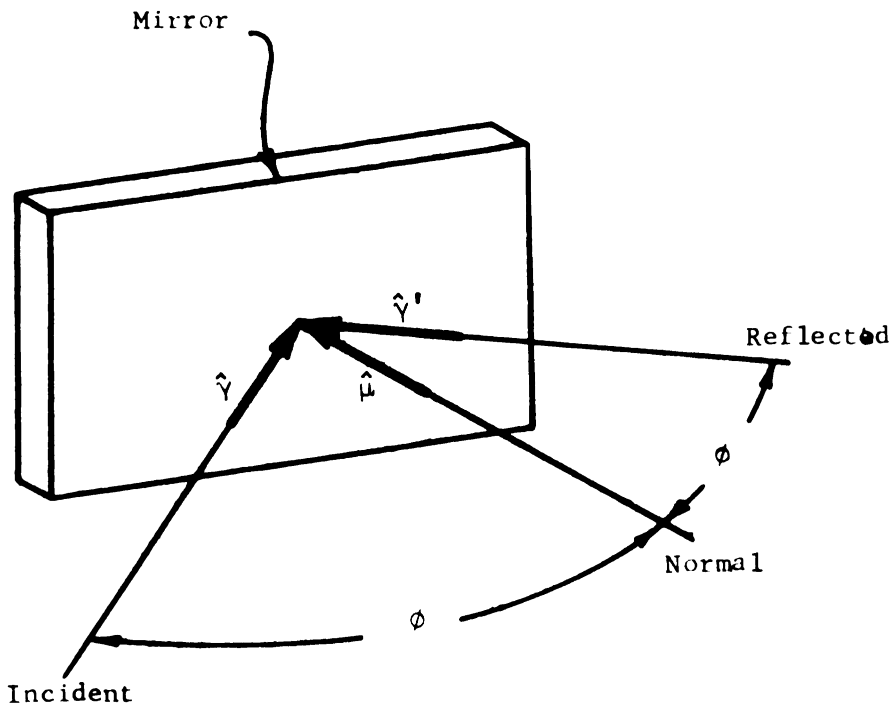

Figure B-2. Unit Vectors at the Mirror

The components of $\hat{\gamma}$ and $\hat{\gamma}'$ may be assumed known, therefore the quantity $\cos 2\phi$ may be evaluated immediately by expanding the last of equations (B-7); that is

$$\cos 2\phi = \gamma_1\gamma_1' + \gamma_2\gamma_2' + \gamma_3\gamma_3' \ .$$

Applying a trigonometric identity gives

$$\cos^2\phi = \frac{1}{2}(1 + \gamma_1\gamma_1' + \gamma_2\gamma_2' + \gamma_3\gamma_3'). \qquad \text{(B-9)}$$

The first two of equations (B-7) may be written in the form

$$\gamma_1\mu_1 + \gamma_2\mu_2 + \gamma_3\mu_3 = \cos \phi$$

$$\gamma_1'\mu_1 + \gamma_2'\mu_2 + \gamma_3'\mu_3 = \cos \phi \ .$$

One can solve for μ_2 and μ_3 in terms of μ_1 from these two equations. The result is

$$\left.\begin{aligned} \mu_2 &= C_1\mu_1 + C_2 \\ \mu_3 &= C_3\mu_1 + C_4 \end{aligned}\right\} \qquad \text{(B-10)}$$

where C_1 through C_4 are defined as follows:

$$C_1 = \frac{\gamma_1'\gamma_3 - \gamma_1\gamma_3'}{\gamma_2\gamma'_3 - \gamma_2'\gamma_3}$$

$$C_2 = \frac{(\gamma_3' - \gamma_3)\cos \phi}{\gamma_2\gamma_3' - \gamma_2'\gamma_3}$$

$$C_3 = \frac{1}{\gamma_3' - \gamma_3}\left[\gamma_1 - \gamma_1' + \frac{(\gamma_2 - \gamma_2')(\gamma_1'\gamma_3 - \gamma_1\gamma_3')}{\gamma_2\gamma_3' - \gamma_2'\gamma_3}\right]$$

$$C_4 = \frac{(\gamma_2 - \gamma_2')\cos \phi}{\gamma_2\gamma_3' - \gamma_2'\gamma_3} \ .$$

Equation (B-8) may be written in the form

$$\mu_1^2 + \mu_2^2 + \mu_3^2 = 1$$

and if μ_2 and μ_3 are eliminated by using equations (B-10) the result is

$$A\mu_1^2 + B\mu_1 + C = 0 \tag{B-11}$$

where

$$A = C_1^2 + C_3^2 + 1$$

$$B = 2(C_1C_2 + C_3C_4)$$

$$C = C_2^2 + C_4^2 - 1.$$

Equation (B-11) is simply a quadratic equation in μ_1, and has the solution

$$\mu_1 = \frac{-B \pm \sqrt{B^2 - 4AC}}{2A}. \tag{B-12}$$

Upon evaluating μ_1 from (B-12) one can substitute the value back into (B-10) to get μ_2 and μ_3. Equation (B-12) gives two roots for μ_1, and at first though one might require that only real roots leading to values of μ_1,μ_2, and μ_3 between $\pm$ 1.0 be retained. This restriction was included in the computer program used to carry out the calculations of this analysis; however in all cases the discriminant $(B^2 - 4AC)$ was negligibly small, and therefore root selection was never a problem. It is anticipated that one could probably show analytically that the discriminant is identically zero if he had the time and patience to carry out the algebraic manipulations involved.

At this point the direction cosines giving the orientation of the mirror normal have been evaluated. The vector $\hat{\mu}$ is shown in Figure B-3. As the mirror rotates about the vertical axis, the angle θ changes by an increment exactly equal to the rotation angle, therefore the desired rotation angle is determined by calculating θ before and after the increment and subtracting the two values to get the net rotation. It is easily seen from Figure B-3 that

$$\theta = \arc \tan \frac{\mu_1}{\mu_2} . \tag{B-13}$$

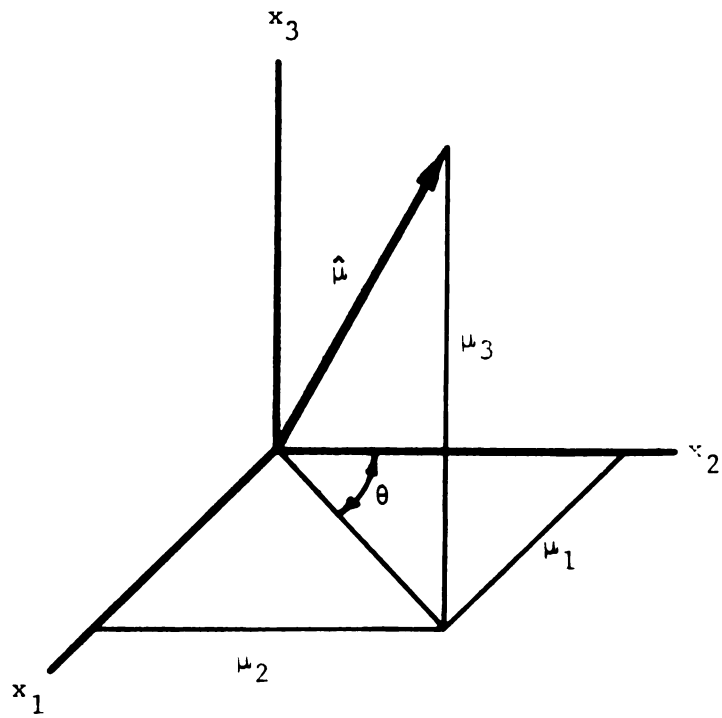

Figure B-3. Components of the Mirror Normal

APPENDIX C

EXPERIMENTAL DATA

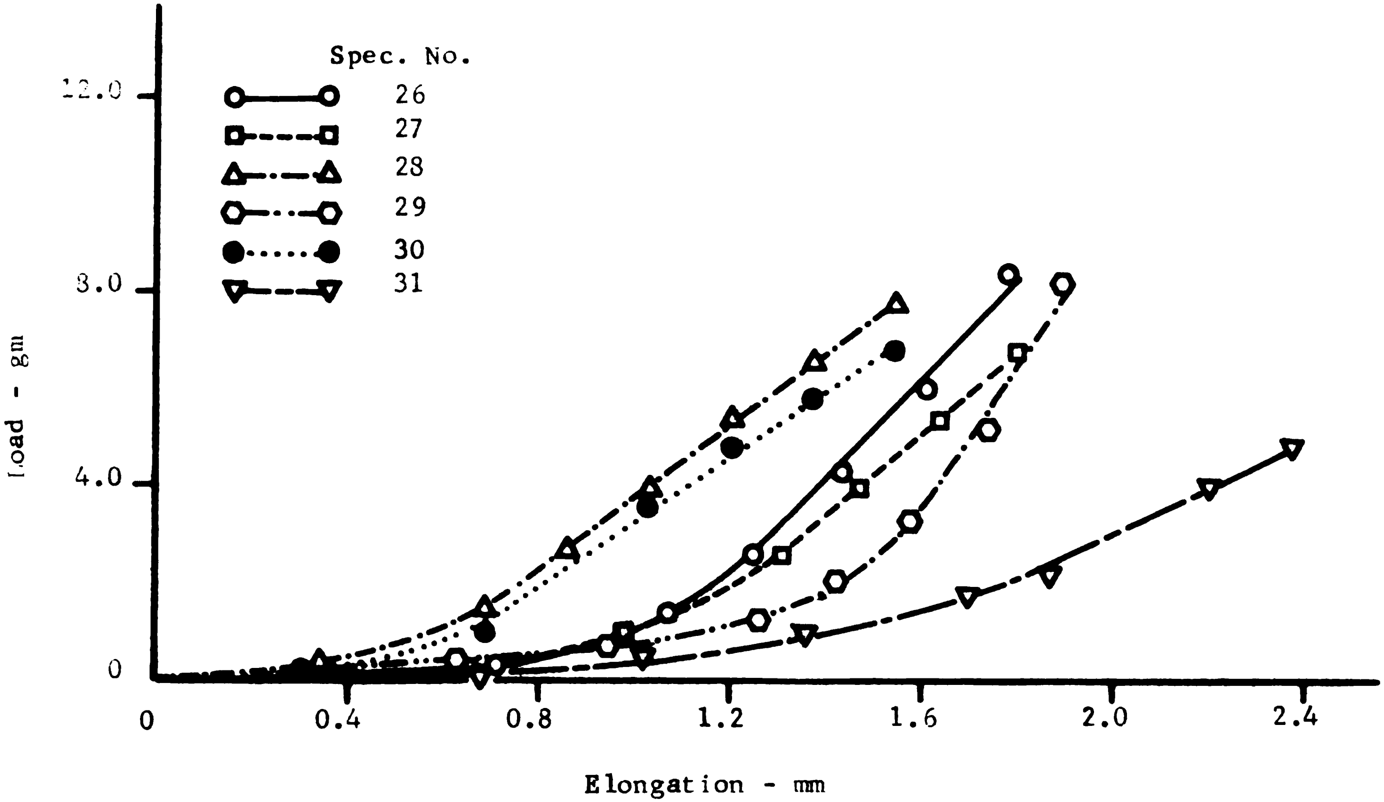

Figure C-1. Tensile Load Versus Elongation - Narrow Peet Specimens

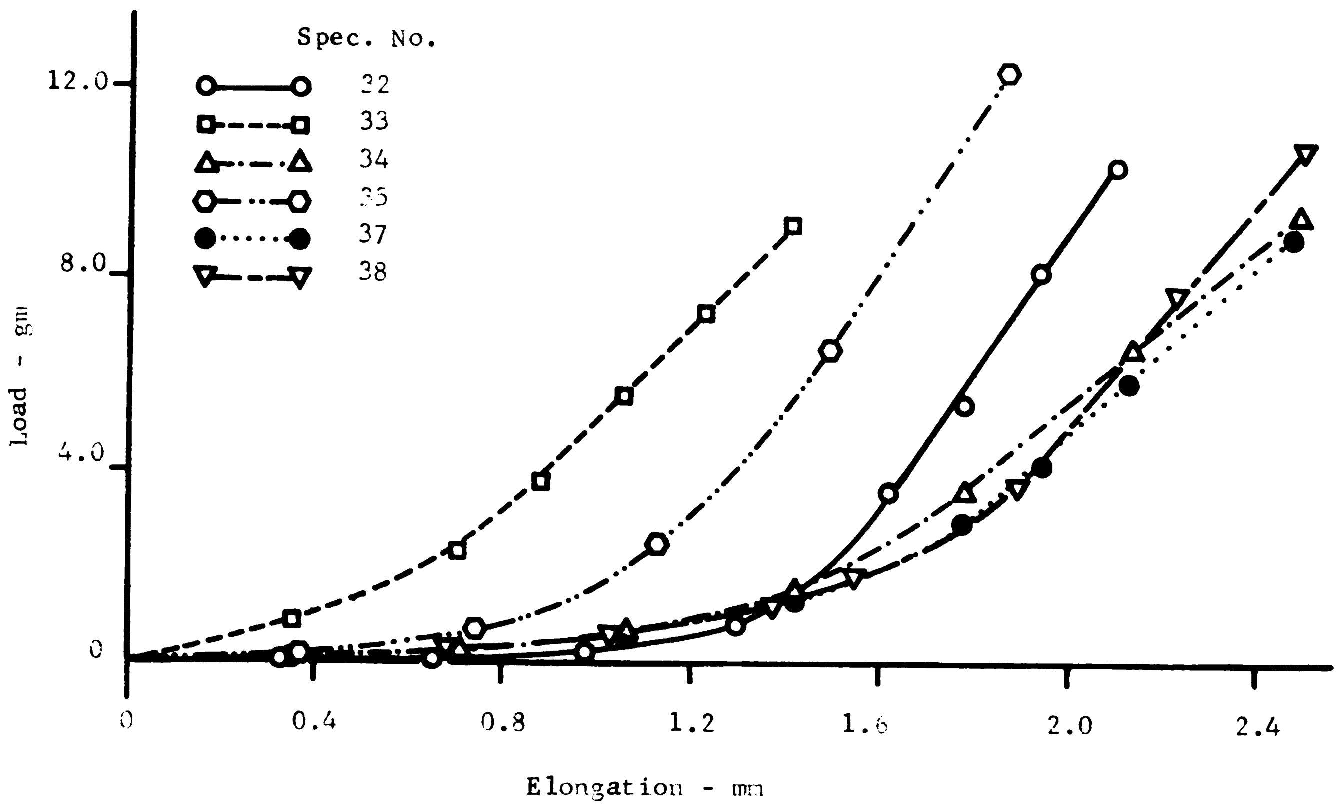

Figure C-2. Tensile Load Versus Elongation - Wide Peel Specimens

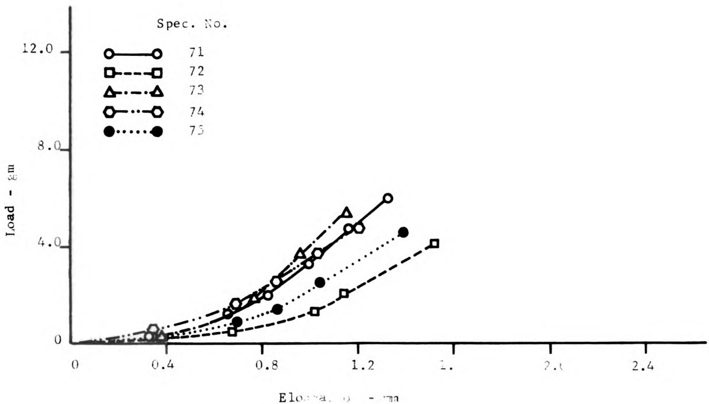

Figure C-3. Tensile Load Versus Elongation - Narrow Me[illegible] Specimens

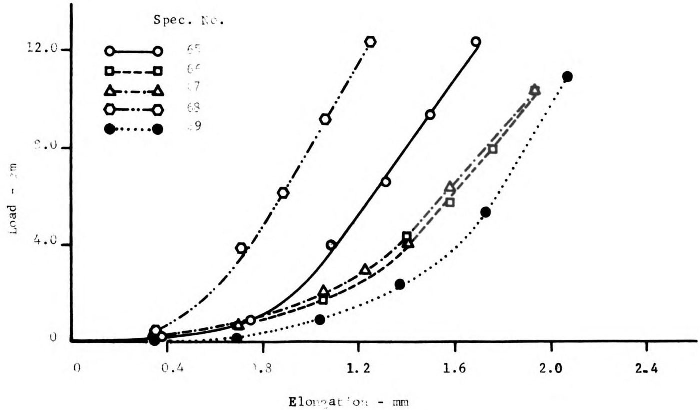

Figure C-4. Tensile Load Versus Elongation - Wide Meats Tab Specimens

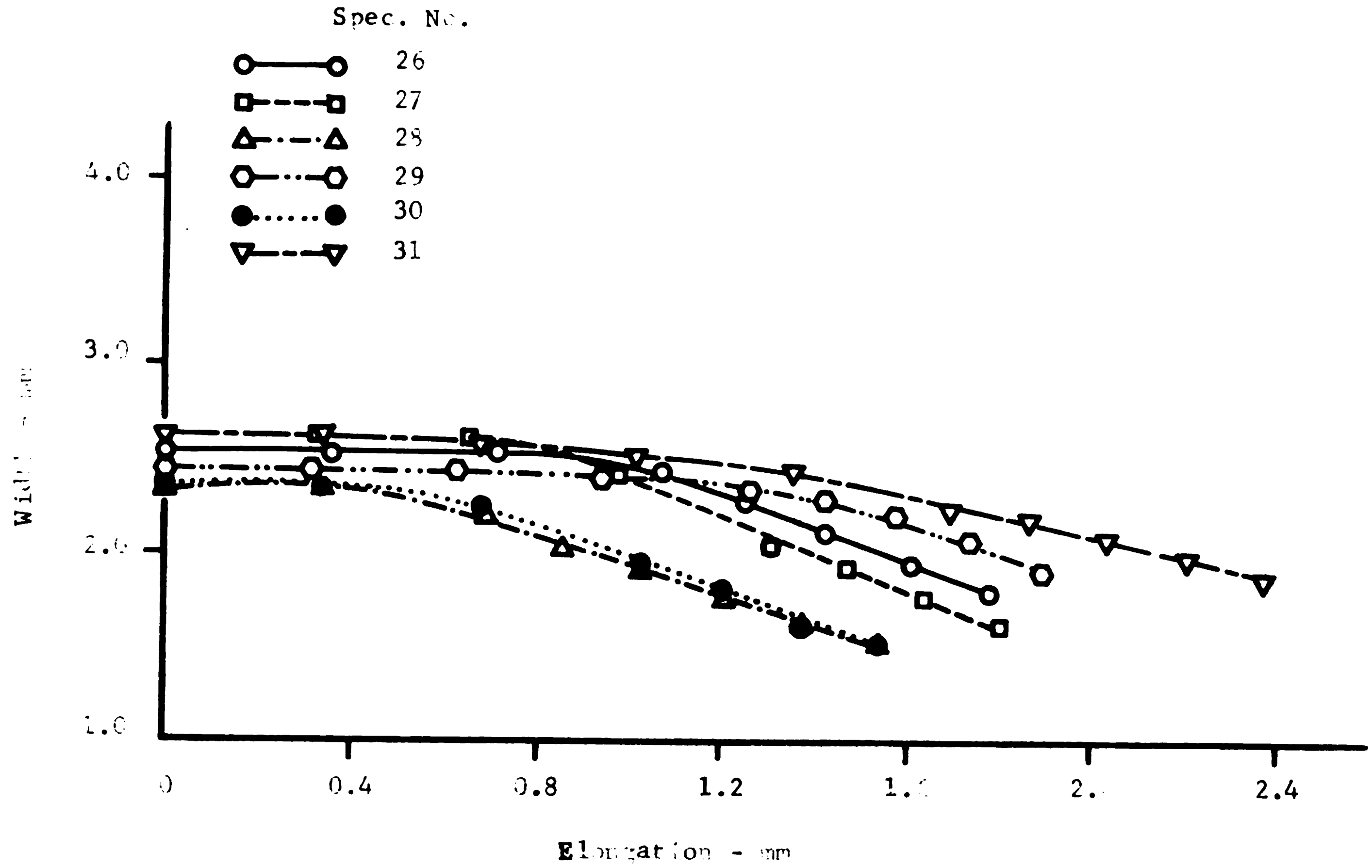

Figure -5. Width Versus Elongation - Narrow Peet Specimens

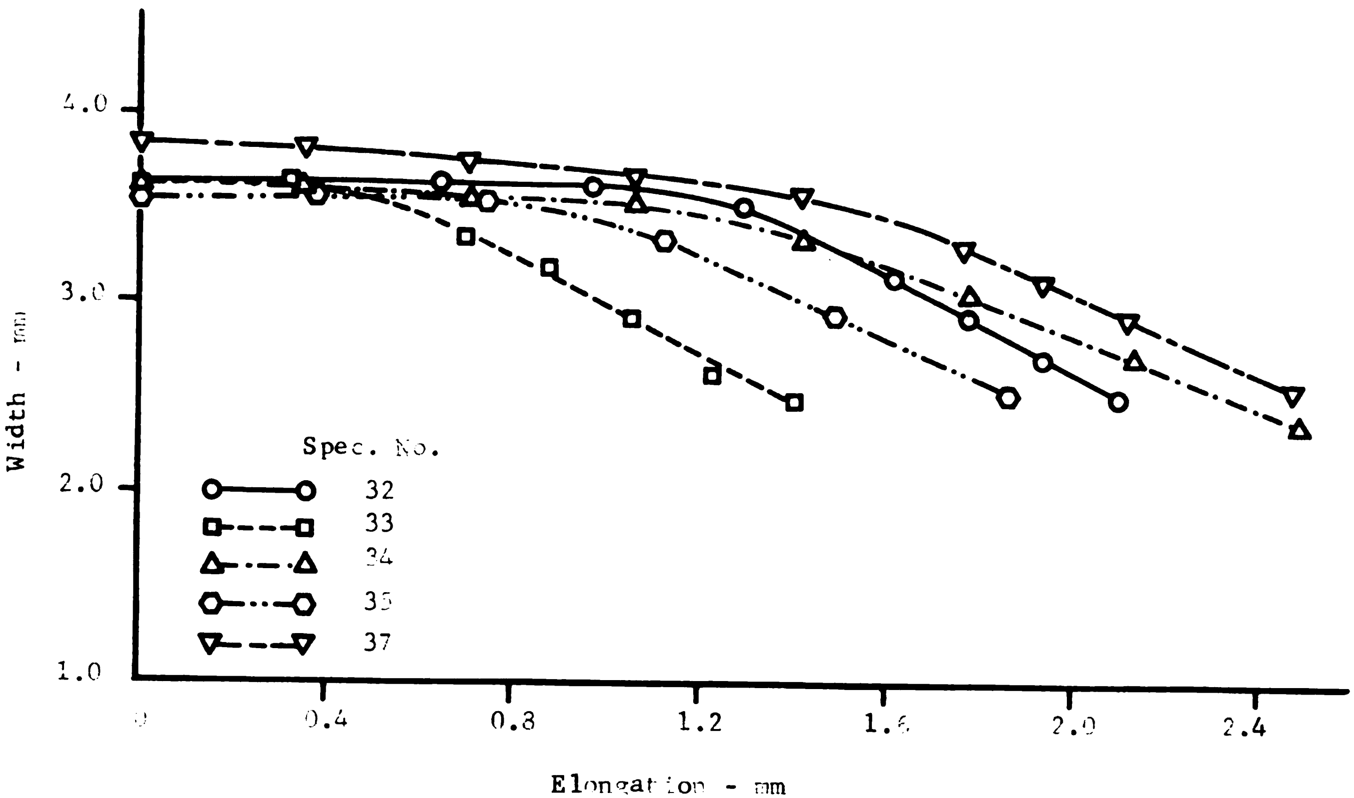

Figure 6-6. Width Versus Elongation - Wide Peet Specimens

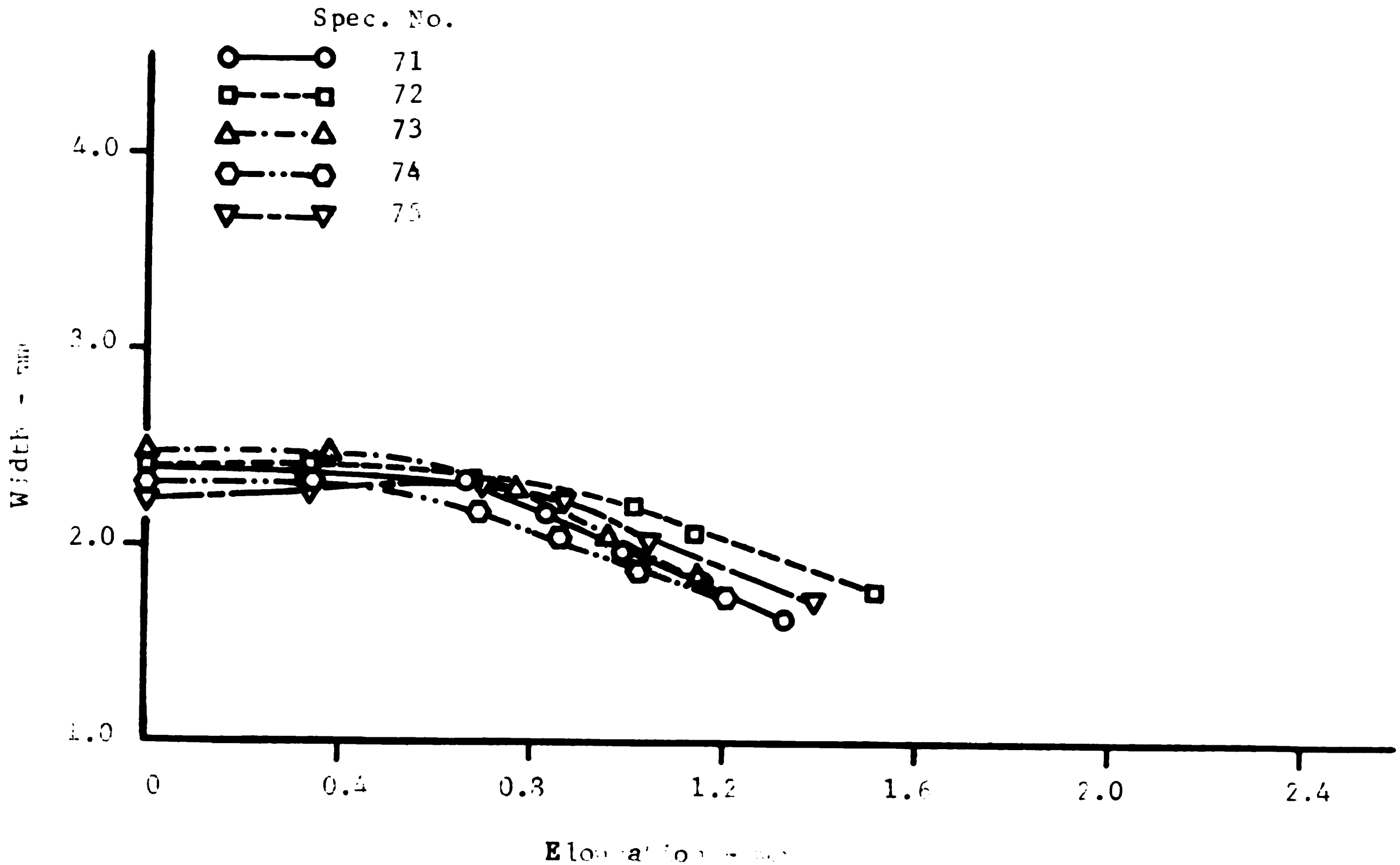

Figure [illegible]. Wi[illegible] Versus Elongation - [illegible] Meats [illegible] Spe[illegible]s

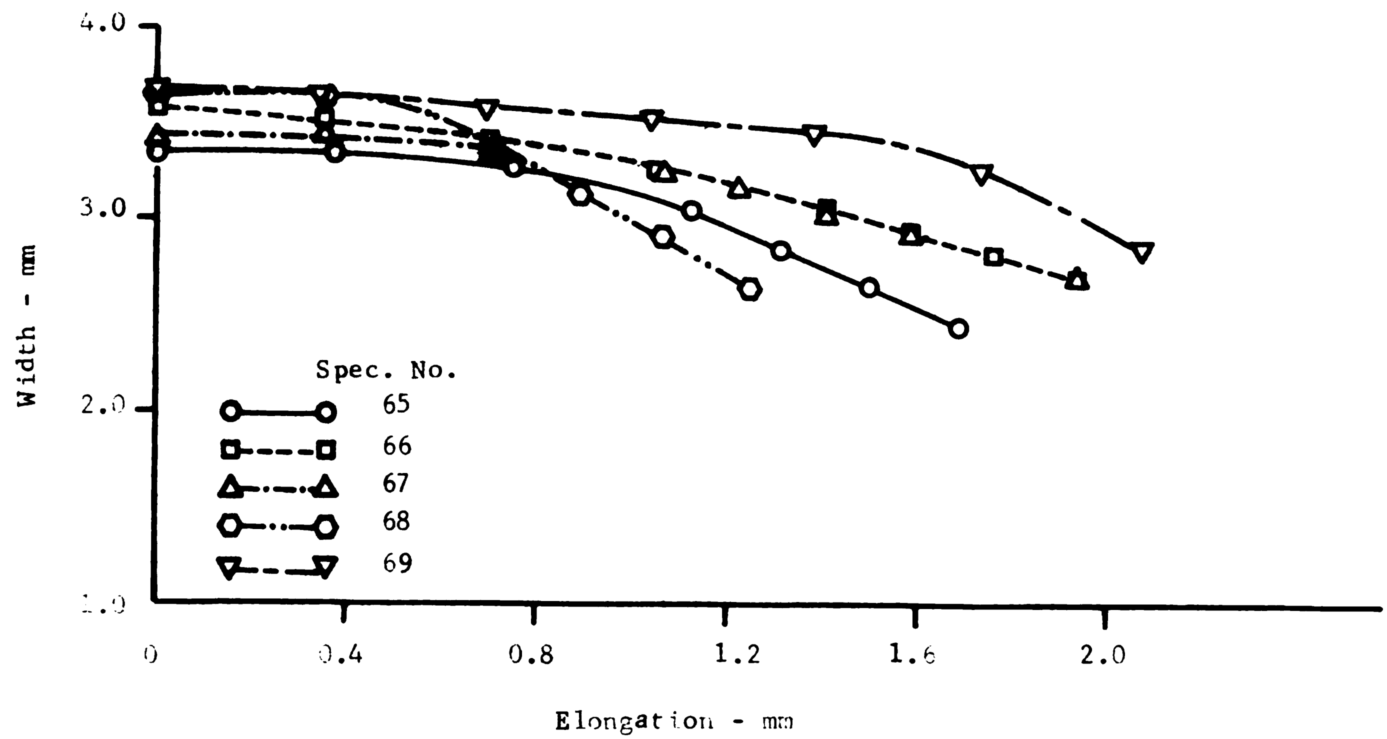

Figure C-[illegible]. Width Versus Elongation - Wide Meats Lab Specimens

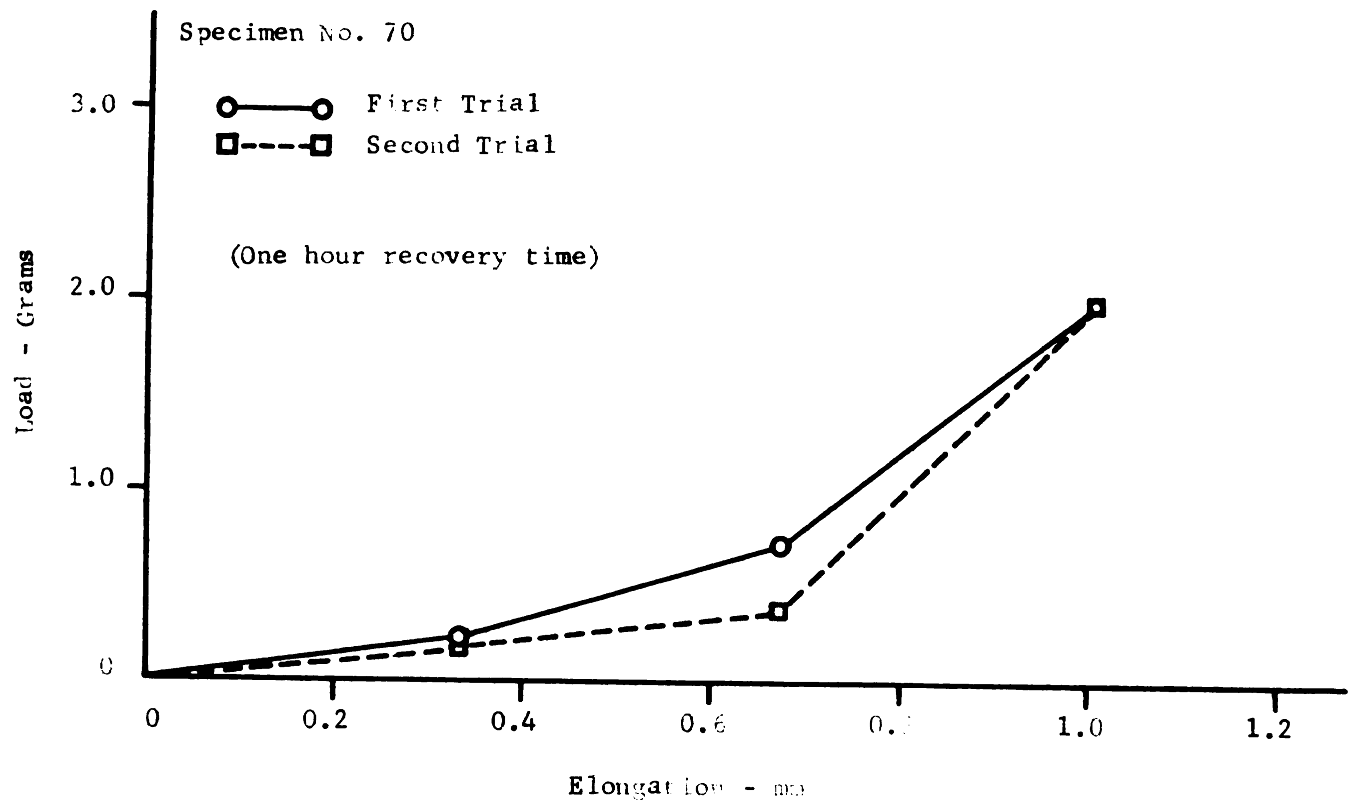

Figure C-9. Tensile Reversibility Test - Wide Meats Lab Specimen

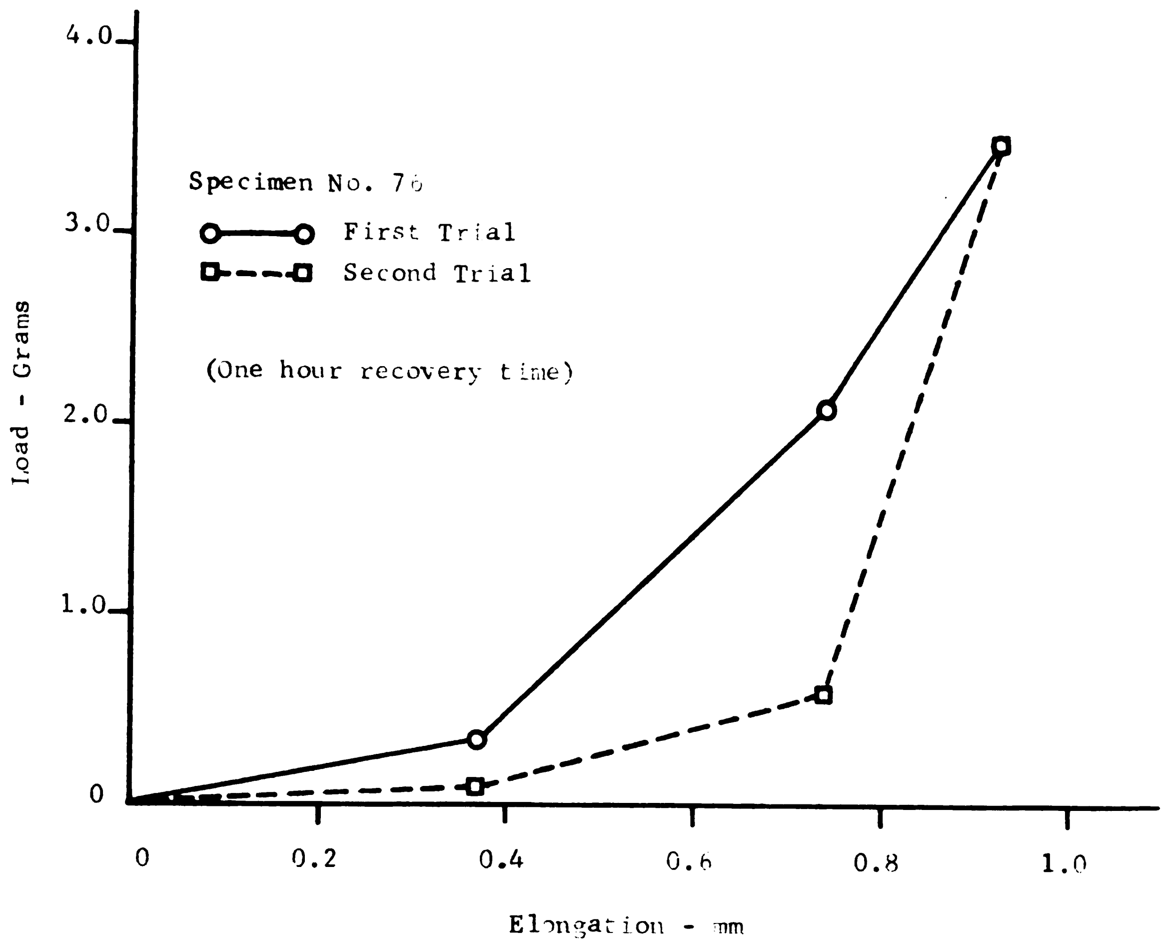

Figure C-10. Tensile Reversibility Test - Narrow Meats Lab Specimen

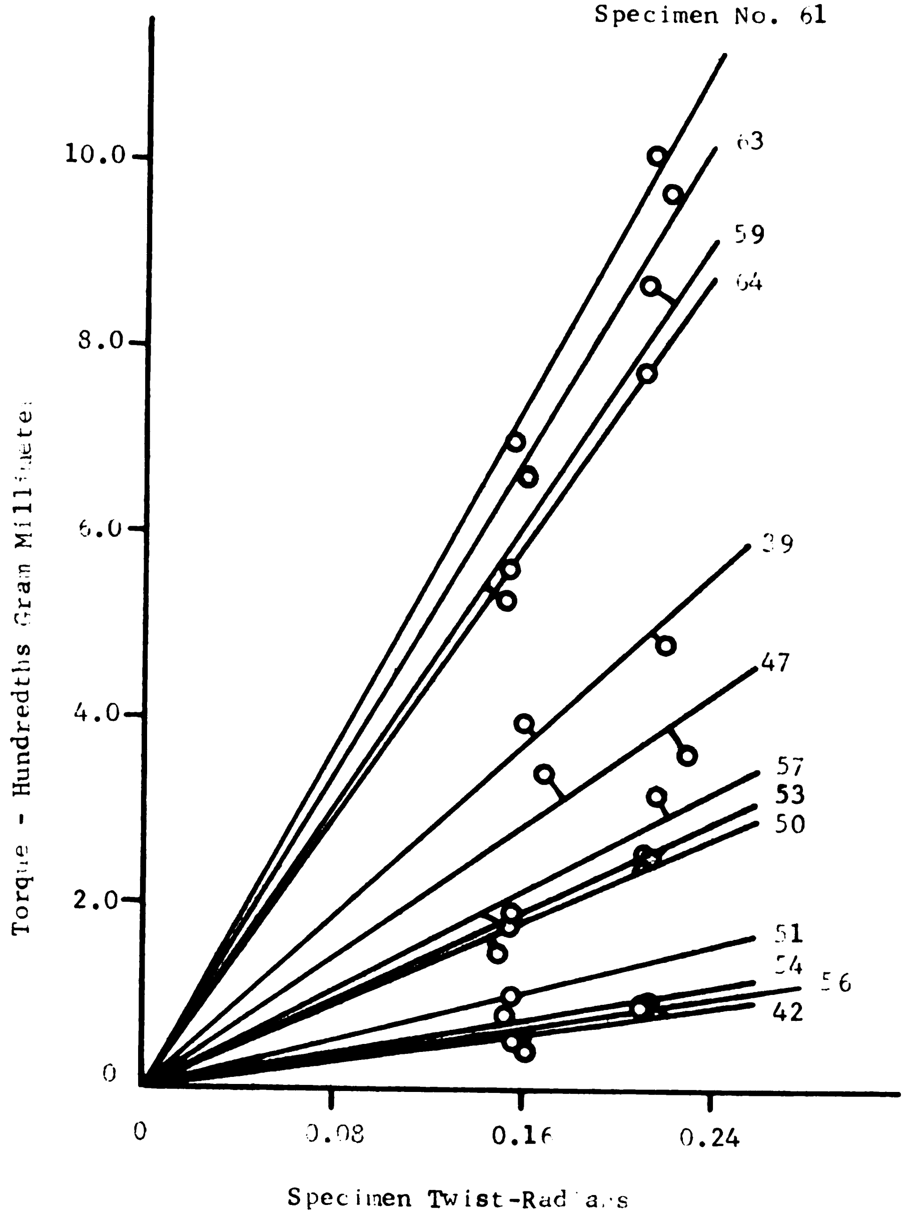

Figure C-11. Torsional Rigidity

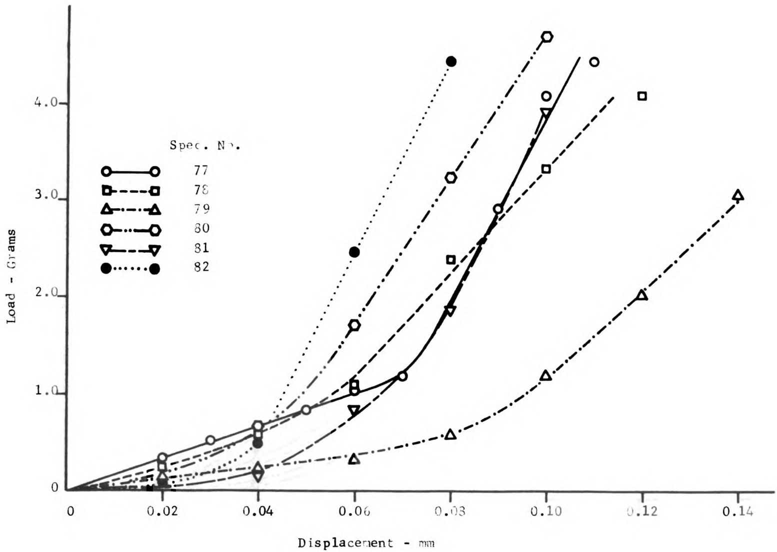

Figure C-12. Uniaxial Strain Test Load Versus Displacement - Meats Lab Specimens

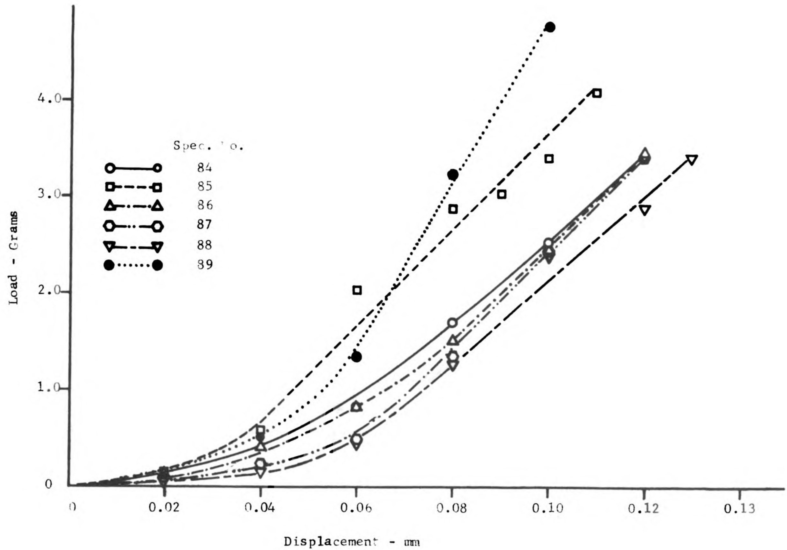

Figure C-13. Uniaxial Strain Test Load Versus Displacement - Peet Specimens

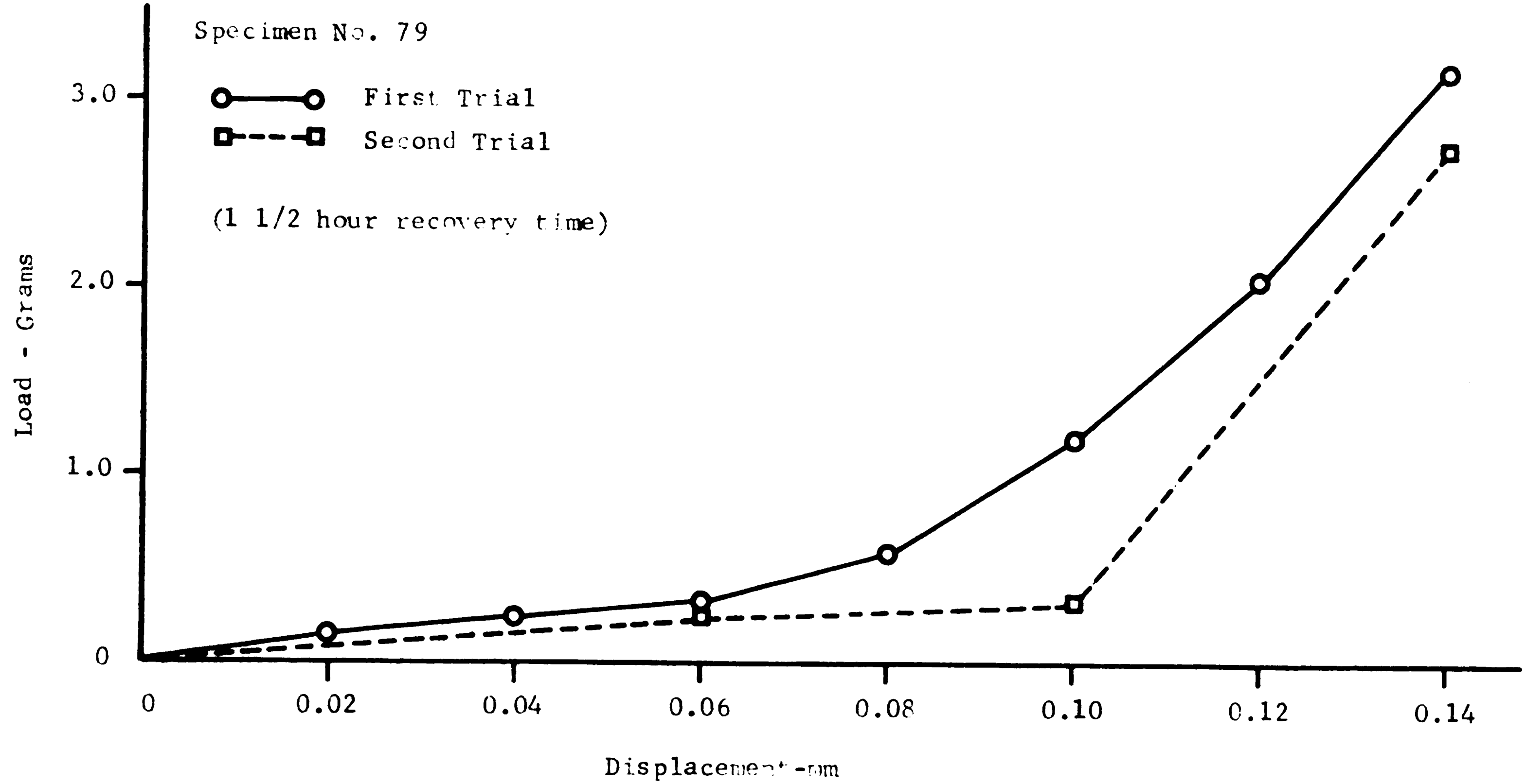

Figure C-14. Uniaxial Strain Reversibility Test - Meats Lab Specimen

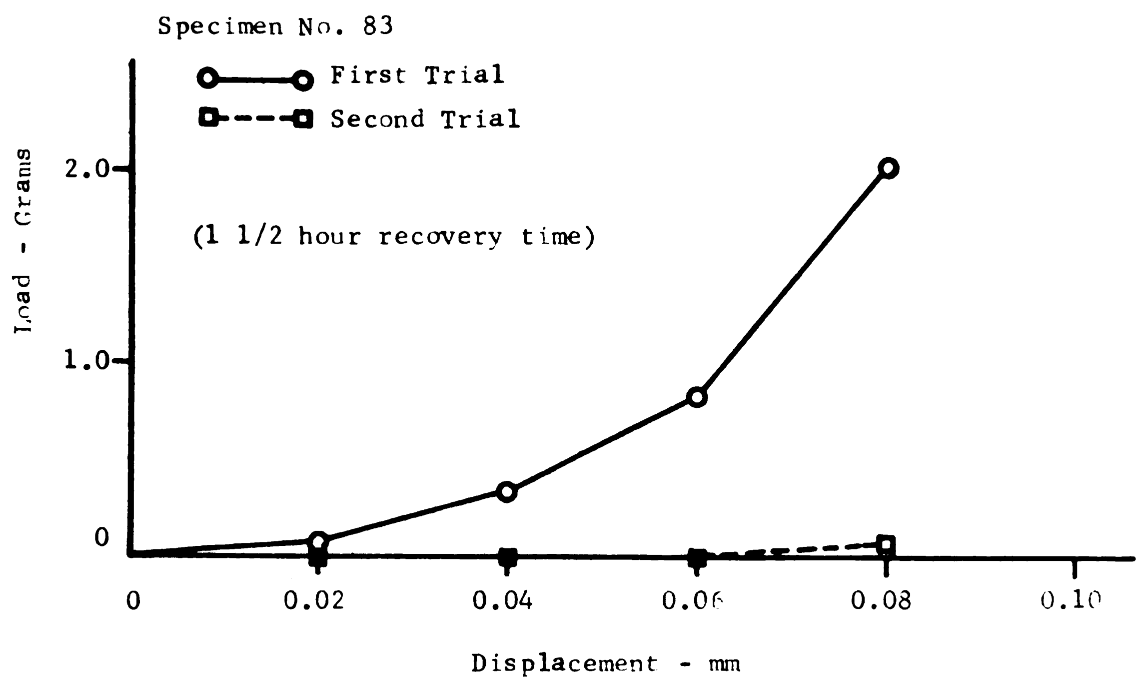

Figure C-15. Uniaxial Strain Reversibility Test - Mears Lab Specimen

APPENDIX D

COMPREHENSIVE LIST OF ASSUMPTIONS

Page 40: Deformations are reversible. An elastic strain-energy function exists.

Page 40: The stresses are linear functions of the strains.

Page 44: The fluid pressure is independent of the state of tissue strain.

Page 48: The parallel fibrils are randomly disposed.

Page 48: The lamella is macroscopically homogeneous, and geometric symmetry implies elastic symmetry.

Page 55: The individual lamellae of the stroma are identical.

Pages 60 & 61: Classical homogeneous plate theory assumptions are in force; that is, normals of the middle-plane of the plate before bending and stretching are deformed into normals of the middle-plane after bending and stretching, and transverse shearing and normal forces have negligible effect on the bending.

Pages 66 & 68: The St. Venant boundary regions of the uniaxial tensile test and torsion test are neglected.

Page 68: The torsion test displacement U_3 is only a first-order approximation. Only the shear stresses are nonzero, and these are uniformly distributed along the length of the specimen.

Page 71: In the uniaxial strain test, "edge effects" at the periphery of the specimen have negligible influence at the plunger.

LIST OF REFERENCES

LIST OF REFERENCES

1. Prince, J., Diesem, C., Englitis, I., and Ruskell, G., Anatomy and Histology of the Eye and Orbit in Domestic Animals, Bannerstone House, Springfield, Illinois, 1960.

2. Wolff, E., Anatomy of the Eye and Orbit, Fifth Edition, H.K. Lewis & Co., London, 1961.

3. The Eye, Vol. I, ed. by Davson, H., Academic Press, New York, 1962.

4. Kestenbaum, A., Applied Anatomy of the Eye, Grune and Stratton, Inc., New York, 1963.

5. Naylor, E.J., "The Structure of the Cornea Revealed by Polarized Light", Quarterly Journal of Microscopical Science, Vol. 94, Part I, pp. 83-88, 1953.

6. Nyquist, G.W., "Rheology of the Cornea: Experiment Techniques and Results", Experimental Eye Research, Vol. 7, pp. 183-188, 1968.

7. The Structure of the Eye, ed. by Smelser, G., Academic Press, New York, p. 348, 1961.

8. Capella, J.A., Kaufman, H.E., and Robbins, J.E., "Preservation of Viable Corneal Tissue," Cryobiology, Vol. 2, No. 3, p. 116, 1965.

9. Stanworth, A., "The Cornea in Polarized Light", British Journal of Ophthalmology, Vol. 33, pp. 485-490, 1949.

10. Schwartz, N.J., "A Theoretical and Experimental Study of the Mechanical Behavior of the Cornea With Application to the Measurement of Intraocular Pressure", Space Sciences Laboratory, Series 6, Issue 31, Univ. of California, July 28, 1965.

11. Kinsey, V.E. and Cogan, D.G., "The Cornea: III. Hydration Properties of Excised Corneal Pieces", Archives of Ophthalmology, Vol. 28, pp. 272-284, 1942.

12. Dohlman, C.H. and Anseth, A., "The Swelling Pressure of the Ox Corneal Stroma", Acta Ophthalmologica, Vol. 35, pp. 73-84, 1957.

13. Hedbys, B.O. and Dohlman, C.H., "A New Method for the Determination of the Swelling Pressure of the Corneal Stroma In Vitro", Experimental Eye Research, Vol. 2, pp. 122-129, 1963.

14. Hedbys, B.O., Mishima, S., and Maurice, D.M., "The Imbibition Pressure of the Corneal Stroma", Experimental Eye Research, Vol. 2, pp. 99-111, 1963.

15. Biot, M.A., "Theory of Elasticity and Consolidation for a Porous Anisotropic Solid", Journal of Applied Physics, Vol. 26, pp. 182-185, 1955.

16. Hedbys, B.O. and Mishima, S., "Flow of Water in the Corneal Stroma", Experimental Eye Research, Vol. 1, pp. 262-275, 1962.

17. System of Ophthalmology, Vol. 4, ed. by Duke-Elder, C.V., Mosby Co., St. Louis, p. 352, 1968.

18. Azzi, V.D. and Tsai, S.W., "Anisotropic Strength of Composites", Experimental Mechanics, Vol. 5, pp. 283-288, Sept., 1965.

19. Chen, C.H. and Cheng, S., "Mechanical Properties of Fiber Reinforced Composites", Journal of Composite Materials, Vol. 1, pp. 30-40, 1967.

20. Holister, G.S. and Thomas, C., Fiber Reinforced Materials, Elsevier Publishing Co. Ltd., Barking, Essex, England, 1966.

21. Fundamental Aspects of Fiber Reinforced Plastic Components, ed. by Schwartz, R.T. and Schwartz, H.S., Interscience Publishers, New York, 1968.

22. Smith, C.G., "Some new types of Orthotropic Plates Laminated of Orthotropic Material", A.S.M.E. Journal of Applied Mechanics, Vol. 20, pp. 286-288, 1953.

23. Reissner, E. and Stavsky, Y., "Bending and Stretching of Certain Types of Hetrogeneous Aeolotropic Elastic Plates", A.S.M.E. Journal of Applied Mechanics, Vol. 28, pp. 402-408, 1961.

24. Dong, S.B., Pister, K.S., and Taylor, R.L., "On the Theory of Laminated Anisotropic Shells and Plates", Journal of the Aerospace Sciences, Vol. 28, pp. 969-975, 1962.

25. Azzi, V.D. and Tsai, S.W., "Elastic Moduli of Laminated Anisotropic Composites", Experimental Mechanics, Vol. 5, pp. 177-185, 1965.

26. Timoshenko, S., and Woinowsky-Krieger, S., Theory of Plates and Shells, Second Edition, McGraw-Hill, New York, 1959.

27. Lele, P., and Weddell, G., "The Relationship Between Neurohistology and Corneal Sensibility", Brain, Vol. 79, pp. 119-154, 1956.

28. Schenck, H., Theories of Engineering Experimentation, McGraw-Hill, New York, 1961.

29. Den Hartog, J.P., Mechanical Vibrations, Fourth Edition, McGraw-Hill, New York, 1956, Chapter II.

30. Sears, F.W., Mechanics, Wave Motion, and Heat, Addison-Wesley, Reading, Mass., 1958, p. 342.